DISS. ETH. NO. 23501

Photoresponsive Polymer-Brush Structures for Smart Surfaces

A dissertation submitted to

ETH ZURICH

for the degree of

Doctor of Sciences ETH

presented by

MATTHIAS DÜBNER

Master of Science ETH in Chemistry

born on the 19th of May 1987

citizen of Germany

accepted on the recommendation of

Prof. Dr. Nicholas D. Spencer, examiner

Prof. Dr. A. Dieter Schlüter, co-examiner

Dr. Celestino Padeste, co-examiner

2016

The pursuit of truth and beauty is a sphere of activity in which we are permitted to remain children all our lives.

A. Einstein (1879 – 1955)

Abstract

The performance of a material is determined by its bulk and its surface properties. As many highly-engineered materials are designed to be robust, inert and stable, they often show passivity in terms of their surface properties. Surface modification of such materials is therefore highly desirable, as it allows the interfacial properties to be controlled in terms of specific interactions or non-interactions towards the environment without completely changing the chemical nature of the parent material. The focus of the presented work was the surface modification of flexible, lightweight and deformable foils of high-performance fluoropolymers such as poly(ethylene-*alt*-tetrafluoroethylene) (ETFE), poly(tetrafluoroethylene) (PTFE), as well as microporous polyolefins such as polypropylene (PP) membranes to achieve light-responsiveness.

Functionalization of surfaces with polymer brushes is very attractive, as it is offers a versatile methodology for the implementation of a high density of functional groups per unit area of the substrate. Such surface-bound macromolecular chains are mechanically and chemically stable due to their covalent attachment at one end to the substrate. Furthermore they can act as a very flexible and responsive extension of the surface into the third dimension. In the applied grafting-from approach, polymer brushes are grown from polymeric substrates via surface-initiated free-radical polymerization (FRP). Radical initiators are created by breaking of covalent bonds in the topmost layer of the polymeric substrates by exposure to argon-plasma or interference exposures with extreme ultraviolet radiation (EUV-interference lithography, EUV-IL) at the Swiss Light Source (SLS). Argon plasma allows simple and straightforward grafting of large areas in the order of several cm^2, while EUV-IL leads to well-controlled grafting of micro- and nanopatterns with high and tunable grafting densities.

Different strategies have been developed for the grafting of patterned light-responsive polymer brushes by means of one- or two-step post-polymerization modification (PPM) of epoxides (glycidyl methacrylate, GMA) and of acids (methacrylic acid, MAA) that were activated as anhydrides. The different PPM approaches allowed the number of photochromic spiropyran (SP) groups attached to the polymer brushes, and as a consequence their light-responsive behavior, to be controlled. SP can open upon UV-light exposure to form zwitterionic, deeply colored and fluorescent merocyanine (MC) and close back to the colorless SP configuration via thermal or visible light-induced relaxation. Switching kinetics were studied

using time-resolved fluorescence microscopy, indicating the importance of the local chemical environment provided by both the polymer brush and added solvents. The measurements showed the predominant influence of polar solvents, which stabilize the MC form, on the ring-closing kinetics. Furthermore, light-induced reversible switches in color and wettability upon alternating UV- and visible light irradiation were demonstrated.

The established PPM approach of grafted polymer brushes has been used to fabricate a microporous pH- and light-responsive membrane that enabled remote control over its transport and interfacial material properties. Morphological changes as a function of grafting level upon argon plasma activation were analyzed by means of atomic force microscopy. pH- and light-induced reversible switches in wettability and permeability upon changing from acidic to basic pH or alternating UV- and visible-light irradiation, respectively, were demonstrated using static water contact angle and flux measurements.

In the following, different thiol-reactive nanopatterned copolymer-brush structures were grafted from polymeric substrates by means of EUV-IL. The copolymer brushes were designed to contain maleimide functional groups as thiol-reactive centers. The number of reactive centers on the grafted brush structures was tailored by varying the monomer ratios in the feed. The maleimide methacrylate (MaMA) was furan-protected (FuMaMA) during the polymerization to avoid *in situ* crosslinking and deprotected after the grafting process. The reactive MaMA units were utilized to conjugate thiol-containing moieties using the nucleophilic Michael-addition reaction, which proceeds at room temperature without the need for any metal-based catalyst. Using this approach, a variety of functionalities was introduced to yield polyelectrolytes, as well as fluorescent and light-responsive polymer-brush structures.

This approach was continued to graft amine- and thiol-reactive copolymer-brushes allowing chemospecific orthogonal PPM of the grafted structures. Epoxides were utilized for chemoselective bio-conjugation of microperoxidase-11 (MP-11) via an amine linker and de-protected maleimides to conjugate photochromic SP thiols using again the nucleophilic Michael-addition reaction. Enzymatic activity was illustrated via a MP-11-catalyzed oxidation of colorless 3,3',5,5'-tetramethylbenzidine (TMB) diamine to deep-blue colored TMB diimine. A dramatic switch in the enzymatic turn-over of TMB according to exposure to either UV- or visible light allowed us to control the enzymatic activity of fabricated photochromic bio-conjugated copolymer brushes grafted from the polymeric substrates.

Zusammenfassung

Die Leistungsfähigkeit eines Materials wird von dessen Bulk- und Oberflächeneigenschaften bestimmt. Viele hochentwickelte Materialien sind jedoch so robust, inert und stabil aufgebaut, dass sich auch ihre Oberflächen passiv verhalten. Oberflächenmodifikation solcher Materialien ist daher sehr wünschenswert, da sie die Kontrolle über die Grenzflächeneigenschaften in Bezug auf deren Interaktionen bzw. Nicht-Interaktionen mit der Umgebung ermöglicht, ohne die chemische Natur des Substrates komplett zu verändern. Der Fokus der vorliegenden Arbeit lag auf der Oberflächenmodifikation von flexiblen, leichten und verformbaren Folien von Hochleistungs-Fluoropolymeren, wie Poly(ethylen-*alt*-tetrafluoroethylen) (ETFE), Poly(tetrafluoroethylen) (PTFE), sowie von mikroporösen Polyolefinen, wie Polypropylen (PP)-Membranen, um Licht-induzierte Veränderungen in deren Oberflächeneigenschaften und –funktionalität hervorzurufen.

Die Funktionalisierung von Oberflächen mit „Polymerbürsten" („Polymer Brushes") ist hierbei sehr attraktiv, da sie eine vielseitige Methodik für die Implementierung hoher Dichten an funktionellen Gruppen pro Oberflächeneinheit bietet. Solche Oberflächen-gebundenen makromolekularen Ketten sind aufgrund ihrer kovalenten Bindung mit einem Kettenende an das Substrat mechanisch und chemisch stabil. Sie können zudem als flexible und schaltbare Erweiterung der Oberfläche in die dritte Dimension dienen. Im hier verwendeten „grafting-from" Ansatz wurden ausgehend von Radikalinitiatoren an einer Polymeroberfläche Polymerbürsten mittels freier radikalischer Polymerisation (FRP) gepfropft. Die Radikalinitiatoren wurden mittels Brechen von kovalenten Bindungen in der äussersten Schicht des Polymersubstrates durch Bestrahlung mit Argon-Plasma oder mittels Interferenzlithographie mit extrem-Ultraviolettstrahlung (EUV-IL) an der Synchrotron Lichtquelle Schweiz („Swiss Light Source", SLS) erzeugt. Argon-Plasma erlaubt eine einfache und direkte Pfropf-Polymerisierung auf grossen Flächen in der Grössenordnung von einigen cm^2, während die EUV-IL dafür genutzt werden kann, präzise definierte Mikro- und Nanostrukturen mit hohen und einstellbaren Pfropfdichten zu erzielen. Verschiedene Strategien wurden entwickelt, um strukturierte Licht-schaltbare Polymerbürsten mittels Ein- oder Zwei-Schritt Post-Polymerisations-Modifikation (PPM) von Epoxiden (Glycidylmethacrylat, GMA) und als Ester oder Anhydrid aktivierten Säuren (Methacrylsäure, MAA) zu pfropfen. Die unterschiedlichen PPM Ansätze ermöglichten, die Anzahl der photochromen Spiropyran (SP)-Gruppen an den Polymerbürsten, sowie deren

Licht-schaltbares Verhalten zu kontrollieren. SP kann sich unter UV-Licht-Einstrahlung öffnen und die zwitterionische, stark-gefärbte Merocyanin (MC) Konformation ausbilden. Durch thermische oder Licht-induzierte Relaxation kann sich das MC wieder zur farblosen SP-Form schliessen. Das Schaltverhalten der SP-modifizierten Bürstenstrukturen wurde mittels Zeit-aufgelöster Fluoreszenzmikroskopie untersucht. Die Untersuchungen ergaben, dass die lokale chemische Umgebung, gegeben durch die Zusammensetzung der Polymerbürsten und das hinzugefügte Lösungsmittel, massgeblich für die Intensität des Schaltverhaltens ist. Sie zeigten den dominanten Einfluss von polaren Lösungsmitteln auf die Ringschlusskinetik, da jene die MC-Form stabilisieren. Darüber hinaus wurde eine reversible, Licht-induzierte Veränderung in der Farbe und der Benetzbarkeit aufgrund von abwechselnder Einstrahlung mit sichtbaren und UV-Licht nachgewiesen.

Der so etablierte PPM-Ansatz für gepfropfte Polymerbürsten wurde dazu genutzt, um mikroporöse pH- und Licht-schaltbare Membranen zu fabrizieren, welche die ferngesteuerte Kontrolle über deren Transport- und Grenzflächeneigenschaften erlaubte. Morphologische Veränderungen als Funktion des Pfropf-Grades („Grafting-Levels") wurden mittels Rasterkraftmikroskopie analysiert. pH- und Licht-induzierte Schaltbarkeit von Benetzbarkeit und Permeabilität wurden durch abwechselnd sauren und basischen pH bzw. durch abwechselnde Einstrahlung mit UV- und mit sichtbarem Licht anhand von statischen Kontaktwinkelmessungen und mittels Durchflussmessungen demonstriert.

Im Folgenden wurden Thiol-reaktive nanostrukturierte Copolymerbürsten von Polymersubstraten mittels EUV-IL gepfropft. Die Copolymerbürsten wurden so synthetisiert, dass sie neben unreaktiven Monomereinheiten Maleimid-Gruppen als Thiol-reaktive Zentren enthielten. Die Anzahl der reaktiven Zentren an den Polymerbürsten wurde hierbei durch das Variieren der Monomerverhältnisse gesteuert. Die reaktiven Maleimidmethacrylat (MaMA) Einheiten waren während der Polymerisation Furan-geschützt (FuMaMA), um *in situ* crosslinking zu vermeiden und wurden nach dem Graftingprozess wieder entschützt. So konnten die reaktiven MaMA Einheiten genutzt werden, um Thiol-terminierte Moleküle mittels nukleophiler Michael-Addition Reaktion zu binden. Diese Reaktion verläuft bei Raumtemperatur, ohne den Bedarf eines Metall-basierten Katalysators. Dieser Ansatz wurde zur Einführung unterschiedlicher Funktionalitäten genutzt, um Polyelektrolyte, sowie fluoreszierende und Licht-schaltbare Polymerbürstenstrukturen zu erhalten.

Derselbe Ansatz wurde erweitert, um Amin- und Thiol-reaktive Copolymerbürsten zu pfropfen, welche die chemospezifische orthogonale PPM der gegrafteten Strukturen ermöglichte. Epoxide wurden für die chemoselektive Biokonjugation von Mikroperoxidase-11 (MP-11) über eine Aminogruppe verwendet. An die Maleimide wurden nachfolgend photochrome SP-Thiole mittels der nucleophilen Michael-Addition Reaktion gebunden. Die enzymatische Aktivität wurde durch eine MP-11-katalysierte Oxidation von farblosem 3,3',5,5'-Tetramethylbenzidin (TMB) Diamin zu dunkelblauem TMB Diimin nachgewiesen. Es zeigte sich ein gravierender Unterschied im enzymatischen Umsatz von TMB in Abhängigkeit der Lichteinstrahlung. Durch abwechselnde Bestrahlung der Proben mit sichtbarem oder UV-Licht, konnte enzymatische Aktivität der photochromen biokonjugierten Copolymerbürsten auf den Polymersubstraten kontrolliert werden.

Abbreviations

AFM	atomic force microscopy
ATR	attenuated total reflectance
ATRP	atom transfer radical polymerization
BCP	block copolymer
CA	contact-angle
CRP	controlled radical polymerization
CuAAC	copper-catalyzed azide alkyne cycloaddition
DA	Diels-Alder
DABCO	1,4-diazabicyclo[2.2.2]octane
DMSO	dimethyl sulfoxide
DPN	dip-pen nanolithography
EBL	electron-beam lithography
EGMA	ethylene glycol methyl ether methacrylate
ETFE	poly(ethylene-*alt*-tetrafluoroethylene)
EUV-IL	extreme ultraviolet interference lithography
FRP	free-radical polymerization
FuMaMA	furan-protected maleimide methacrylate
GL	grafting level
GMA	glycidyl methacrylate
HSQ	hydrogen silsesquioxane
IR	infrared
LB	Langmuir-Blodgett
LbL	layer by layer
LCST	lower critical solution temperature
MAA	methacrylic acid
MaMA	maleimide methacrylate
MMA	methyl methacrylate
MC	merocyanine
MCT	mercury cadmium telluride

MES	mercaptoethane sulfonate
MP-11	microperoxidase-11
μCP	micro-contact printing
NHS	*N*-hydroxysuccinimide
NMP	nitroxide-mediated radical polymerization
PAA	poly(acrylic acid)
PAcEMA	poly(2-(acetoacetoxy)ethyl methacrylate)
PAzPMA	poly(3-azidopropyl methacrylate)
PDMAEMA	poly(*N*,*N*-dimethylaminoethylmethacrylate)
PE	poly(ethylene)
PEG	poly(ethylene glycol)
PEGMA	poly(ethylene glycol) methyl ether methacrylate
P(EGMA)	poly(ethylene glycol methyl ether methacrylate)
PFP	pentafluorophenyl
PGMA	poly(glycidyl methacrylate)
PMAA	poly(methacrylic acid)
PMMA	poly(methyl methacrylate)
PNIPAAM	poly(*N*-isopropyl acrylamide)
PP	poly(propylene)
P(PEGMA)	poly(poly(ethylene glycol) methyl ether methacrylate)
PPM	post-polymerization modification
PPMA	poly(propargyl methacrylate)
PTFE	poly(tetrafluoroethylene)
P4VP	poly(4-vinylpyridine)
RAFT	reversible addition fragmentation chain transfer
rDA	retro Diels-Alder
SAM	self-assembled monolayer
SI-ROMP	surface-initiated ring opening metathesis polymerization
SIP	surface-initiated polymerization
SP	spiropyran
SP-NH$_2$	spiropyran amine
SP-SH	spiropyran thiol

SLS	Swiss Light Source
TEA	triethylamine
THF	tetrahydrofuran
TMB	3,3',5,5'-tetramethylbenzidine
TMS	tetramethylsilane
UV	ultraviolet
Vis	visible
XIL-II	X-ray interference lithography beamline
XPS	X-ray photoelectron spectroscopy

Table of Contents

1.   General Introduction

1.1   Polymer Brushes for Surface Modification

The modification of surfaces has a very long history going back some 7000 years, when wooden objects were covered with lacquer from tree sap as a protective layer in ancient Asian cultures. Back then it was already known that the performance of a material is determined by its bulk properties, as well as the structure and composition of its surface. Over the millennia, surface modifications have moved from simple coatings to highly engineered thin films, controlling the interfacial properties of a material by the deposition of ultrathin organic films onto their surface without completely changing the chemical nature of the underlying material (*stealth effect*).[1]

The advantage of coatings is based on the maintenance of the beneficial parent material bulk properties while the surface properties can be dramatically improved as they allow control over specific interactions or non-interactions towards the environment. Coatings serve usually as protection barrier against a hostile environment (*e.g.* corrosion, chemical or mechanical degradation) to optimize friction, adhesion, adsorption of molecules or wetting of solvents, used for industrial coatings, barriers, packaging, lubricants, biointerfaces and for microelectronics.[2-4]

Ultrathin coatings have been fabricated *via* self-assembly or directed-assembly methods by means of physical interactions or chemical bonds. The fabrication method used strongly defines the physical properties, such as film thickness and long-term stability of the formed coatings. Depositions based on physical forces are usually carried out from solution, where the solvent evaporates during the process. Technologically important and rather simple methods include spin-coating, dip-coating, doctor-blade coating and roll-to-roll coating. Further, more sophisticated methods, which allow higher precision in terms of internal structure and thickness, have been developed, including Langmuir-Blodgett (LB) films, layer by layer (LbL) deposition as well as adsorption of polymers. These technologies benefit from their simplicity, but lack in long-term stability due the weak interactions between the film and the surface, leading to desorption, displacement, dewetting or delamination.[5]

In contrast to physical interactions, an irreversible attachment through chemical bonds provides a much better long-term stability. Frequently employed techniques are based on either chemical modifications, self-assembled monolayers (SAMs) or polymer brushes.[6] SAMs are formed *via* interactions of functional anchoring groups and molecule-molecule interactions

attaching small molecules in a well-controlled and highly ordered fashion to the surface. The disadvantage of this approach is the intrinsically limiting nature of the 2D-arrangement, as the maximal density of functional groups is defined by their cross-sectional area, as well as the limited accessibility of functional groups due to the high packing density. In contrast to SAMs, polymer brushes are very flexible chains which are mechanically and chemically stable due to their covalent attachment at one end to the substrate, and they can act as an extension of the surface in a third dimension, leading to a high density of functional groups per unit area of substrate (*skyscraper approach*).[1, 7]

In addition, polymer brushes are very interesting from a physical point of view as they possess very unique properties due to their confined environment. The degrees of freedom for end-tethered macromolecules are reduced, allowing the chains to adopt rather unusual conformations, and, in a good solvent, leading to stretching, even of uncharged polymers, due to repulsive interactions with other chains. Important interaction parameters include, but are not limited to, grafting density, surface concentration, osmotic pressure and solvent quality. In addition, the conformational changes of surface-bound chains cause a change in entropy, energy and friction. While non-stretched coils show only a moderate increase of the energy stored in the system according to a slight molecular deformation (*entropy elasticity*), the energy difference for stretched chains in the brush conformation is much larger for the same small deformation, leading to very strong differences for shearing or penetration of surface-bound chains compared to free macromolecular coils.[8]
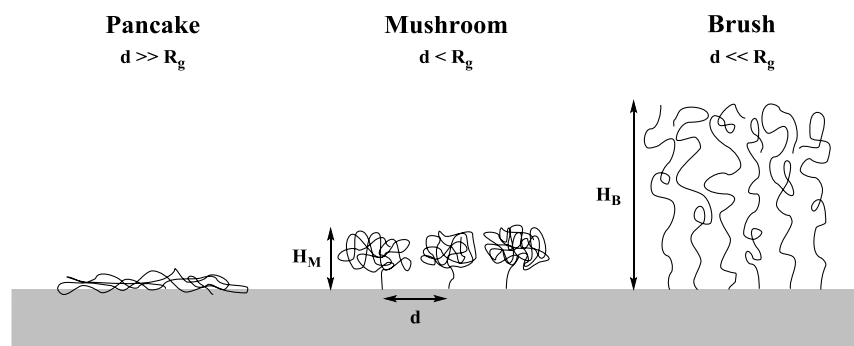
1.2   Polymer-Brush Formation

Figure 1.1: Three different possible conformations (a) pancake, (b) mushroom and (c) brush of surface-attached polymer chains in dependence of the grafting density.

In general, three conformations of surface-bound polymer chains are described in the literature, depending on their grafting density on the surface[9]: pancake for very low, mushroom for medium and polymer brush for very high grafting densities (Figure 1.1). The pancake-like regime is achieved in a bad solvent or in the dry state when the grafting density is very low, so that neighboring chains do not "feel" each other and if the chain segments strongly interact with the underlying surface. If the interaction between the surface and the macromolecule is rather weak or even repulsive, in a good solvent chains form random coils with a "stem"-linker, the so-called mushroom-like conformation. In a third case, when grafting density is very high, repulsive segment-segment interactions between neighboring chains force the chains to stretch away from the surface, forming the so-called polymer brushes.
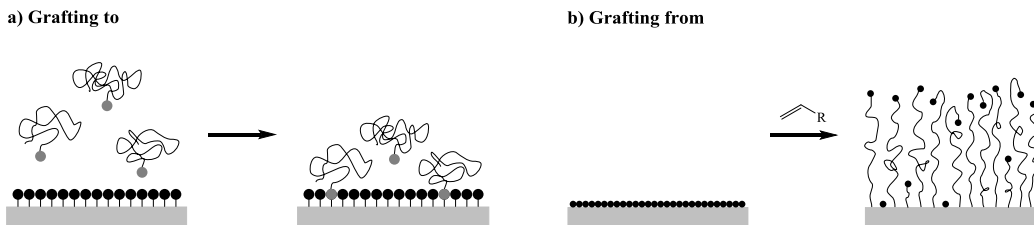
Figure 1.2: Schematic illustration of (a) the low grafting density yielding grafting-to and (b) the grafting-from approach, yielding high grafting density.

Robustly grafted macromolecular chains can be fabricated either *via* the grafting-to or *via* the grafting-from approach (Figure 1.2). In the grafting-to approach, pre-synthesized, well-defined and -characterized polymers are chemically attached *via* functional anchor groups to the surface, leading to a chemically homogenous film, but typically one with mushroom-like structures and very low film thicknesses, due to the relatively low grafting density. Higher grafting densities are kinetically and thermodynamically hindered as additional chains must diffuse against an ever-increasing concentration gradient on the surface, slowing down the immobilization dramatically with increasing coil overlap.[10] Another strict limitation is the choice of polymers to be attached to the surface, as unwanted interactions of functional side groups compete with anchoring groups for the reactive surface, especially for highly functionalized or charged polymers.[11]

In the grafting-from approach – which has first been described by Prücker and Rühe[12] – macromolecules are grown *in situ* from surface-bound initiators *via* surface-initiated

polymerization (SIP). Initiators are thereby either generated or chemically bound in an additional step prior to the polymerization on the surface, allowing – due to the small nature of the initiator – very high grafting densities and therefore leading to more brush-like structures. Chain growth can be started thermally either through a chemical or a photochemical process *via* living or free-radical polymerization (FRP).

a) Atom transfer radical polymerization (ATRP)
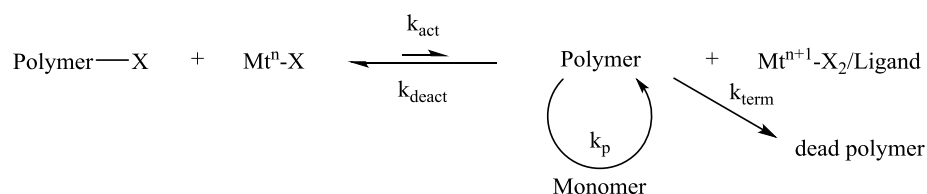
b) Reversible addition fragmentation chain transfer (RAFT) polymerization
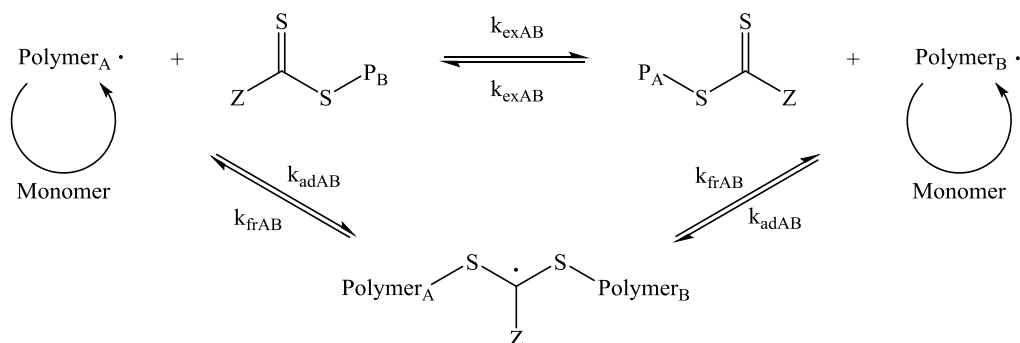
c) Nitroxide-mediated polymerization (NMP)
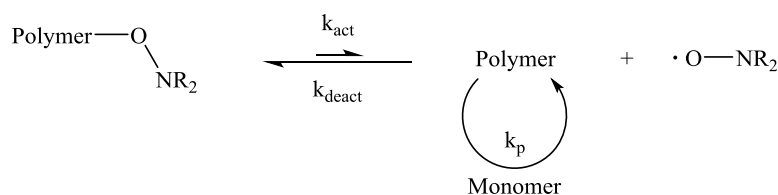
Scheme 1.1: Generalized propagation steps of controlled radical polymerization methods: (a) atom transfer radical polymerization (ATRP), (b) reversible addition fragmentation chain transfer (RAFT) and (c) nitroxide-mediated polymerization (NMP).

Living or controlled radical polymerization (CRP) methods, such as atom-transfer radical polymerization (ATRP), reversible addition-fragmentation chain transfer (RAFT), and nitroxide-mediated polymerization (NMP) benefit from a controlled, linear chain growth, leading to very narrow molecular weight distributions (low polydispersity) under relatively mild reaction

conditions without any side reactions. Scheme 1.1 shows the reaction mechanisms of CRPs which are based on an equilibrium between an active state, a short-living propagation radical, and a so-called dormant state, a long-living chain end which is capped with a labile end-group such as a halogen (ATRP), a chain transfer agent (RAFT) or a stable, free counter-radical (NMP). The equilibrium is predominantly in the dormant state, as the radical recombination back-reaction with the pendant group is much faster than the chain-growth reaction with free monomers, allowing individual chain-growth for only a very short time. In addition, the stability of this dormant state allows stopping and restarting the reaction and consequently the fabrication of more advanced configurations with control over their sequence, such as block-copolymers (BCPs). The drawbacks of CRPs are the extensive preparation and purification steps, the high sensitivity towards air and moisture, very long reaction times, and the limited brush length or weak attachment of the initiator to the surfaces. Furthermore, they are – to some extent – based on expensive metal catalysts, which dramatically limit their applications in *in vivo* experiments, as those catalysts are toxic to biomolecules or cells. These limitations can be overcome by means of FRP methods, as they do not require any expensive or toxic catalysts and lead to much thicker brushes within very short reaction times. The trade off in this approach is the less controlled nature in terms of molecular weight distributions and sequence of the formed brushes.

In general, surface-initiated polymerizations allow the growth of polymer brushes starting from a wide spectrum of monomers on surfaces of different topologies. Such covalently grafted structures open a broad field of applications from microelectronics to biomedicine, as such layers have long-term stability, *i.e.* as they can be exposed to good solvents without being dissolved, displaced or removed from the surface. Although brushes have been predominantly synthesized on gold or silicon substrates, the industrial focus is constantly expanding towards the functionalization of more functional, flexible and cost effective high-performance polymers, such as polyolefins (*e.g.* PE, PP) and fluoropolymers (*e.g.* ETFE, PTFE).

1.3   Structured Polymer Brushes

Patterning of polymer brushes is of particular interest, as it allows the spatial, chemospecific modification of surfaces useful for a wide range of applications from microfluidics to lab-on-a-chip devices for bio-sensing or drug-release processes.[13] The flexibly and swelling potential makes covalently attached brush structures ideal bio-interphases, as they can act as soft

cushions on the surfaces. This feature is of particular significance, since proteins tend to denature on hard, solid surfaces.

Pattern formation can be achieved by means of patterned deposition of initiators, spatially deactivation of initiators, through local addressing, confinement of monomer access or *via* spatially addressed chemical transformation of precursors. In this fashion, patterned polymer brushes have been fabricated *via* additive deposition methodologies such as micro-contact printing (μCP)[14, 15], dip-pen nanolithography (DPN)[16], capillary force lithography[17], scanning-probe lithography[18, 19], or *via* resist-based methodologies such as electron-beam lithography (EBL)[20, 21], photolithography[22, 23] and EUV-interference lithography (EUV-IL)[24, 25].

EUV-IL has further been used as a direct patterning methodology, as it allows the functionalization of flexible polymer foils with polymer brushes of sub-micron resolution. Depending on the mask design, a number of different periodic structures with resolutions down to 100 nm can be produced using a single exposure. The EUV-light is used to crack chemical bonds in the outermost area of the polymeric substrate and to form radicals which serve as initiators for subsequent surface-initiated graft polymerizations. The produced radical density can be varied from one to the next exposure field and with exposure dose, leading to a well-controlled formation of radical patterns in the micrometer to nanometer scale. Upon contact with ambient air, the radicals react to form semi-stable peroxides and hydroperoxides. The process sequence used to generate the structured brushes is shown schematically in Figure 1.3. Upon heating and degassing in a monomer solution, the (hydro-)peroxides are cleaved off to revive the initiator radicals, which start the growth of well-defined polymer brush structures. Typical grafting densities between 0.5 − 1 chains per nm^2, depending on the monomer used, were reported for polymer brushes grafted from ETFE[25].
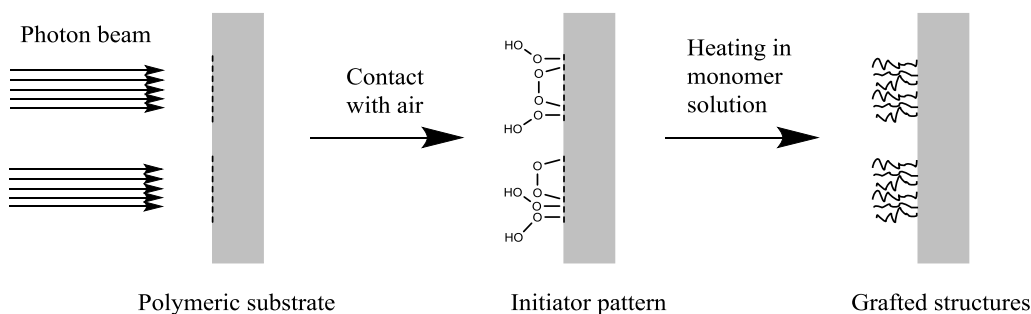

Figure 1.3: Formation of radiation-induced growth of polymer brushes on polymeric substrates.

The limitations of this method are the very sophisticated equipment needed (synchrotron), the need for ultra-high vacuum and the limited size of patterned fields (µm to mm range). But these drawbacks are compensated by the very fast processing of exposures, simultaneous sample preparation and the very simple single-step polymerization processes once the surfaces have been activated. The potential use of polymer-brush structures on flexible polymeric materials is of particular interest for organic electronics and the quest for all-polymeric devices.

1.4   Post-Polymerization Modification of Polymer Brushes

The implementation of a particular functionality onto polymers is strongly dominated by the availability of functional monomers and whether or not functionalized monomers have to be synthesized. The fabrication of functional polymer brushes can be achieved using two fundamentally different approaches: One approach is *via* the coupling of the functional group to a suitable monomer, followed by the graft-polymerization reaction and the second approach is using post-polymerization modification (PPM) for coupling of the functional group to previously grafted brushes.[26]

If the functional group is first conjugated to the monomer, functionalized monomers have to be synthesized in various difficult synthetic steps, including tedious purification, to obtain a well-characterized and pure monomer for the graft reaction. Another drawback of this approach is that the reactivity of the conjugated monomer is drastically influenced by the bulkiness, the chemical nature and reactivity of the coupled moiety so that the grafting reaction conditions have to be optimized for each monomer individually.[27]

In contrast, PPM benefits from its simplicity, as commercially available monomers can be used for the graft-polymerization. Further, functional precursor polymers facilitate the establishment of libraries of functional polymers, without the need to optimize the individual polymerization conditions for varieties of monomers carrying different functional groups. Furthermore, no tedious purification steps are necessary, as unreacted material can simply be washed out from the grafted brushes. However, the main drawback of this method is the limited control over the coupling efficiency which is controlled by the diffusion of the reactant moieties through the polymeric network, as well as the yield of the coupling reaction.[28, 29]

Often, reactions on surfaces proceed with poor efficiency due to slow kinetics and undesired side reactions, caused by the heterogeneity of the system. In contrast, efficient and

chemospecific transformations,[28, 30, 31] collectively grouped as "click" reactions,[32-38] have drawn tremendous attention in recent decades. Some coupling reactions that are known to react in very high to quantitative yields are listed in Scheme 1.2.
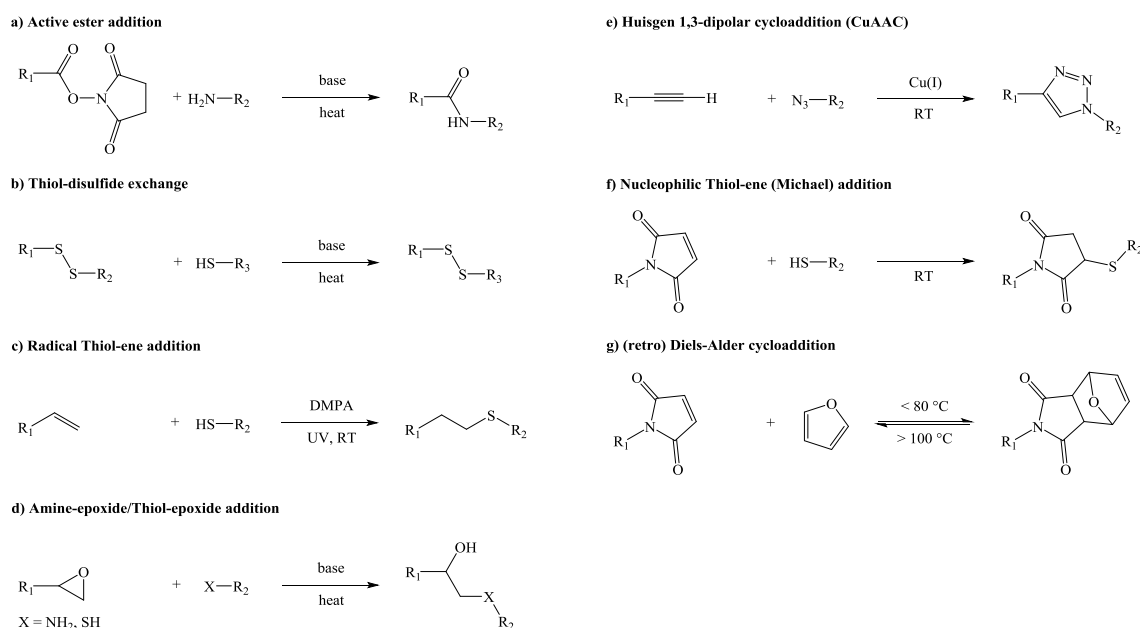
Scheme 1.2: Different classes of reactions that can be used for the preparation of functional polymers by means of post-polymerization modification (PPM).

The most frequently used PPM is probably the conjugation of amines to active esters such as *N*-hydroxysuccinimide (NHS) (Scheme 1.2a). The drawbacks of this approach include the limited solubility of NHS-containing polymers, except in DMSO or DMF, as well as side reactions such as succinimide ring-opening and the formations of *N*-substituted glutarimides, which necessitates the presence of a proton acceptor such as triethylamine (TEA)[39]. Alternatively, pentafluorophenyl (PFP) esters offer higher reactivity, better hydrolytic stability and allow conjugation in a broad range of solvents[40].

A biologically important PPM is the reversible Thiol-disulfide exchange (Scheme 1.2b), which takes place in the modulation of enzymes[41], viral entry[42], and protein folding[43]. This equilibrium reaction is strongly pH dependent[44] and reversible *via* reduction or other thiols present[45] in the reaction solution.

In the radical thiol-ene reaction, thiols are added to C=C bonds to form the anti-Markovnikov product (Scheme 1.2c). This reaction can be mediated either *via* a radical or a UV-

light source[46]. Potential side reactions are intramolecular cyclization[47] of any vinylic groups in proximity, which leads to a need for low temperatures and high concentrations of thiols.

As a result of their ring-strain, epoxides are highly reactive groups and react with nucleophiles such as amines and thiols in the presence of a base (Scheme 1.2d). Epoxides have frequently been used for PPM as they are stable towards radical polymerization conditions[48]. The main drawback of the amine-epoxy reaction is the potential crosslinking of primary amines, as the formed secondary amines can further react with non-reacted neighboring epoxides[49]. This side-reaction can be circumvented by the use of thiols in the Thiol-epoxy[50] reaction.

The probably most recognized "click" reaction is the copper-catalyzed Huisgen 1,3-dipolar cycloaddition between azides and alkynes (CuAAC) (Scheme 1.2e) as it reacts with quantitative yields in aqueous, as well as organic solvents[51, 52]. Matyjaszewski[53] demonstrated the growth of azide-containing poly(3-azidopropyl methacrylate) (PAzPMA) *via* ATRP, while the counter approach to form poly(propargyl methacrylate) (PPMA) did not show any controlled growth due to side reactions. Although the CuAAC reaction offers a powerful tool for well-controlled PPM, a major drawback is the use of Cu(I) as catalyst, as it forms complexes with the formed triazole ring[54] and as it limits the biocompatibility, due to its toxicity to cells[55-59]. As a consequence of this, "click" reactions that avoid the use of metal catalysts – such as the strain-promoted alkyne-azide cycloaddition – have experienced a major increase in their utilization.[60-65]

Another coupling reaction that is often referred to as "click" chemistry is the nucleophilic thiol-ene reaction (Scheme 1.2f).[65-69] Due to its usually fast reaction kinetics, this Michael-type hydrothiolation of a C=C bond is a very robust technique, leading to high or quantitative yields, with little or no byproduct, under ambient, non-stringent reaction conditions.[70, 71]

Maleimides are versatile functional groups for thiol-ene reactions, as they show fast kinetics because of their two electron-withdrawing carbonyl groups in a cis-configuration, combined with bond-angle relaxation and release of strain in the ring upon thiol-addition.[72-74] Since the maleimide group contains a polymerizable double bond, maleimide monomers require efficient protection during polymerization, as well as efficient deprotection after the polymerization.[75-77]

The ability to reversibly deactivate/activate maleimides by means of Diels-Alder (DA) and retro Diels-Alder (rDA) reactions, respectively, is based on their high reactivity as dienophiles with a variety of dienes (Scheme 1.2g).[38, 78] The rDA reaction usually takes place at higher temperature compared to the forward reactions and can be used to form thermo-

responsive polymer structures[79]. Notably, the simple DA/rDA reactions require no additional reagents and generate no byproducts,[80, 81] thus making them attractive for obtaining masked polymers and re-activating dormant polymers into "clickable" form.

Maleimide-furan adducts have been applied for the generation of reversible covalent assemblies,[82-84] self-healing polymers,[85, 86] thermally responsive dendrons,[87] segmented block dendrimers,[88] and polymers with a tunable crosslinking density.[89, 90]

Such efficient PPM reactions may be used to introduce new types of moieties into the repeat units of grafted brush structures. Modification of grafted brushes takes place from the top and may cause diffusion limitations according to very high grafting densities and an increasing amount of bound moieties. Of particular interest is the copolymerization of different functional monomers, as they can help to overcome these limitations and allow for orthogonal functionalization *via* chemospecific and quantitative modification of different repeat units under characteristic reaction conditions, to create multifunctional or smart surfaces.

1.5   Responsive Polymer Brushes

Responsive surfaces are of great interest due to their stimulus-induced switching of properties on demand. Switching originates from responsiveness to a certain trigger such as temperature[91], pH[92], redox potential[93], mechanical stress[94], ionic strength[95], solvents[96], an external electric field[97] or light[98]. The adjustment of temperature and pH conditions are very simple, environmentally benign, low-energy methods[99] which makes them probably the most commonly used stimuli in material science.

Thermo-responsive polymers exhibit a phase transition when taken through their lower critical solution temperature (LCST), causing a change from a swollen, hydrophilic amorphous-like state to a collapsed, hydrophobic configuration, resulting in a change in solubility and hydration of the polymer chains. The most prominent example of such temperature-sensitive polymers is poly(*N*-isopropyl acrylamide) (PNIPAAM), which undergoes a phase transition at 32 °C, *i.e.* close to human body temperature.[100, 101] Applications for thermo-responsive polymer brushes are mainly in field of bio-interfaces and range from tissue and cell growth surfaces[102-104], through separation processes[105, 106] and microfluidic devices[107], to drug delivery[108].

Typical pH-responsive polymers are weak polyelectrolytes, *i.e.* polymerized weak acids such as poly(acrylic acid) (PAA)[99], poly(methacrylic acid) (PMAA)[109] or bases such as poly(*N,N*-dimethylaminoethylmethacrylate) (PDMAEMA)[110] or poly(4-vinylpyridine) (P4VP)[111]. They undergo conformational transitions depending on the pH conditions. The response of poly-acids towards pH occurs *via* deprotonation above their particular pKa values, which induces a swelling of the charged polymer and accordingly after protonation below their pKa values induces a collapse of the non-charged polymer.[112] pH-responsive materials have predominantly been used for the surface modification of membranes for chemical separation processes such as for oil/water mixtures[113], for proteins[114] and metal ions[115], as well as in biotechnological applications such as biosensors[116], drug-delivery systems[117] or non-fouling surfaces[118].

Reports on light-responsiveness on surfaces are not as frequent as for responsiveness towards temperature or pH, probably due to the lack of commercially available photo-responsive monomers. Nevertheless, among the stimuli that could be applied, the use of light is most attractive[119], since light is a remote trigger, which means that closed systems can be actuated and no chemical contamination is introduced. Photons can be specifically directed to a surface and delivered with high spatial and temporal precision over long distances. It enables remote-controlled influence on material properties such as wettability, swelling properties and interactions with ions and biomolecules. To impart the property of photo-responsiveness to such surfaces, photochromic organic moieties have to be either incorporated in or attached to the surface. These moieties then undergo a light-induced, most often reversible conformational change, which also causes a change in physical properties such as dipole moment, dielectric constant, refractive index, oxidation-reduction potential or color.

The principal switches explored to date have included gated photochromism (diarylethenes[120], dithienylethenes[121]), pericyclic reactions (fulgides[122], fulgimides[123]), cis/trans-isomerization (stilbenes[124], azobenzenes[125]) and heterolytic cleavage/ring-opening reactions (spiropyrans[101], spirooxazines[126], chromenes[127]) (Scheme 1.3).

Among these photochromic groups, spiropyrans (SPs) are known to show the largest response in dipole moment[128] due to zwitterion formation. Therefore, incorporated into grafted polymer brushes, they show the largest switch in wettability, as well as in swelling behavior, in the presence of an appropriate, polar solvent. SPs consist of a heterocycle and a chromene moiety, which are orthogonally linked through a spiro-carbon atom. The photochromism of SPs has been studied intensively since the first publication by Hirshberg[129] in the 1950s and is based

on the reversible transformation[130-132] of the ring-closed colorless SP and the zwitterionic, deeply colored merocyanine (MC) (Scheme 1.3d). The heterolytic cleavage of the sp^3 carbon-oxygen bond in the pyran ring is caused by UV-light and can be reversed back to the thermodynamically stable form upon heating or irradiation with visible light.

a) Gated Photochromism: Diarylethenes
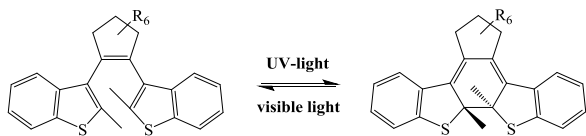
c) Cis/Trans-Isomerization: Azobenzenes
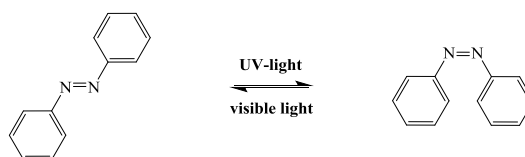
b) Pericyclic Reactions: Fulgides
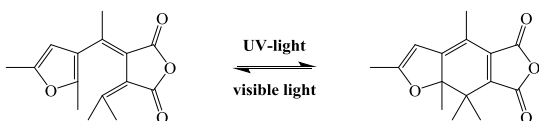
d) Heterolytic Cleavage Reactions: Spiropyran
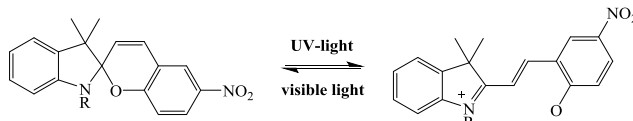
Scheme 1.3: Photochromic molecular switches (a) gated photochromism, (b) pericyclic reactions, (c) cis/trans-isomerization and (d) heterolytic cleavage reactions upon reversible exposure to visible and UV-light.

Studies of photochromic monolayer systems have shown changes in surface free energy upon photoisomerization. This effect was used to control the movement of liquid droplets with light[133], for example. In a comprehensive review on nanoparticles functionalized with molecular switches, the importance of a flexible attachment of the switching molecules for their functionality was emphasized. Flexibility was achieved by introducing spacers or attaching the photoactive species to polymer brushes[134]. Photochromic brushes have been grafted from oxide surfaces by surface-initiated ring-opening metathesis polymerization (SI-ROMP)[135] and atom transfer radical polymerization (ATRP) on silica surfaces and colloids[136, 137].

Photochromic surfaces open a wide field of applications, such as photonic devices[138], photosensitive glasses and lenses[139], optical memories and switches[140-142], microfluidic devices[143], switchable biomaterials[144, 145], controllable drug delivery[146-149], diffusion and ion transport through channels or membranes[150-152], as well as variable wettability or self-cleaning surfaces[153].

1.6   Smart Bio-conjugated Surfaces

Responsive bio-conjugated materials have gained increasing attention in recent years as they open a broad field of applications in lab-on-a-chip systems for the detection of physical variables (temperature, pH and light), as biosensors (analytes, biomolecules and cells), delivery systems (drugs, proteins, enzyme and genes), in medical diagnostics and imaging, as well as for regenerative medicine (therapy, tissue engineering and injectable implants) and in biotechnology (bioseparators and biofuel cells).[154-167]

Various methods have been applied for the immobilization of biomolecules including physical adsorption on solid supports, entrapment in hydrogels, channels or capsules and covalent attachment to modified surfaces.[168-171] Bio-conjugation of enzymes is very attractive as enzymes show high substrate specificity and can operate as recognition elements for individual targets under biologically relevant conditions. However, to retain a high level of enzymatic activity, immobilization should employ mild chemical modifications, allow large quantities to be irreversibly immobilized, and provide a relatively large surface area for enzyme-substrate interactions.[172]

Adsorption on flat rigid surfaces is limited in terms of providing a mechanically stable system and can lead to deformation and therefore deactivation of enzymes, while chemical bond formation *via* flexible linkers has not shown any significant decrease in activity, compared to the free biomolecules.[173, 174] Thus, solid supports have to be covered with soft layers of, for example, self-assembled monolayers (SAMs) or polymer brushes as spacers.[157, 175-177] As pointed out in Chapter 1.1, compared to SAMs, polymer brushes are more mechanically and chemically stable and lead to a higher density of functional groups and as a consequence allow more biomolecules to be immobilized per unit area.[7] Hence, varying the brush thickness of enzyme-conjugated systems allows the number of catalytic centers[178] to be tuned, and the output of signals *i.e.* for UV/vis or fluorescence spectroscopy to be controlled.

Enzymes and proteins have been bound to polymer brushes on flat gold or silicon surfaces *via* a number of functional groups including epoxides, carboxylic acids, hydroxyls, aldehydes, maleimides, thiols and amines.[7, 90, 179] Epoxy groups are well suited for bioconjugation as they react irreversibly and site-specifically *via* ring-opening reactions with nucleophilic amine or thiol groups, which are abundant in biomolecules.[180-183]

Combining bio-conjugated systems with stimulus responsiveness is very desirable, as it allows for a better control over localization, release of payload and rapid imaging of pathological events by modulating of the properties of the environment in the near vicinity. First pH-responsive protein brushes[184], DNA brushes[185], as well as polymer-enzyme conjugates to control electrochemical properties of electrodes[186-191] and thermo-responsive polymeric systems to control the release of fouling[192], hemoglobin[193] and cells[194-197] have been described.

Despite the benefits of light as an external trigger (Chapter 1.5), reports on light-controlled bioactivity are surprisingly very rare. Random incorporation of typically photochromic azobenzenes into enzymes was used for photo-controlled bio-catalysis by reversible deformation of active centers caused by the cis/trans transformation of the molecular photo-switches upon light exposure[198-201] and for optobioelectronics by means of photochromic spiropyran (SP)-containing SAMs on Au electrodes that allow or restrict electron transfer between the electrodes and enzymes[144, 202, 203]. Photo-responsiveness has been used to tailor cell adhesion[204] and indirectly to trigger protein capture in thermo-responsive polymer brushes *via* light-to-heat-transfer[205]. Poloni *et al.*[206] reported photo-controlled deactivation of lipase immobilized on an azobenzene-containing SAM-modified quartz surface. The drawback of these approaches is the direct connection of the photo-switches to the enzymes, which, in most cases, causes an irreversible deformation and therefore deactivation of the enzyme.

The aim of this project was to combine the listed advantageous methods by grafting of homo- and copolymer brushes from polymeric substrates, carrying functional groups – such as epoxides, activated acids or maleimides – which allow PPM with *e.g.* photochromic SP. We were taking advantage of different activation methods to graft large areas *via* argon plasma and micro- and nanopatterned brushes by means of EUV-IL. Chemospecific PPM of particular repeat units allowed the introduction of certain functionalities to the brushes without the need of tedious synthesis and purification steps and optimization of single grafting procedures. Copolymerization of different functional monomers gave access for orthogonal PPM of grafted macromolecules, allowing the creation of multifunctional photochromic bio-conjugated copolymer brushes on polymeric substrates and the fabrication of smart surfaces.

2.   Methods and Experimental Procedures

2.1   Materials

Substrates: Extruded, 100-µm-thick ETFE foils (Nowoflon, ET-6235 Nowofol GmbH, Siegsdorf, Germany) and PTFE foils (Angst + Pfister AG, Zurich, Switzerland) were placed between two 4" silicon wafers and hot pressed for 5 to 20 minutes at 220 °C with an applied pressure of 4 MPa, in order to obtain flat surfaces. Similarly, 120-µm-thick PP foils (Kolma 59 464, Kolma AG, Wabern, Switzerland) were hot pressed for 20 minutes at 140 °C with an applied pressure of 4 MPa. 30-µm-thick microporous polypropylene (PP) membranes (Treo-Pore®-PDA 30, Treofan Germany GmbH & Co. KG, Raunheim, Germany) with a porosity of > 60 % were used as received. All samples were rinsed with ethanol prior to use.

Chemicals: Chemicals were purchased from Sigma-Aldrich (Buchs, Switzerland), VWR (Zurich, Switzerland) or FLUKA (Buchs, Switzerland) and were used as received. Water for rinsing or as a solvent was of Millipore® quality (Quantum® Ex / Q-Gard® 2, Merck Millipore, Zug, Switzerland). The spiropyran amine has been synthesized *via* a procedure similar to that described in the literature[207, 208] with minor changes to enhance the overall yield (Chapter 3.5.1).

Monomers: The monomers glycidyl methacrylate (GMA), methyl methacrylate (MMA), ethylene glycol methyl ether methacrylate (EGMA) and poly(ethylene glycol) methyl ether methacrylate (PEGMA, molecular weight 300 Da), were passed through an alumina column before use. Methacrylic acid (MAA) was purified *via* distillation. The furan-protected monomer (FuMaMA), was received from the group of Professor Sanyal (Boğaziçi University, Turkey), synthesized according to a procedure described in the literature.[209]

TMB solution: The 3,3',5,5'-tetramethylbenzidine (TMB) analyte solution was a mixture of two solutions: Solution A, in which TMB (0.4 mM) was dissolved in an acetone/methanol (1/9) mixture, and solution B, which was an aqueous solution of citric acid monohydrate (0.1 M), potassium hydroxide (KOH, 0.1 M) and hydrogen peroxide (H_2O_2, 2 mM). The mixture of 150 µL of solution A in 3 mL solution B was freshly prepared, stirred vigorously for 1 min prior to each experiment.

2.2   Experimental Procedures

2.2.1   Extreme-Ultraviolet Interference Lithography

ETFE, PTFE and PP samples were exposed to extreme ultraviolet (EUV) light at the EUV interference lithography (EUV-IL) beamline at the Swiss Light Source (SLS). EUV-IL combines high resolution capabilities with high throughput, according to step-and-repeat exposures and very high flux available at the synchrotron source. In contrast to "writing" with e-beam exposures, EUV-IL can be used to pattern entire areas in a single exposure without moving the sample. Exposures were performed in vacuum (< 5 x 10^{-6} mbar). The beamline uses undulator light (42 poles, 212 mm period) with a central wavelength of 13.5 nm (92.5 eV photon energy) and ~ 3 % spectral bandwidth. Coherence is hereby achieved *spatially* due to the small size and divergence of the electron beam in the storage ring and *temporally* due to the spectral bandwidth ($\Delta\lambda/\lambda$) of the undulator. The incident EUV power on the sample was 0.5 - 42 mW cm^{-2}, and the delivered dose was controlled using a fast beam shutter.

Patterned structures are usually created by irradiation through partially transparent silicon nitride (Si_3N_4) membranes with linear chromium gratings of different periods on a single chip. Coherent beams diffract along the gratings and interfere at a certain distance along the beam direction. These interfering beams are used to create periodic patterns such as lines, dots, rings, crosses or more complex geometries – depending on the number of interfering beams. EUV-IL patterns are usually created into positive-tone resist, such as poly(methyl methacrylate) (PMMA) or negative-tone resist materials, such as hydrogen silsesquioxane (HSQ), where the irradiation leads to either chain scission or crosslinking, respectively. In our case, 2, 4 and 6 interfering beams were used to create patterns of radicals in the topmost layer of polymeric surfaces (attenuation length in ETFE $\sim$ 72 nm), which were used as initiators for subsequent surface-initiated graft polymerizations. Alternatively, masks with a window of 3 mm x 3 mm were used to produce large-area exposures to analyze macroscopic properties. The bond-breaking process is expected to be very efficient, as the photon energy is by more than an order of magnitude higher than typical bond energies in polyolefins and fluorinated polymers. The resolution of the nanostructures is limited by the length and polydispersity of the formed polymer chains *via* free-radical polymerization and not by the exposure process. In order to improve the pattern resolution, controlled radical polymerization methods, *i.e.* reversible addition fragmentation chain

transfer (RAFT) has been employed to achieve line arrays with a periodicity down to 100 nm[210].
The irradiated samples were stored in a deep freezer at -80 °C.

2.2.2   Low-Pressure Argon Plasma Activation

Flat-pressed ETFE, PTFE or PP samples were cut into 1.2 cm × 1.2 cm pieces. After
thorough rinsing with isopropanol and acetone, the pieces were dried in a stream of nitrogen and
attached to glass microscope slides with KAPTON® poly(imide) adhesive foil (Nitto P-221
AMB, Permapack AG, Rorschach, Switzerland). This foil was also used to cover part of the
sample, in order to shield it from the plasma. The samples were then activated with vacuum
argon plasma (Femto, Diener Electronics, Jettingen, Germany) operated with 40 KHz/30 W for
between 30 seconds and 10 minutes. Plasma-treated samples were allowed to stand in air for
10 minutes and were then rinsed with isopropanol and blown dry with nitrogen prior to grafting.

2.2.3   Grafting and Modification

PGMA: Activated samples were reacted in a solution of glycidyl methacrylate (20 %-vol)
and poly(ethylene glycol) (20 %-vol) in dioxane for 1 h at 60 °C. The grafted samples were
rinsed with dioxane and immersed in each isopropanol and DCM and treated in an ultrasonic bath
for 15 min. *PGMA-SP:* Post-polymerization modification was carried out in a solution of 42.3 mg
spiropyran amine (0.1 mmol) and 11.2 mg 1,4-diazabicyclo[2.2.2]octane (DABCO, 0.1 mmol) in
3 mL dioxane for 18 h at 60 °C.

PMAA: Activated samples were reacted in a solution of methacrylic acid (20 %-vol) in
3 mL 0.1 M HCl for 2 h at 70 °C. The grafted samples were rinsed in H_2O and immersed each in
H_2O and acetone in an ultrasonic bath for 15 min. *PTFAMA:* In the first post-polymerization step
the PMAA brush samples reacted in a solution of 98 µL triethylamine (0.7 mmol) and 122 µL
perfluorophenyl trifluoroacetate (0.7 mmol) in 3 mL THF for 18 h at RT. *PMA-SP:* In the second
modification step the trifluoroacetic methacrylic anhydride brush samples reacted in a solution of
42.3 mg spiropyran amine (0.1 mmol) in 3 mL THF for 18 h at RT.

P((EG)$_x$MA-co-FuMaMA): Activated samples were placed in a monomer solution
(3 mmol) of the furan-protected maleimide methacrylate and ethylene glycol monomethyl ether
methacrylate in 3 mL dioxane containing 20 %-vol poly(ethylene glycol), degassed with nitrogen

and heated for 2 h to 70 °C. Copolymerization with methyl methacrylate, or with poly(ethylene glycol) monomethyl ether methacrylate was carried out analogously. The mole fraction of the different monomers in the solution was varied, but the total monomer concentration was kept constant. *P((EG)$_x$MA-co-MaMA):* The deprotection of the maleimide moieties was carried out by heating the substrates under vacuum for 1 h at 110 °C. *P((EG)$_x$MA-co-MaMA-SR):* The Michael additions of the different thiols (0.1 mmol) were carried out in *N,N*-dimethylformamide (DMF, 3 mL) at ambient temperatures overnight.

P(GMA-co-FuMaMA): Grafting of copolymer brushes was carried out on activated samples placed in a monomer solution (3 mmol) of the furan-protected maleimide methacrylate and glycidyl methacrylate in 3 mL dioxane containing 20 %-vol poly(ethylene glycol). Solutions were degassed with nitrogen and heated for 1 h to 70 °C. The mole fraction of the monomers in the solution was varied, but the total monomer concentration was kept constant. *P(GMA-co-MaMA):* The deprotection of the maleimide moieties was carried out by heating the substrates under vacuum for 30 minutes at 110 °C. *P(GMA-MP-11-co-MaMA):* Covalent attachment of microperoxidase-11 (MP-11) was carried out on activated P(GMA-*co*-MaMA) samples in a solution of MP-11 (0.1 mmol) and DABCO (0.1 mmol) in 3 mL *N,N*-dimethylformamide (DMF) at 60 °C for 1 h. *P(GMA-MP-11-co-MaMA-SP):* The Michael additions of the spiropyran thiol (SP-SH) was carried out in a subsequent step, in a solution of SP-SH (0.1 mmol) in 3 mL DMF at ambient temperatures for 1 h.

2.3   Analytical Techniques

2.3.1   Attenuated Total Reflectance – Infrared (ATR–IR) Spectroscopy

Spectra were recorded on a Hyperion 3000 IR microscope (Bruker, Fällanden, Switzerland) using an ATR-IR objective with an anvil-shaped germanium crystal with about 8000 μm^2 contact area (Bruker, Fällanden, Switzerland). The ATR crystal contacted the surface with a preset and constant pressure. A Globar source and a KBr beamsplitter were used. Light was collected using dedicated optics and sent to a liquid-nitrogen-cooled mercury cadmium telluride (MCT) 250 μm x 250 μm detector (Infrared Associates, Stuart, FL, USA). The detector is sensitive between 500 and 10,000 cm^{-1}. Reference spectra were recorded just prior to the actual measurement. Measurements have been carried out on micro-structured (Ø = 100 μm) areas of

high radical density. OPUS spectroscopy software (version 6.5, Bruker, Fällanden, Switzerland) was used for data processing.

2.3.2   Ultraviolet-visible (UV/vis) Spectroscopy

UV/vis transmission spectra were acquired in a range from 200-800 nm in a single-channel mode for solid polymeric substrates and in a two-channel mode for solutions under continuous stirring on a UV/VIS/NIR spectrometer (Lambda19, PerkinElmer, Schwerzenbach, Switzerland) equipped with a deuterium lamp and a halogen light source.

Chapter 6: Measurements in solution (1.5 mL) were carried out with TMB analyte solution as both, reference and detection solution. The mixture was freshly prepared prior to each experiment. To avoid a naturally blue color appearing after some time also in enzyme-free solutions, reaction times were limited to one hour each. Measurements were carried out in the presence of grafted ETFE samples with a size of 18 mm^2, which were either exposed to visible or UV-light prior to the experiment or *in situ*.

2.3.3   Nuclear Magnetic Resonance (NMR) Spectrometry

^{1}H-NMR spectra were recorded on a Bruker 300 MHz spectrometer using deuterated chloroform ($CDCl_3$) or dimethyl sulfoxide (d^6-DMSO) as a solvent and tetramethylsilane (TMS) as the reference.

2.3.4   Atomic Force Microscopy (AFM)

Chapter 3: Measurements were performed in TappingMode^{TM} in air on a Dimension IIIa instrument (Veeco, Mannheim, Germany). Silicon nitride (Si_3N_4) cantilevers with a tip radius of 20 nm, a spring constant of 40 N m^{-1} and a resonance frequency of 325 kHz (NSC15/AlBS, Mikromasch, San Jose, CA, USA) were used for obtaining images in both height and amplitude mode. Images were processed with second-order flattening procedures (Nanoscope software, Veeco, Mannheim, Germany).

Chapter 4: AFM scans in height mode were acquired *via* TappingMode[TM] in air on a Dimension Icon instrument (Bruker, Karlsruhe, Germany) using proprietary Si_3N_4 cantilevers with a tip radius of 7 nm, a spring constant of 26 N m^{-1} and a resonance frequency of 300 kHz.

Chapter 5: AFM scans in height and peak force mode were acquired ScanAssistMode[TM] in air on a Dimension Icon instrument (Bruker, Karlsruhe, Germany). ScanAsistAir[TM] Si_3N_4 cantilevers with a tip radius of 12 nm, a spring constant of 0.4 N m^{-1} and a resonance frequency of 70 kHz (Bruker, Karlsruhe, Germany). First-order flattening procedures (NanoScope Analysis 1.5 software, Bruker, Karlsruhe, Germany) were applied to all measured data.

2.3.5   Water-Contact-Angle (CA) Determination

Chapter 3+5: Water drops of 3 μL volume were placed on the sample with an automated G23 E Mk2 syringe system (Krüss GmbH, Hamburg, Germany) and images were recorded with a G2 & DO3426 contact-angle-measuring system (Krüss GmbH, Hamburg, Germany). Contact-angle (CA) evaluation was performed with DSA 2 software (version 2.5, Krüss GmbH, Hamburg, Germany). The error in contact-angle determination is estimated to be ± 2 °.

Chapter 4+6: A DataPhysics OCA 25 contact-angle-measuring system (DataPhysics GmbH, Filderstadt, Germany) was used for determination of static contact angles of 3 μL water droplets.

2.3.6   Fluorescence Microscopy and Image Evaluation

Fluorescence images were recorded with an Olympus IX81 fluorescence microscope (Olympus Deutschland GmbH, Hamburg, Germany) equipped with an OBS MegaView camera (Olympus Deutschland GmbH, Hamburg, Germany). The temperature within the fluorescence microscope was kept constant at 37 °C. Only images recorded during the same session with identical settings were compared. Fluorescence evaluation was performed with cell[R] software (version 2.2, Olympus Deutschland GmbH, Hamburg, Germany).

2.3.7   Flux Measurements

Membrane samples were placed between two PE frits (20 µm, Carl Roth GmbH+Co. KG, Karlsruhe, Germany) in a 6 mL SPE column (PP, Carl Roth GmbH+Co. KG, Karlsruhe, Germany). The column end was connected to a vacuum pump (SC920, KNF Lab, KNF Neuberger GmbH, Freiburg, Germany) to produce a minor under-pressure of $\Delta p = 250$ mbar. Samples were placed in the relevant aqueous solutions for 1 hour prior to measurements. For pH-responsive measurements, the flux was determined by the time for 5 mL of water, HCl (0.1 M) or NaOH (0.1 M) to pass through the membrane. For light-responsive measurements, samples were exposed for 30 seconds to UV-light prior to use.

3.   Light-Responsive Polymer Surfaces *via* Post-Polymerization Modification of Grafted Polymer-Brush Structures[1]

3.1   Abstract

Light-induced reversible switching of surface properties in well-defined areas enables the creation of remote-controlled smart surfaces. In this work, we took advantage of the unique high resolution structuring capabilities of extreme ultraviolet (EUV) interference lithography to produce nanostructured photoresponsive polymer brushes. Patterns of poly(glycidyl methacrylate) (PGMA) and poly(methacrylic acid) (PMAA) were grafted from two different 100-µm-thick fluoropolymer substrates using a radiation-initiated grafting-from approach based on free-radical polymerization. Photochromic properties were introduced *via* novel one- or two-step post-polymerization modifications with spiropyran (SP) derivatives, which allowed us to control the number of photochromic groups on the polymer brushes. Depending on the degree of functionalization and the local chemical environment, the SP moieties can open upon UV-light exposure to form zwitterionic, deeply colored and fluorescent merocyanines (MCs) and close back to the colorless SP configuration *via* thermal or visible light-induced relaxation. Switching kinetics were studied using time-resolved fluorescence microscopy and compared with kinetic measurements of the SP moiety in solution. The results indicated the importance of the local chemical environment provided by both, the polymer brush and added solvents, on the intensity of the switching and showed the predominant influence of polar solvents, which stabilize the MC form, on the ring-closing kinetics. To allow further characterization of the polymer brush arrangements on a macroscopic scale, similar, but unstructured brush systems were grafted from fluoropolymers after large-area activation using EUV radiation or argon plasma. In particular, all the steps of the post-polymerization modification were characterized in detail using attenuated total reflection infrared (ATR-IR) spectroscopy. Furthermore, a light-induced reversible switch in static contact angle of up to 15° for PGMA-SP brushes and up to 30° for PMA-SP brushes, upon alternating UV- and visible light irradiation was demonstrated.

3.2   Introduction

High-performance polymers, such as poly(tetrafluoroethylene) (PTFE) and poly-(ethylene-*alt*-tetrafluoroethylene) (ETFE) have advantageous bulk properties, useful in a multitude of applications such as electrical insulation of cables and wiring[211], filters and linings for chemical industry[212], convection barriers for solar cells[213, 214], as well as non-sticking and self-cleaning surfaces[215]. Their high stability and chemical inertness also dominate their surface properties, often leading to limitations in specific applications where chemical functionalization would be advantageous.

Light-responsiveness can be imparted to such surfaces by means of attachment of robust, flexible photochromic polymer brushes (Chapter 1.1). To avoid tedious synthetic procedures and purification steps, post-polymerization modification (PPM) offers a simple and elegant alternative approach (Chapter 1.4), allowing the grafting of relatively cheap commercially available monomers. Theato *et al.*[216] used PPM to create spiropyran (SP)-containing polymer brushes that were grafted *via* reversible addition-fragmentation chain transfer (RAFT) polymerization from silica surfaces. Despite the benefits of controlled radical polymerization (CRP) drawbacks are their extensive preparation and purification steps, long reaction times, and, to some extent, the limited brush length or weak attachment of the initiator to the surfaces (Chapter 1.2).

Polymer micro- and nanografting by free-radical polymerization (FRP)[24, 25, 217] is a technology based on extreme ultraviolet (EUV) interference exposures available at the XIL-beamline of the Swiss Light Source (SLS), to grow well-defined patterns of polymer brushes on polymeric substrates such as polyolefins (*e.g.* PE, PP) and fluoropolymers (*e.g.* ETFE, PTFE). The control of this process is achieved *via* an interference lithography setup that allows the creation of well-defined patterns of radicals on the micrometer-to-nanometer scale. These serve as initiators for the polymerization process. Unlike CRP, no additional adsorbed initiators need to be pre-attached to the surface. Reaction times range from 1 to 2 hours, yielding periodic brush structures whose dry thickness exceeds that produced by CRP methods by more than one order of magnitude.

We demonstrate a universal, metal-free approach to the fabrication of covalently attached photochromic polymer brushes on polymer surfaces. New PPM strategies are shown, including a

modification of grafted poly(glycidyl methacrylate) (PGMA) and poly(trifluoroacetic methacrylic anhydride) (PTFAMA), derived from grafted poly(methacrylic acid) (PMAA).

3.3   Results and Discussion

3.3.1   Grafting of Micro- and Nanostructures

The EUV lithography setup for the creation of nano-patterned polymer brushes is shown in Figure 3.1. The photon energy of the undulator light is 92.5 eV ($\lambda = 13.5$ nm), which is well suited for cracking chemical bonds and therefore creating radicals on polymer surfaces. Patterns on the surface of ETFE and PTFE foils are generated by interference of beams diffracted at grating structures. Using these radicals as initiators, micro- and nanostructured polymer brushes are covalently grafted from substrate polymer surfaces. Exposures through a typical mask with diffraction gratings lead to line arrays with a period from 1 µm down to 100 nm for two interfering beams and to dot arrays with a period from 1.4 µm down to 140 nm, respectively. The size of the patterned fields for small-period patterns is in the range of 200 µm^2.

Our aim was to increase the contrast of these nano-patterned brushes applying a newly established interference mask that combines six diffracted beams in one hexagonal interference pattern[218]. AFM images of nano-patterned brush areas defined by 6-interfering EUV-beams are given in Figure 3.2. With the applied FRP technique, hexagonally patterned PGMA and PMAA brush structures were obtained. Six dots with a width of 700 nm are placed around a cavity of 150 nm in diameter. A cross-section of the AFM image indicates a very homogenous distribution of the brush structures over the entire patterned array. The profile of the grafted interference structures will help us in the future to analyze the photoresponsive behavior of the brushes by looking at the swelling behavior of the dots, as well as the dot-to-cavity ratio in the dry state and particularly in solvents of different polarity.

For grafted PGMA and PMAA, the dry brush thickness was found to increase roughly with the square root of dose (Figure A 3.1). The FRP conditions used allow us to create polymer structures that exceed 1.7 µm in height for GMA and 800 nm for MAA brushes. The drastic differences in height for the two monomers can be explained by the polymerization kinetics, which lead to a 2–3 times faster grafting process for PGMA. The thickness of the polymer brushes in the nanostructured areas (Figure 3.2) can be up to an order of magnitude smaller than

in the areas of high radical density – a consequence of the much lower dose in regions patterned by interfering diffracted beams.
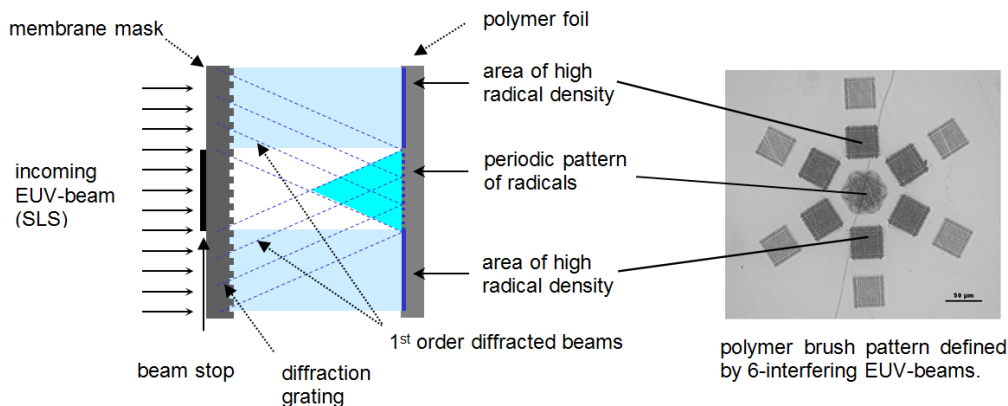
Figure 3.1: EUV 6-beam interference lithography setup for creation of nanopatterned polymer brushes, as performed at SLS. The beamline uses undulator light of 92.5 eV photon energy ($\lambda = 13.5$ nm), which is well suited to creating radicals on polymers.

Figure 3.2: AFM images (a, b) and cross-section (c) of a PGMA nanostructure. The structure was defined by 6-interfering EUV-beams. Structure dimensions: width = 700 nm, height = 150 nm.

3.3.2   Post-Polymerization Modification

Our strategy was to synthesize a spiropyran (SP) moiety with a primary amine linker and to covalently bind it to previously grafted PGMA or PMAA bushes in a one or two-step post-

polymerization modification (PPM), resulting in different spacer lengths between the polymer backbone and the SP units.
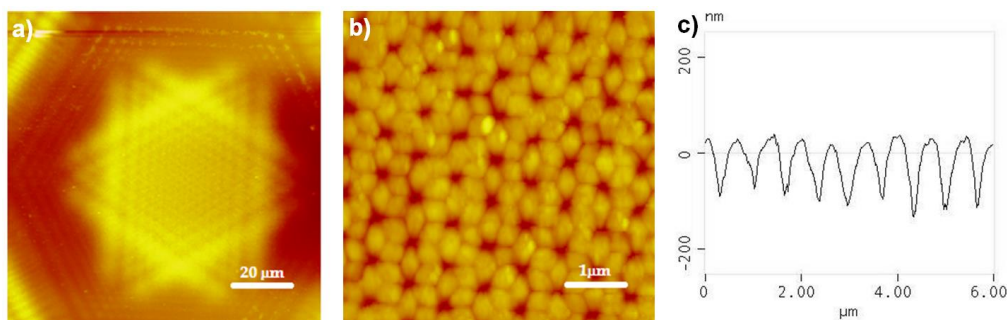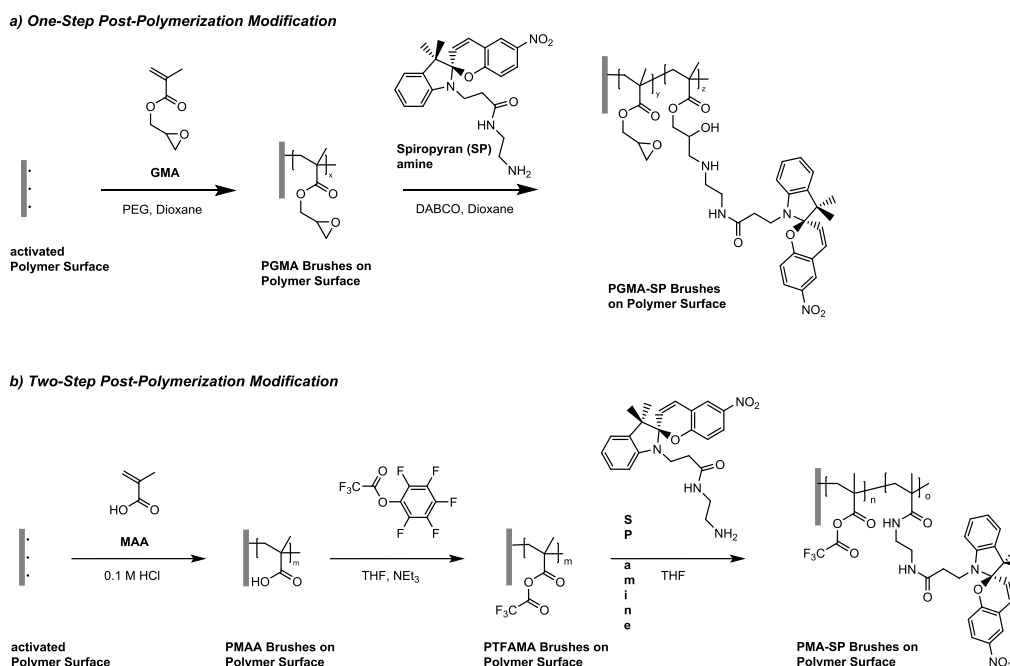

Scheme 3.1: (a) Strategy for synthesis of light-responsive polymer brushes *via* post-polymerization modification (PPM) of PGMA brush structures. Chemical linking of the spiropyran (SP) moiety to the polymer brushes is achieved through coupling of the primary amine linker to the epoxide. (b) Strategy for synthesis of light-responsive polymer brushes *via* two-step PPM of PMAA brush structures. Chemical linking of the SP moiety to the polymer brushes is achieved through coupling of the primary amine linker to the fluorinated anhydride.

Further, the different modification strategies result into two different brush types, carrying moieties of different reactivity. On the one hand, very reactive epoxides and on the other hand, rather unreactive anhydrides which allowed us to tune the number of photochromic moieties on the polymer brushes. In the one-step post-polymerization process, the primary amine performs a nucleophilic attack on the epoxide groups of the PGMA, leading to a ring-opening and formation of a secondary alcohol (Scheme 3.1a).

In the two-step PPM, the carboxylic acid groups of the grafted PMAA brushes are first transformed to fluorinated anhydrides (PTFAMA). In the second step, a nucleophilic substitution is carried out on the anhydride groups, binding the SP amine moieties and cleaving off trifluoro acetic acid (Scheme 3.1b).

In order to monitor the functionalization of the polymer brush, a surface-sensitive technique is required. When measuring IR in transmittance, the thickness of the substrate material (100 μm) naturally leads to a dominance of C-H and C-F bands of ETFE and PTFE over the polymer brush bands. The polymer foils completely absorb the IR radiation over a large wavenumber range. In contrast, the use of an IR-Microscope equipped with an objective for attenuated total reflectance (ATR) renders the measurement surface sensitive and greatly diminishes the contribution of the substrate. Furthermore, it allows the measurement of defined areas, in this case of 100 μm in diameter.

Sample spectra of substrate (PTFE, black), grafted PGMA brushes (red) and further functionalized SP-containing PGMA-SP brushes (blue) acquired with the ATR microscope are shown in Figure 3.3a. For spectra on ETFE and list of peaks with assignments for both substrates see Appendix (Figure A 3.2 and Table A 3.1). The two peaks at 1212 cm^{-1} and 1135 cm^{-1} in all three curves stem from C-F vibrations of PTFE. Upon grafting of PGMA, additional bands appear at 1485 cm^{-1}, 1450 cm^{-1}, 1390 cm^{-1}, 1218 cm^{-1} and 1088 cm^{-1}, which can be ascribed to C-O and C-C vibrations of the ether-like epoxide groups and a very significant additional band at 1730 cm^{-1} clearly indicating an ester C=O bond.

After PPM of the PGMA brushes, broad bands appear around 3375 cm^{-1} and 3245 cm^{-1}. These bands could be interpreted as O-H and N-H stretches, as well as H-O$^{..}$H bonds of the secondary alcohol formed and the covalently attached amine of the linker. Additional strong peaks at 1658 cm^{-1} and 1587 cm^{-1} support the assumption of a covalently attached SP moiety, as these could be interpreted as N-H bending of the amine and amide moieties. An appearance of the peak at 1059 cm^{-1} and the shoulder around 1218 cm^{-1} and in particular the disappearance of the band at 1088 cm^{-1} indicate the opening of the ether-like epoxide group and a covalent attachment of the SP moiety. From the ATR-IR spectra on ETFE and PTFE the efficiency of the PPM is estimated to be around 90-95 %. The shift and broadening of the C=O band at 1727 cm^{-1} can be explained by an overlap of the band for the ester groups of the backbone and the newly bound amide groups of the SP amine. Further, peaks at 1516 cm^{-1} and 1338 cm^{-1}, characteristic for nitro groups, as well as peaks at 1470 cm^{-1}, 874 cm^{-1} and 796 cm^{-1}, can be ascribed to C=C and C-H vibrations of the aromatic skeleton. The same vibrations can be assigned on ETFE (Figure A 3.2).

For the alternative synthetic approach, sample spectra of substrate (PTFE, black), grafted PMAA brushes (red), modified PTFAMA (purple) and further functionalized SP-containing PMA-SP brushes (blue) are given in Figure 3.3b. Again, the two peaks at 1212 cm^{-1} and

1135 cm^{-1} in all three curves are assigned to C-F vibrations of the substrate. Upon grafting of PMAA additional bands appear at 3159 cm^{-1}, 2596 cm^{-1} and 962 cm^{-1}, which can be ascribed to O-H vibrations of the carboxyl groups and a very significant additional band at 1699 cm^{-1}, as well as the broad band at 1631 cm^{-1}, clearly indicating a carboxylic C=O bond.
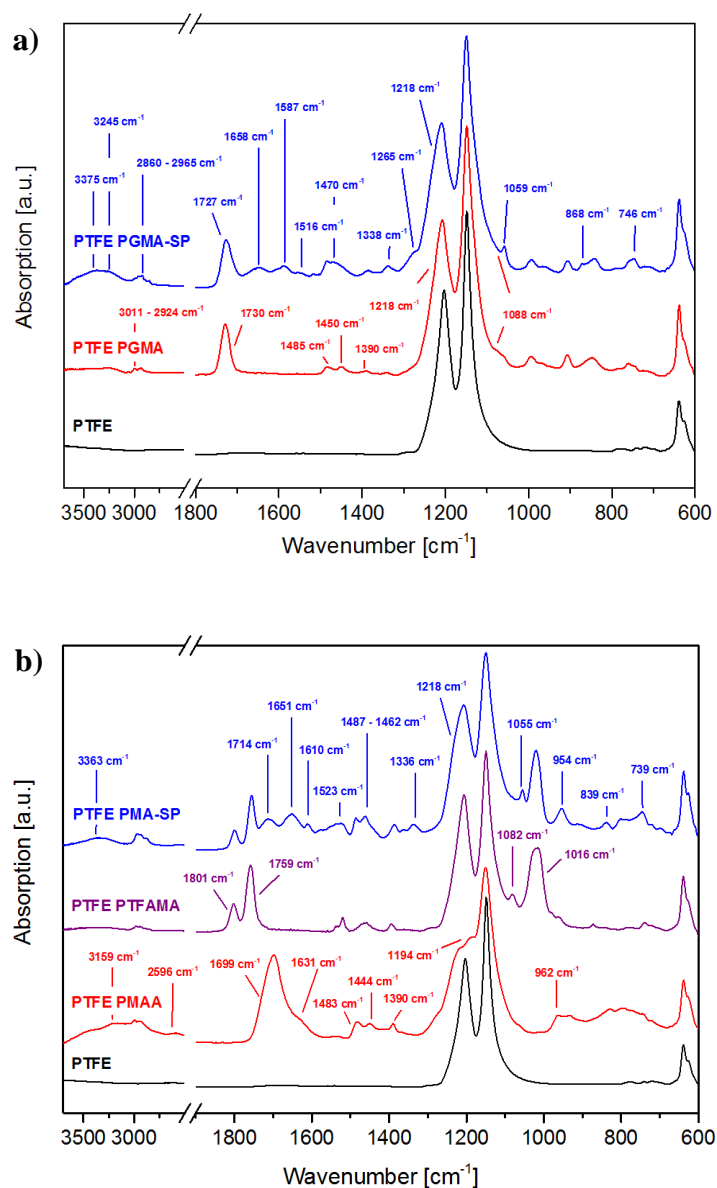

Figure 3.3: ATR-IR spectra of thick (a) PGMA and spiropyran (SP)-carrying PGMA-SP and (b) PMAA, PTFAMA and SP-carrying PMA-SP brush structures grafted from PTFE with the relevant bands marked with arrows.

After the first PPM step, all characteristic peaks for the COOH groups disappear, indicating a quantitative transformation of the carboxylic to the fluorinated anhydride groups. An appearance of the double band at 1801 cm^{-1} and 1759 cm^{-1}, characteristic of C=O anhydrides, strongly supports this assumption − in contrast to literature claiming the formation of the pentafluorinated phenylic ester upon similar reaction conditions[208] (Figure A 3.4). Further, peaks at 1082 cm^{-1} and at 1016 cm^{-1} can be ascribed to C-O and C-F vibrations, respectively.

The second PPM step of the PTFAMA brushes on the other hand seems not to be quantitative. The band intensities of the precursor moieties are clearly reduced, but still detectable. The efficiency of the second PPM process is estimated to be around 50 %. Nevertheless, as for the PGMA brush approach, strong bands due to the SP-modified PMA-SP brushes appear at 3363 cm^{-1}, 1651 cm^{-1} and 1610 cm^{-1}, indicating N-H vibrations for amides. In contrast to the first approach, there is no additional broad band appearing around 1587 cm^{-1} for N-H bending and the band around 3360 cm^{-1} for N-H stretching is much weaker, both clearly indicating an absence of amines and a covalent attachment of the spiropyran moiety as an amide moiety to the backbone.

Additional strong peaks at 1714 cm^{-1}, 1523 cm^{-1} and 1336 cm^{-1} can be ascribed to the amide C=O and N-O stretches of the SP moiety. Further, peaks at 1487–1462 cm^{-1}, 1218 cm^{-1}, 1055 cm^{-1}, as well as peaks at 954 cm^{-1}, 839 cm^{-1} and 739 cm^{-1} can be ascribed to C=C, C-H and C-O vibrations of the aromatic skeleton. The same vibrations can be assigned on ETFE (Figure A 3.3).

3.3.3 Color Switching on Macrostructures

To determine the color-switching behavior, large-area brush structures have been generated. For this purpose, the fluorocarbon foils have been irradiated with EUV-light (92.5 eV) at the SLS with no interference mask. Using the same intensities as for interference exposures to yield exposure doses 0.5 mJ cm^{-2} to 21.5 mJ cm^{-2}, areas of 1.7 mm x 1.7 mm of increasing brush thickness have been created (Figure 3.4).

SP-containing PGMA-SP structures show a bright yellow color, which intensifies with greater brush thickness. Upon UV-light irradiation, there is no color change visible. In contrast, the SP-containing PMA-SP brushes appear almost transparent under visible light, and show a strong color switch to deeply purple-colored polymer brush structures upon UV-light irradiation.

The color intensity is again enhanced at increasing brush thickness caused by the higher EUV dose. The absence of color change in the PGMA-SP structures could be interpreted as a consequence of the chemical environment provided by the PGMA brush structure. Here only a minority of subsurface SP moieties seem to open upon UV-light irradiation. Hence, the rather strong yellow color in the closed SP state might overlap a weak purple signal. A possible explanation for this effect is the high density of SP moieties that are limiting the photoresponsiveness and therefore the color change. The attachment as an amide to the anhydride brushes on the other hand provides an environment of more flexible, partly fluorinated anhydride backbone, as well as a lower density of SP moieties and could therefore favor the ring-opening process of the SP upon UV-light irradiation, explaining the strong switch in color.
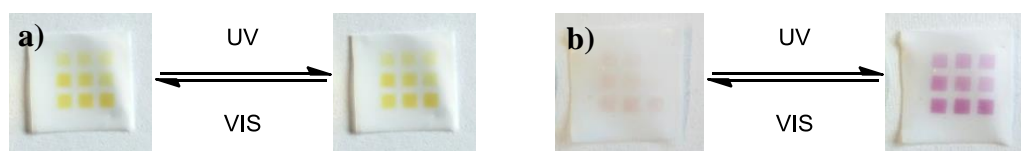

Figure 3.4: Reversible color switching of micro-structured brushes upon visible and UV-light irradiation. While spiropyran (SP)-functionalized PGMA-SP brushes on PTFE (a) appear yellow and do not appear to switch in color, PMA-SP brush structures on PTFE (b) switch from transparent to deeply purple-colored brush surfaces. This process is reversible for more than 5 cycles.

3.3.4   Switching of Wettability on Large-Area Surfaces

Surface wettability is indicative of the surface free energy, and can be determined *via* static contact-angle (CA) measurements of water droplets on the sample surface. A modification of the surface chemistry of substrates is usually accompanied by a change in static CA following the Young Equation. Large-area surfaces have been generated for analyzing macroscopic properties of photoresponsive polymer brushes. In an argon-plasma chamber, cm^2-scale patterns of radicals were created to graft PGMA and PMAA brushes from 100-µm-thick ETFE and PTFE foils. The surface free energy of the hydrophobic fluorocarbon polymers was drastically enhanced following the PGMA grafting process, leading to a more hydrophilic surface (Table 3.1). After PPM, the SP-containing PGMA-SP brushes showed a reversible switch of up

to 15° in static water CA from 82° (PGMA-SP) to 67° (PGMA-MC) upon alternating visible and UV-light irradiation (Figure 3.5) which is within the range of SP-containing surfaces[137, 208, 219].

	static CA [°]* on PTFE			static CA [°]* on ETFE		
Substrate	110	±	2	104	±	2
a) One-Step Post-Polymerization Modification:						
PGMA	58	±	2	57	±	3
PGMA-SP	82	±	3	81	±	3
PGMA-MC	67	±	3	67	±	4
b) Two-Step Post-Polymerization Modification:						
PMAA	41	±	2	42	±	3
PTFAMA	95	±	3	95	±	2
PMA-SP	97	±	2	96	±	3
PMA-MC	67	±	3	68	±	3

*average of five measurements

Table 3.1: Static water contact-angle measurements 100-µm-thick PTFE and ETFE foils, without polymer brushes, and (a) with grafted PGMA and spiropyran (SP)-carrying PGMA-SP brushes under visible light (PGMA-SP) and UV light (PGMA-MC) and (b) with grafted PMAA, PTFAMA and SP-carrying PMA-SP brushes under visible light (PMA-SP) and UV light (PMA-MC).

After grafting PMAA on both substrates, the surface modification is again evident from a strong enhancement of the surface free energy (Table 3.1). The PPM of the PMAA to the fluorinated anhydride carrying PTFAMA brushes can be detected *via* a strong reduction in surface free energy, leading to a static CA change from 41° to 95°. The higher water CA was due to the fluorinated methyl groups of the acetic acid anhydride. Upon the second functionalization step, the SP-containing PMA-SP brushes showed a reversible switch of up to 30° in static CA measurements from 97° to 67° upon alternating visible and UV-light irradiation (Figure 3.5). This switch is in the range of the most intense reversible switches described in the literature[208]. Switching of both types of surfaces was reversible for at least 10 cycles.

The switching in CA for SP-containing brushes is strongly dependent on the chemical environment provided by the brush. On the PGMA-SP brushes the hydrophobic SP moieties are

dominant upon visible and UV-light irradiation, due to their high density. The wettability of the PMA-SP brushes on the other hand, is mostly determined by the more hydrophobic fluorinated methyl groups in visible light, as the SP are less abundant; upon UV irradiation however, the formed hydrophilic MC is dominant, leading to the same CA for PMA-MC as for PGMA-MC. Although the different brush types show different switching in color, both lead to the same CA upon UV-light irradiation. Since the wettability is only dependent on the outermost moieties this supports the theory of having SP moieties that are capable of opening and closing freely on the outermost surface on both brush types. The substrate on the other hand seems not to play a role in terms of the surface free energy for each modification step, as the values are equal within the error range for ETFE and PTFE. This shows that the PPM approaches work universally on different fluorocarbon polymer substrates and could also, in principle, be transferred to other polymers, such as polyolefins.
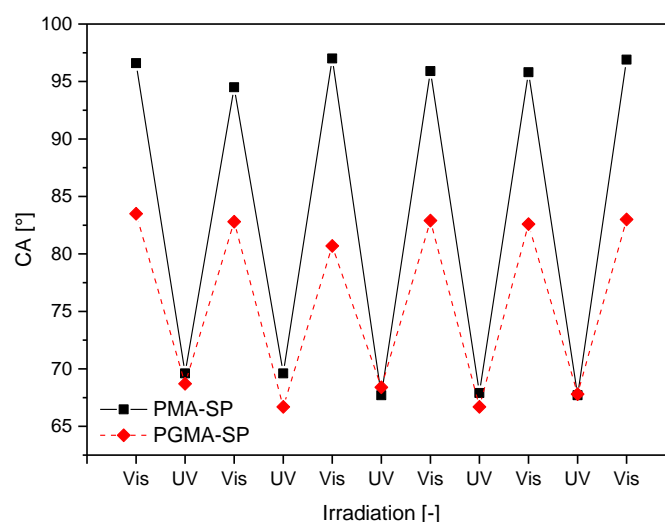

Figure 3.5: Static contact-angle measurement of water droplets (3 μL): Reversible switching between visible and UV-light irradiation leads typically to a switch in contact angle from 82° to 67° for PGMA-SP (red) and from 97° to 67° PMA-SP (black) brush surfaces. This process is reversible for more than 5 cycles.

3.3.5   Fluorescence Kinetic Studies of Nanostructures

For comparison the fluorescence kinetics of the SP amine was first determined in solution (for details see Appendix). Without excitation, the closed, thermodynamically stable SP form shows no absorption band in the visible region. Irradiated with UV light ($\lambda_{Ex} = 350$ nm) the SP amine changes its conformation to the planar MC form and shows strong absorption band at 540 to 580 nm, depending on the solvent used (Figure A 3.5). The planar conformation of the MC opens the possibility for the electrons to delocalize over the entire molecule and absorb light in the visible range. This absorption is used to excite fluorescence in the red area at about 628 nm. The fluorescence increases with increasing UV exposure. The emission half-life ($T_{1/2}$) has been determined for each solvent after an initial exposure to UV light for 330 seconds (Table 3.2). In general, $T_{1/2}$ for the thermodynamically less stable MC form increases with polarity. The extreme elongation of $T_{1/2}$ in ethanol can be ascribed to hydrogen bonding of the solvent with the phenolate group of the open MC form.

The fluorescence-emission kinetics of patterns of SP-containing PGMA-SP and PMA-SP brushes were analyzed in the dry state and in solvents of different polarities using fluorescence microscopy (Figure 3.6 and Figure A 3.8). Again, upon an initial excitation by UV-light ($\lambda_{Ex} = 360$ nm, 30 s) the open MC is formed, which can then be excited *via* subsequent continuous irradiation using a second excitation wavelength ($\lambda_{Ex} = 555$ nm). This excitation leads to an emission of red fluorescence ($\lambda_{Em} = 630$ nm) on the generated arrays of micro- and nano-patterned polymer brushes. As a consequence of the much higher brush thickness in the dry state – and therefore the higher number of binding sites – the areas of high radical density show stronger fluorescence emission. However, the periodic interference patterns also show a clear – albeit much weaker – emission.

The intensity of the emission that appears is roughly the same in the beginning in the different solvents for both brush environments, showing a slightly enhanced emission in THF and DCM and a reduced emission in EtOH and water. To determine the fluorescence kinetics in the different environments, the individual $T_{1/2}$ was evaluated from the relative brightness of the fluorescent parts of the images (Table 3.2; Figure A 3.9 and Figure A 3.10). In the dry state, $T_{1/2}$ is 2.3 s for PGMA-SP brushes, while in a non-polar solvent such as toluene it fades much more rapidly, after approximately 1.7 s. With increasing polarity, $T_{1/2}$ seems to recover, until in polar solvents, such as THF, DCM and ethanol, the emission reaches a lifetime twice as long as in the

dry state. Similar fluorescence kinetics depending on the chemical environment provided by the solvent could be observed for PMA-SP brush structures (Table 3.2).
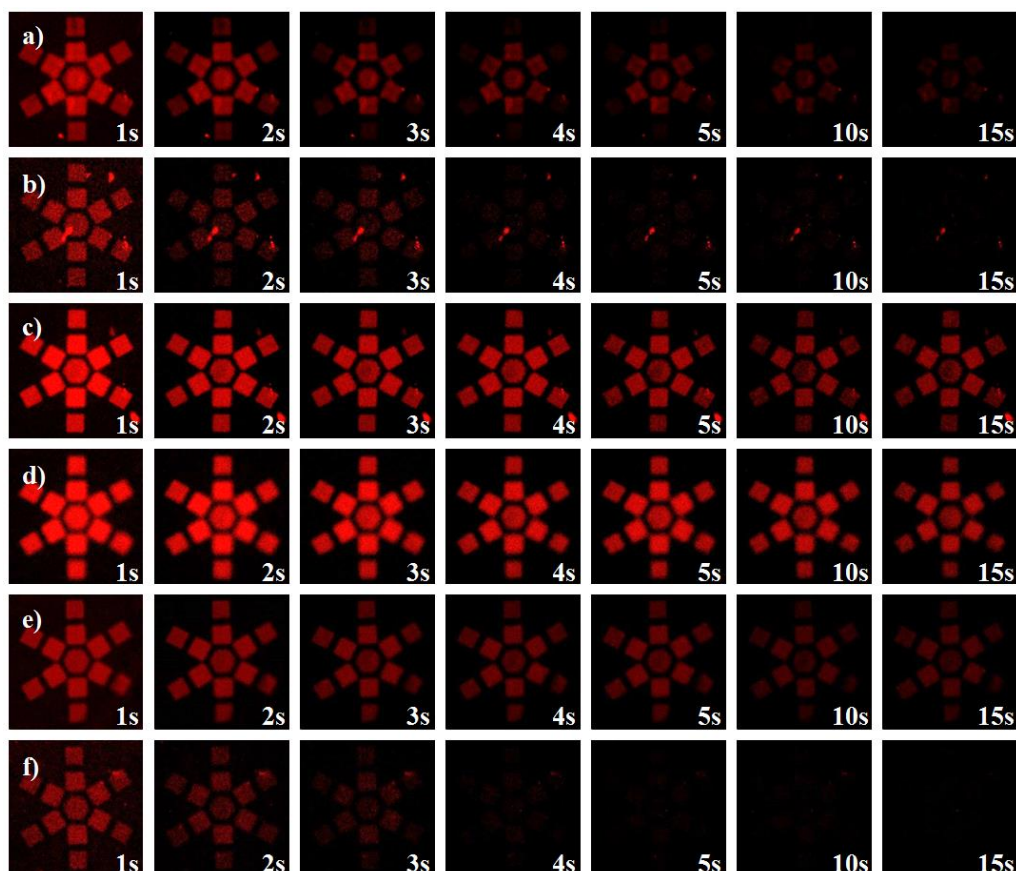

Figure 3.6: Fluorescence kinetic studies of spiropyran (SP)-containing PGMA-SP brush structures after an initial excitation with UV-light (λ = 360 nm, 30 s). The red fluorescence was observed under excitation with visible light (λ_{Ex} = 555 nm) in the dry state (a), toluene (b), THF (c), DCM (d), ethanol (e) and in water (f).

In general, suitable solvents enhance the fluorescence emission by solvating the polymer brushes, giving them the ability to swell and shrink. Non-polar solvents destabilize the open merocyanine form and therefore shorten $T_{1/2}$, while polar solvents stabilize the open MC form and extend their emission life-time. The results in water do not follow this principle, as SP-containing brushes are expected not to be soluble in water. The generally much shorter $T_{1/2}$ for PMA-SP brushes can be considered to be a consequence of the higher flexibility provided by the brushes, allowing the SP moieties to move freely and therefore open and close much faster. The

fluorescence kinetics is therefore dependent on both the brush chemistry, as well as on the solvent surrounding it.

Fluorescence kinetics in solution, as described before, show the same dependencies as the brushes but on a much slower time scale, due to different relaxation pathways as well as the different temperatures. Note that the measurements in solution were carried out under thermal relaxation in the dark at $T = 20\,°C$, while the brush structures were relaxed *via* visible light irradiation at $T = 37\,°C$.

		Fluorescence Emission Half-life $T_{1/2}$ (sec) in									
	Dry			Toluene			THF		DCM	EtOH	H_2O
In Solution											
SP amine	-			120 ± 30		105 ± 30		570 ± 90	5520 ± 210		-
On Polymer-Brush Structures											
PGMA-SP	2.3 ± 0.3			1.7 ± 0.2		4.4 ± 0.3		5.2 ± 0.8	4.8 ± 0.8		2.4 ± 0.5
PMA-SP	1.2 ± 0.2			1.4 ± 0.2		2.2 ± 0.3		2.3 ± 0.3	2.9 ± 0.3		1.7 ± 0.2

Table 3.2: Fluorescence emission half-life ($T_{1/2}$) of thermal degradation in the dark of SP amine in different solvents (c = 1.0 x 10^{-6} M), as well as $T_{1/2}$ under visible light for SP-containing PGMA and PMA brushes after initial irradiation with UV-light.

Due to the lower dry thickness, as well as the lower coupling yield, the number of SP moieties on PMA-SP brushes is expected to be less than 1/5 that of the PGMA-SP brushes. The fact that the initial fluorescence emission on the PMA-SP brushes is similar under all conditions to that of PGMA-SP shows that there is also a clear dependence on the chemical environment provided by the two different brushes. On PMA-SP almost all spiropyrans moieties seem to have the ability to open to the merocyanine form, while on the PGMA-SP only a small fraction is capable of this.

Considering the switching behavior in color, as well as in wettability, the coupling *via* the secondary amine onto PGMA brushes seems to separate the surface modification into two phases – a bulk and a surface phase. The PGMA-SP brushes may create a greater rigidity, which hinders the opening of SPs in the bulk phase. Only the outermost SPs are then capable of responding towards the UV-light activation and therefore causing a much weaker fluorescence emission. The rigidity might originate from SP stacking or crosslinking of secondary amine groups with

unreacted epoxides. The PMA-SP brushes on the other hand seem to provide a much higher flexibility, due to their lower coupling yield which allows the majority of the SP to open, therefore producing much stronger fluorescence emission, given the dry thickness and coupling yield. This would be in agreement with prior results in color switching and CA measurements, which demonstrated a rather weak switching behavior for PGMA-SP and a strong switching behavior for PMA-SP brush structures.

3.4   Conclusions

We have used free-radical polymerization (FRP) and two different post-polymerization modification strategies *via* simple coupling reactions to generate photochromic polymer brushes on fluoropolymer surfaces. The photochromic brushes carry covalently attached spiropyran (SP) as pendant groups. Initiator radicals have been created by extreme ultra-violet (EUV) light at the Swiss Light Source (SLS), which allow us to reproducibly grow polymer brushes from interference patterns on a micrometer to nanometer scale, up to a few hundred nm in height.

The demonstrated ATR-IR spectra clearly show the grafting of PGMA and PTFAMA derived from PMAA brush structures and their post-polymerization modification (PPM) with the spiropyran (SP) amine. The patterned SP-containing polymer brushes were successfully shown to be smart surfaces that switch in color, in their fluorescence behavior, and in wettability, using light as external stimulus.

Fluorescence emission and half-life ($T_{1/2}$) of the photochromic brushes were analyzed in the dry state and in solvents of different polarity. Solvents enhance the initial emission compared to the dry state and determine $T_{1/2}$. Non-polar solvents lower $T_{1/2}$, while polar solvents enhance the emission life-time. The polymer-brush chemistry and coupling yield also define the emission kinetics, as the more rigid, highly functionalized PGMA-SP brushes extend, while more flexible and less functionalized PMA-SP brushes reduce $T_{1/2}$. These fluorescence kinetics studies show a clear relation to the SP amine in solution and demonstrate the importance of the brush chemistry, as well as the solvent environment for the spiropyran-merocyanine isomerization.

Further, the UV-light-induced spiropyran-merocyanine isomerization causes a switch in wettability, demonstrated *via* a contact-angle change over a range of 15° for PGMA and 30° for PMA functionalized brush structures which is within the range of SP-containing surfaces. Nevertheless, a strong color switch from transparent to deep purple is only detectable for SP-

modified PMA-SP and not for PGMA-SP brushes. PGMA-SP brushes appear bright yellow and do not switch in color upon alternating visible and UV-light irradiation.

      With the future application potential of smart surfaces in mind, a detailed understanding of the parameters that determine the photoresponsiveness of these engineered brush structures is valuable for the development of further, more complex responsive systems. The advantage of the unique possibilities at the XIL-beamline to control the grafting process in terms of spatial resolution and grafting density defined by the exposure process allows us to characterize the produced structures and their photoresponse on the nanometer scale.

3.5   Appendix

3.5.1   Experimental Procedures
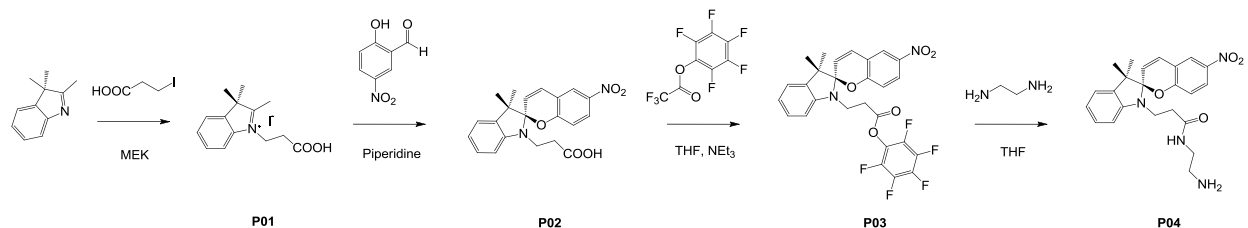
Scheme A 3.1: Synthetic route to spiropyran (SP) moieties with different linkers, which can be covalently bound to previously grafted polymer-brush structures.

1-(2-carboxyethyl)-2,3,3-trimethyl-3*H*-indol-1-ium   iodide   (P01):   2,3,3-trimethylindolenine (5.01 mL/ 30.59 mmol) and 3-iodopropanic acid (6.35 g/ 30.17 mmol) were diluted in 10 mL MEK and stirred under argon for 5 hours under reflux. The precipitate was suspended in 50 mL H_2O and washed three times with 50 mL DCM. The organic layers were combined and washed three times with 25 mL water. The aqueous layers were combined, filtered and the solvent removed at high vacuum, receiving P01 as pale yellow solid in a 97 % yield (10.52 g/ 29.29 mmol). ^{1}H-NMR (300 MHz, CDCl$_3$): 1.55 (s, 6 H, 2 CH$_3$), 2.89 (s, 3 H, CH$_3$), 3.00 (t, 2 H, $^3J_{H,H} = 6.88$ Hz, C$\underline{H}_2$COO), 4.67 (t, 2 H, $^3J_{H,H} = 6.76$ Hz, NC$\underline{H}_2$CH$_2$COO), 7.64-7.58 (m, 2 H, CH$_{arom}$), 7.84-7.89 (m, 1 H, CH$_{arom}$), 7.97-8.03 (m, 1 H, CH$_{arom}$).

3-(3',3'-dimethyl-6-nitrospiro[chromene-2,2'-indolin]-1'-yl) propionic acid (P02): P01 (4.83 g/ 13.31 mmol), 2-hydroxy-5-nitrosalicylaldehyde (2.28 g/ 13.34 mmol) and piperidine (1.60 mL/ 16.04 mmol) were diluted in 20 mL MEK and stirred under argon for 3 hours under reflux. The reaction mixture was cooled to RT overnight, yielding the raw product as a yellow precipitate, which was filtered, washed with MEK (10 mL) and cold MeOH (10 mL) and dried under high vacuum to yield P02 as a bright yellow-green solid in a 88 % yield (4.44 g/ 11.67 mmol). ^{1}H-NMR (300 MHz, DMSO-d6): 1.08 (s, 3 H, CH$_3$), 1.19 (s, 3 H, CH$_3$), 2.41-2.64 (m, 2 H, C$\underline{H}_2$COOH), 3.41-3.56 (m, 2 H, NC$\underline{H}_2$CH$_2$), 6.00 (d, 1 H, $^3J_{H,H} = 10.39$ Hz, C$_q$$\underline{H}$C=CHPh), 6.67 (dd, 1 H, $^3J_{H,H} = 8.26$ Hz, $^5J_{H,H} = 0.78$ Hz, CH$_{arom}$), 6.81 (dt, 1 H, $^3J_{H,H} = 7.45$ Hz, $^5J_{H,H} = 0.75$ Hz, CH$_{arom}$), 6.87 (d, 1 H, $^3J_{H,H} = 9.04$ Hz, CH$_{arom}$), 7.11-7.16 (m,

2 H, CH$_{arom}$), 7.22 (d, 1 H, $^3J_{H,H}$ = 10.36 Hz, C$_q$HC=C$\underline{H}$Ph), 8.01 (dd, 1 H, $^3J_{H,H}$ = 8.98 Hz, $^4J_{H,H}$ = 2.85 Hz, CH$_{arom}$), 8.22 (d, 1 H, $^4J_{H,H}$ = 2.79 Hz, CH$_{arom}$), 12.23 (s, 1 H, COOH).

Perfluorophenyl-3-(3',3'-dimethyl-6-nitrospiro[chromene-2,2'-indolin]-1'-yl)-propanoate (P03): P02 (2.68 g/ 6.97 mmol) was diluted in a solution of triethylamine (2.45 mL/ 17.50 mmol) in 35 mL abs. THF. A solution of PFP trifluoroacetate (3.07 mL/ 17.50 mmol) in 15 mL abs. THF was added dropwise to the reaction mixture. The solution was stirred for 8 hours under argon at RT. DCM (50 mL) was added to the reaction mixture and washed three times with 50 mL H$_2$O. The organic layer was dried over MgSO$_4$ and the solvent removed at high vacuum. The crude product was recrystallized from 15 mL of a cyclohexane/toluene mixture (3:1, v/v) producing P03 as a beige solid in a 97 % yield (3.68 g/ 6.73 mmol). ^{1}H-NMR (300 MHz, DMSO-d6): 1.10 (s, 3 H, CH$_3$), 1.21 (s, 3 H, CH$_3$), 2.99-3.27 (m, 2 H, C$\underline{H}_2$COOH), 3.47-3.70 (m, 2 H, NC$\underline{H}_2$CH$_2$), 6.00 (d, 1 H, $^3J_{H,H}$ = 10.39 Hz, C$_q$$\underline{H}$C=CHPh), 6.78-6.91 (m, 3 H, CH$_{arom}$), 7.15-7.19 (m, 2 H, CH$_{arom}$), 7.24 (d, 1 H, $^3J_{H,H}$ = 10.52 Hz, C$_q$HC=C$\underline{H}$Ph), 8.01 (dd, 1 H, $^3J_{H,H}$ = 9.05 Hz, $^4J_{H,H}$ = 2.39 Hz, CH$_{arom}$), 8.22 (d, 1 H, $^4J_{H,H}$ = 2.52 Hz, CH$_{arom}$).

N-(2-aminoethyl)-3-(3',3'-dimethyl-6-nitrospiro[chromene-2,2'-indolin]-1'-yl)propan-amide (P04): P03 (1.75 g/ 3.17 mmol) was diluted in 20 mL abs. THF. A solution of ethylenediamine (2.15 mL/ 31.85 mmol) in 10 mL abs. THF was added dropwise to the reaction mixture and the solution stirred for 4 h under argon at RT. DCM (50 mL) was added to the reaction mixture and washed five times with 50 mL H$_2$O. The organic layer was dried over MgSO$_4$ and the solvent removed at high vacuum yielding P04 as a yellow solid in a 98 % yield (1.31 g/ 3.10 mmol). ^{1}H-NMR (300 MHz, DMSO-d6): 1.06 (s, 3 H, CH$_3$), 1.18 (s, 3 H, CH$_3$), 1.36 (s, 2 H, NH$_2$), 2.23-2.42 (m, 2 H, C$\underline{H}_2$COOH), 2.94-2.99 (m, 2 H, NH$_2$C$\underline{H}_2$), 3.29-3.51 (m, 2 H, NC$\underline{H}_2$CH$_2$), 5.96 (d, 1 H, $^3J_{H,H}$ = 10.39 Hz, C$_q$$\underline{H}$C=CHPh), 6.65 (d, 1 H, $^3J_{H,H}$ = 7.90 Hz CH$_{arom}$), 6.79 (t, 1 H, $^3J_{H,H}$ = 7.39 Hz, CH$_{arom}$), 6.85 (d, 1 H, $^3J_{H,H}$ = 8.98 Hz, CH$_{arom}$), 7.08-7.14 (m, 2 H, CH$_{arom}$), 7.18 (d, 1 H, $^3J_{H,H}$ = 10.49 Hz, C$_q$HC=C$\underline{H}$Ph), 7.90 (s, br., CON$\underline{H}$CH$_2$), 7.99 (dd, 1 H, $^3J_{H,H}$ = 8.95 Hz, $^4J_{H,H}$ = 2.79 Hz, CH$_{arom}$), 8.23 (d, 1 H, $^4J_{H,H}$ = 2.73 Hz, CH$_{arom}$).

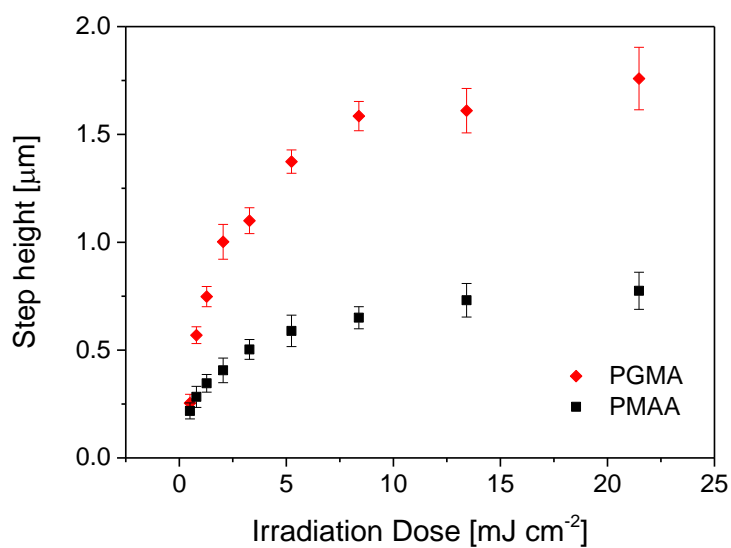### 3.5.2   Atomic Force Microscopy (AFM)

Figure A 3.1: Brush thickness of PGMA and PMAA structures grafted from ETFE surfaces, as a function of the EUV-light (92.5 eV) irradiation dose. Step heights have been derived from AFM images in non-patterned areas of high radical density.

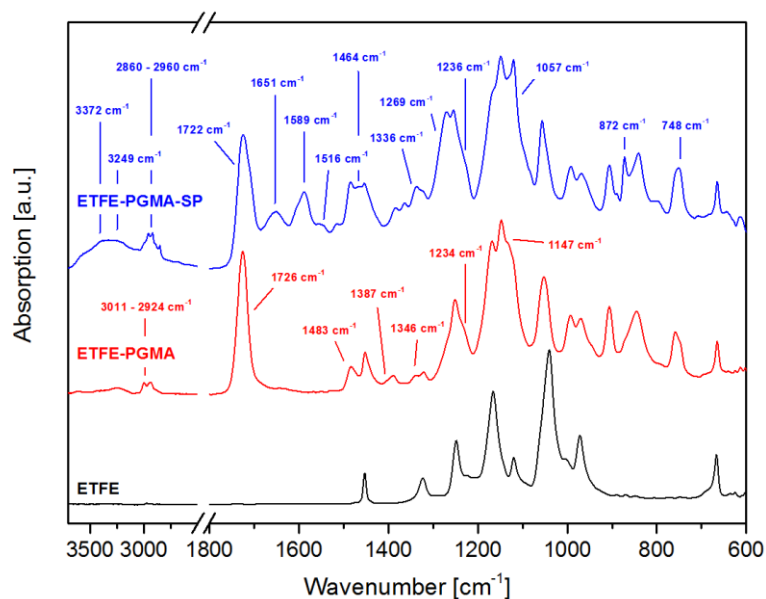### 3.5.3   Attenuated Total Reflectance – Infrared (ATR–IR) Spectroscopy

Figure A 3.2: ATR-IR spectra of thick PGMA and spiropyran-carrying PGMA-SP brush structures grafted from ETFE with the relevant bands marked with arrows.
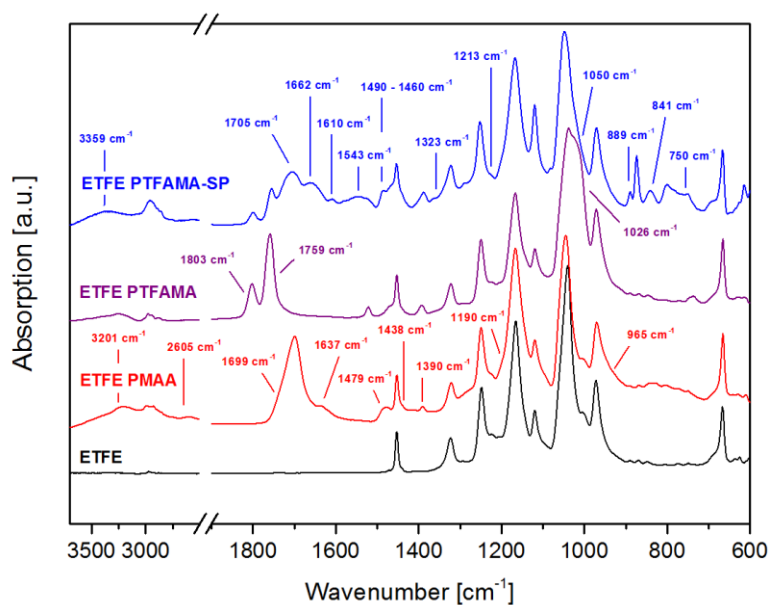

Figure A 3.3: ATR-IR spectra of thick PMAA, PTFAMA and spiropyran-carrying PMA-SP brush structures grafted from ETFE with the relevant bands marked with arrows.

		Wavenumber [cm^{-1}] on PTFE	Wavenumber [cm^{-1}] on ETFE
PGMA	υ(C-H)$_{st}$	3011 – 2924	3011 – 2924
	δ(C-H)$_b$	1483, 1387, 1346	1483, 1387, 1346
	υ(C=O)$_{ester}$	1730	1726
	υ(C-O)$_{acyl}$	1218	1234
	υ(C$_{alkoxy}$-H)$_{ether}$	1088	1147
PGMA-SP	υ(N-H)$_{st}$	3375	3372
	υ(N-H)$_{b, amide}$	1658	1651
	υ(N-H)$_{b, amine}$	1587	1589
	υ(C-H)$_{st}$	2965 – 2860	2965 – 2860
	υ(C-H)$_{arom., metasubst.}$	868, 746	872, 748
	υ(O-H)$_{st}$	3245	3249
	υ(C=O)$_{ester+amide}$	1727	1722
	υ(N-O)$_{asym}$	1516	1516
	υ(N-O)$_{sym}$	1338	1336
	υ(C=C)$_{st, arom.}$	1470	1464
	υ(C-N)	1265	1269
	υ(C$_{Ph}$-O)	1218	1236
	υ(C$_{alkoxy}$-O)$_{alcohol}$	1059	1057

Table A 3.1: List of signals appearing in ATR-IR spectra of thick PGMA and SP-carrying PGMA-SP brush structures grafted from ETFE and PTFE.

		Wavenumber [cm^{-1}] on PTFE	Wavenumber [cm^{-1}] on ETFE
PMAA	υ(O-H)$_{COOH^{\cdots}H}$	3159	3201
	υ(O-H)$_{COOH}$	2596	2605
	υ(O-H)$_{COOH}$	962	965
	υ(C=O)$_{COOH}$	1699	1699
	υ(C=O)$_{COO^-}$	1631	1637
	δ(C-H)$_b$	1483, 1444, 1390	1479, 1438, 1390
	υ(C-O)$_{acyl}$	1194	1190
PTFAMA	υ(C=O)$_{anhydride}$	1801, 1759	1803, 1759
	υ(C$_{alkoxy}$-O)	1082	1090
	υ(C-F)	1016	1026
PMA-SP	υ(N-H)$_{st}$	3363	3359
	υ(C=O)$_{anhydride}$	1801, 1759	1803, 1759
	υ(C=O)$_{amide}$	1714	1705
	υ(N-H)$_{b,\,amide}$	1651	1662
	υ(C-H)$_{st}$	2970 – 2860	2970 – 2860
	υ(C-H)$_{arom.,\,metasubst.}$	954, 839, 739	889, 841, 750
	υ(N-O)$_{asym}$	1523	1543
	υ(N-O)$_{sym}$	1336	1323
	υ(C=C)$_{st,\,arom.}$	1487 – 1462	1490 - 1460
	υ(C$_{Ph}$-O)	1218	1213
	υ(C$_{alkoxy}$-O)	1055	1050
	υ(C-F)	1016	1026

Table A 3.2: List of signals appearing in ATR-IR spectra of thick PMAA, PTFAMA and SP-carrying PMA-SP brush structures grafted from ETFE and PTFE.
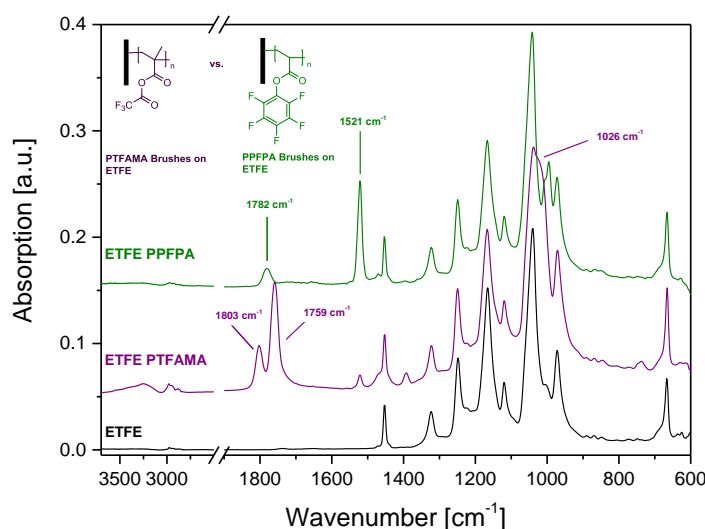
Figure A 3.4: ATR-IR spectra of thick PPFPA in comparison to PTFAMA brush structures grafted from ETFE with the relevant bands marked with arrows. The shift for the C=O vibration for the ester compared to the formed anhydride brushes, as well as the absence of a dominant peak at 1521 cm^{-1} for C=C vibrations of the aromatic ester, proves that not the PFP ester, but the trifluoro anhydride has been formed.

3.5.4   Photochromic Properties of Spiropyrans in Solution

To understand the photoresponsive behavior of spiropyran (SP)-containing brushes, we needed to fully understand the photochromic behavior of SPs in solution first. Therefore, the photochromic behavior of SP moiety P04 was analyzed in solvents of different polarity (Figure A 3.5). Before irradiation with UV-light, the solutions appear colorless or weakly colored, depending on the solvent used. With irradiation of UV-light ($\lambda_{Ex} = 350$ nm) weak fluorescence emission appears in the dark and all solutions show a strong color change. After irradiation with visible light, all solutions decolorize again completely. This process is reversible for more than 20 cycles and depends on the polarity of the solvent.

The absorption behavior of spiropyran moiety P04 (c = 1.0 x 10^{-6} M) was analyzed in detail in toluene, DCM, THF and ethanol (Figure A 3.6). Without excitation, the closed thermodynamically stable SP form shows no absorption band in the visible region. Once irradiated with UV light ($\lambda_{Ex} = 350$ nm) P04 in toluene changes its conformation to the planar

merocyanine form and with irradiation time shows an increasingly strong absorption band at 578 nm and a shoulder around 545 nm. The appearance of the shoulder can be ascribed to the formation of dimers or aggregates of the nitro-substituted SPs in non-polar solvents. With increased polarity, neither a shoulder nor a second absorption band appear in THF (λ_{Max} = 569 nm) or ethanol (λ_{Max} = 536 nm), as polar solvents stabilize the merocyanine (MC) open form. From kinetic analysis of thermal relaxation of the individual absorption maxima of P04, the absorption half-life ($T_{1/2, Abs}$) has been determined for each solvent. In general, $T_{1/2, Abs}$ of the thermodynamically less stable MC form increases with polarity. The 9-fold increase of $T_{1/2, Abs}$ in ethanol can be ascribed to hydrogen bonding of ethanol with the phenolate group of the open MC form. The fluorescence behavior of P04 ($c = 1.0 \times 10^{-6}$ M) was analyzed in detail in toluene, DCM, THF and EtOH (Figure A 3.7). Upon excitation by UV-light (λ_{Ex} = 350 nm), only a very weak fluorescence signal can be detected. The planar conformation of the MC opens the possibility for the electrons to delocalize over the entire molecule and absorb light of another wavelength. If the solutions are excited with a second excitation wavelength, according to their absorption spectrum, the fluorescence emission is strongly enhanced. In toluene a strong emission band appears in the red area at 628 nm with excitation at the absorption maximum (λ_{Ex} = 570 nm), increasing with irradiation time. From kinetic analysis of thermal relaxation of the individual emission maxima of P04 the emission half-life ($T_{1/2, Em}$) has been determined for each solvent (Table 3.2). In general, $T_{1/2, Em}$ of the thermodynamically less stable MC form increases with polarity. The 50-fold elongation of $T_{1/2, Em}$ in ethanol can be ascribed to hydrogen bonding of ethanol with the phenolate group of the open MC form.
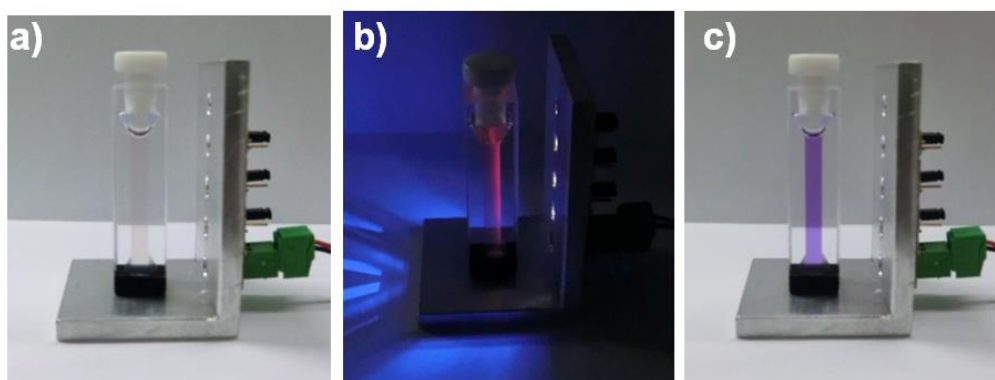

Figure A 3.5: A solution of SP-Amine in toluene ($c = 1.0 \times 10^{-6}$ M) before UV-light exposure (a), under UV-light (b) and after UV-light irradiation (c). After 5 min irradiation with visible light the solution decolorizes completely. This process is reversible for more than 20 cycles.
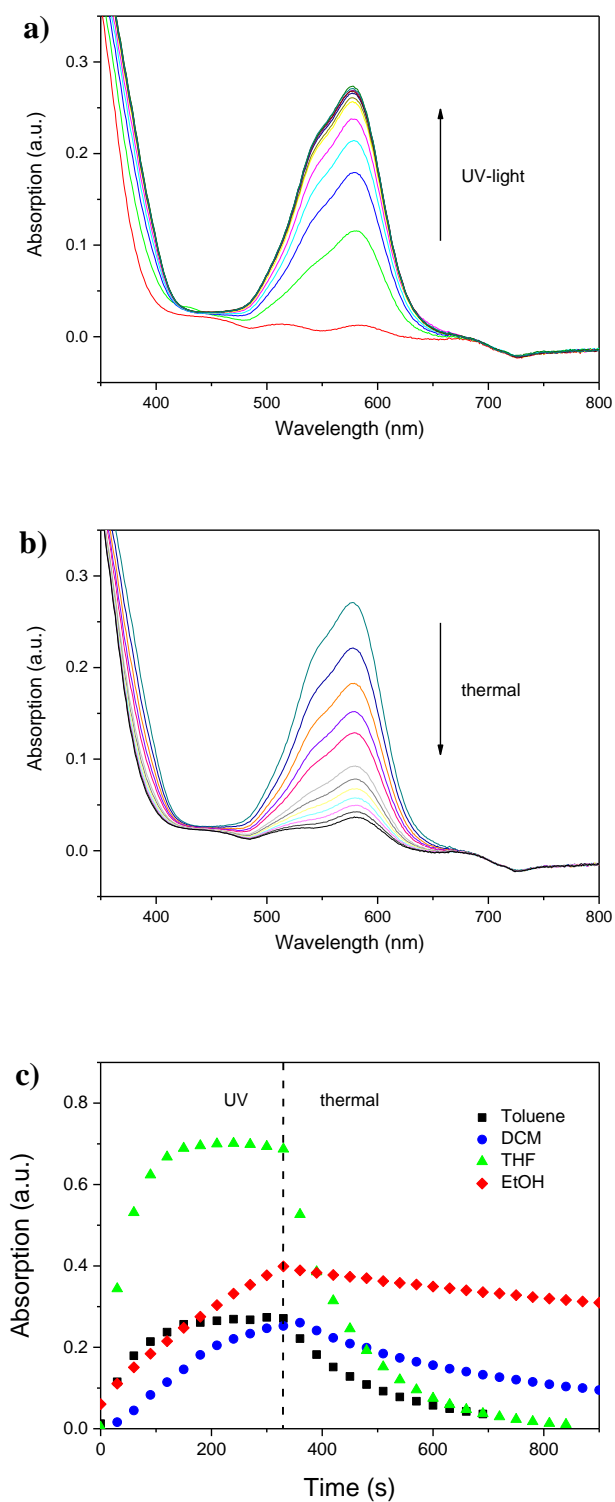
Figure A 3.6: Absorption spectra of a solution of SP-Amine P04 (c = 1.0 x 10^{-6} M) in toluene (a, b), and kinetics at absorption maximum in toluene, DCM, THF and EtOH (c) under UV-light irradiation (λ_{Ex} = 350 nm) and thermal relaxation in steps of 30 sec.
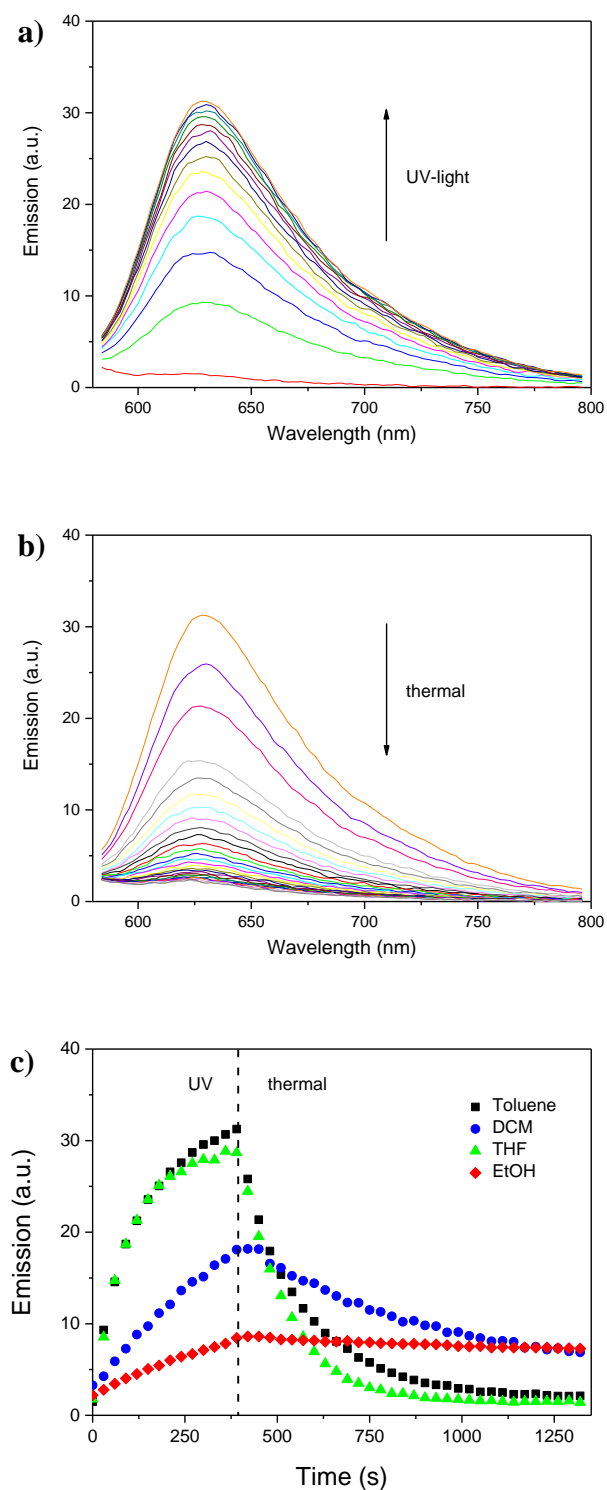
Figure A 3.7: Fluorescence spectra of a solution of SP-Amine P04 (c = 1.0 x 10^{-6} M) in toluene (a, b) and kinetics at emission maximum in toluene, DCM, THF, EtOH (e) under UV-light irradiation and thermal relaxation in steps of 30 sec.

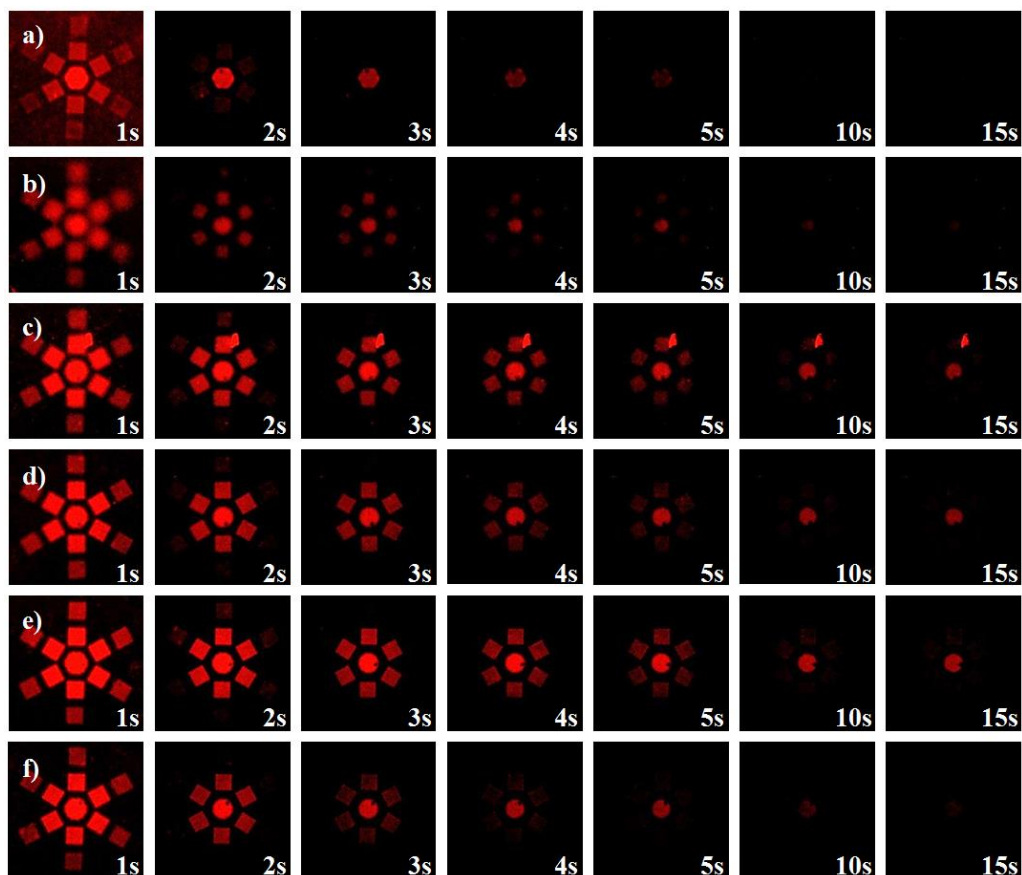### 3.5.5   Fluorescence Kinetics on Polymer Surfaces

Figure A 3.8: Fluorescence kinetic studies of spiropyran (SP)-containing PMA-SP brush structures after an initial excitation with UV-light (λ = 360 nm, 30 s). The red fluorescence was observed under excitation with visible light (λ_{Ex} = 555 nm) in the dry state (a), toluene (b), THF (c), DCM (d), ethanol (e) and in water (f).

Figure A 3.9: Determination of emission half-life ($T_{1/2}$) of SP-containing PGMA-SP brush structures after an initial excitation with UV-light ($\lambda = 360$ nm, 30 s). The intensity of the red fluorescence signal was determined under excitation with visible light ($\lambda_{Ex} = 555$ nm) in the dry state (a), toluene (b), THF (c), DCM (d), ethanol (e) and in water (f).
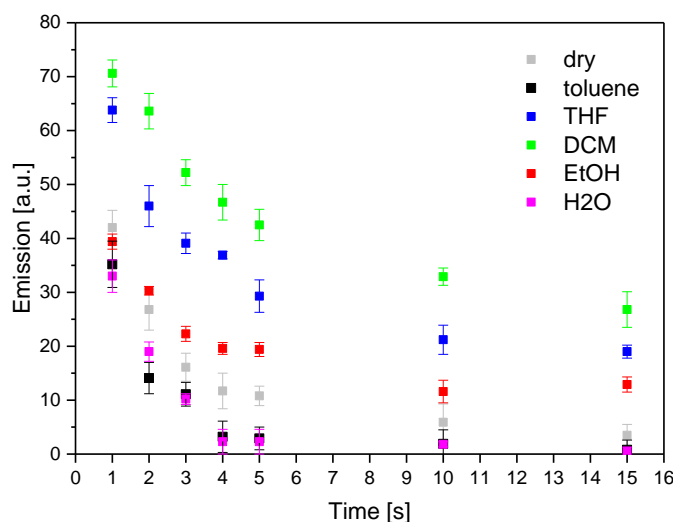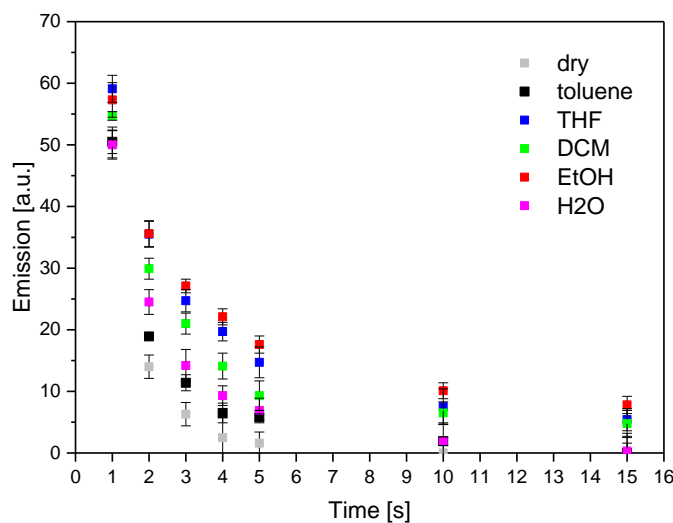

Figure A 3.10: Determination of emission half-life ($T_{1/2}$) of SP-containing PMA-SP brush structures after an initial excitation with UV-light ($\lambda = 360$ nm, 30 s). The intensity of the red fluorescence signal was determined under excitation with visible light ($\lambda_{Ex} = 555$ nm) in the dry state (a), toluene (b), THF (c), DCM (d), ethanol (e) and in water (f).

4. From pH- to Light-Response: Post-Polymerization Modification of Polymer Brushes Grafted onto Polymeric Membranes[2]

4.1 Abstract

We demonstrate a new approach to fabricating a microporous pH- and light-responsive membrane that enables remote control over its transport and interfacial material properties. pH-responsiveness was imparted to a commercial 30-μm-thick polypropylene membrane *via* grafting of poly(methacrylic acid) (PMAA) brushes from the substrate using an argon plasma-induced free-radical graft polymerization. Morphological changes as a function of grafting level were analyzed by means of atomic force microscopy. Conversion into a light-responsive membrane was performed *via* a two-step, post-polymerization modification to covalently attach photochromic spiropyran moieties to grafted PMAA polymer brushes. Characterization of the functionalization of the polymer brushes was carried out with attenuated total reflectance infrared and UV/vis spectroscopy. pH- and light-induced reversible switches in wettability and permeability upon changing from acidic to basic pH or alternating UV- and visible light irradiation, respectively, were demonstrated using static water contact angle and flux measurements. Additionally, light-responsive membranes show a switch in color which was characterized *via* UV/vis spectroscopy.

4.2 Introduction

Smart membranes that are sensitive to their environment have received tremendous attention in recent years as they enable the rapid, remote-controlled switching of their transport and interfacial properties [100, 116, 220-226]. They are designed materials that have properties such as swelling behavior, permeability or interactions with ions and biomolecules that can be changed reversibly in a controlled way by means of external stimulation. Switching originates from responsiveness to a certain trigger such as pH[92], temperature[227], metal ions[228], electric field[229] or light[152]. Membranes that are sensitive towards pH have been fabricated using a variety of

---

[2] This chapter is the basis for a manuscript to be submitted to ACS Applied Materials & Interfaces. The experimental part has been integrated in Chapter 2. The supplementary information has been added as an appendix at the end of this chapter.

processes including formation of polymer networks, chemical modification of the bulk material or *via* grafting of polymer brushes on their surfaces.

Polypropylene (PP) membranes are low-cost materials that show advanced bulk properties in terms of their mechanical strength, dimensional stability and chemical inertness[230]. However, this is associated with a high degree of hydrophobicity, low reactivity and poor biocompatibility. Modification of such commercial substrates to improve their surface properties is therefore very attractive[32]. Conventional simple methods include coating and grafting processes. The easily implemented dip- or spin-coating techniques have the disadvantages of pore blockage and weak adhesion forces to the parent polymer[231]. Grafting of polymer brushes covalently either *via* "grafting-to" or "grafting from" is a very powerful, efficient and simple method to covalently attach new functionalities, allowing a fast response to environmental stimuli due to flexible mobile chain ends, while retaining the desirable bulk properties of the parent material (Chapter 1). Different techniques have been established as a pre-treatment to activate polymeric membranes to bind *e.g.* RAFT chain-transfer agents for graft polymerization, namely *via* plasma[232], ozone (O_3)[233], UV-light[234] or for direct polymerization *via* γ-irradiation[235]. Plasma activation is a fast, dry and environmentally friendly way, which has been heavily exploited in industry for activation and cleaning of surfaces in order to form homogenous coatings[236, 237].

Typically, pH-responsive polymers are weak polyelectrolytes (Chapter 1.5), which undergo conformational transitions depending on the pH conditions. The response of poly-acids towards pH occurs *via* deprotonation above their particular pKa values, which induces a swelling of the charged polymer and − when grafted to a membrane − to a decrease in pore size. Alternatively, protonation below their pKa values induces a collapse of the non-charged polymer and an increase in pore size[112]. pH-responsive membranes have been used for chemical separation processes such as for oil/water mixtures[113], for proteins[114] and metal ions[115], as well as in biotechnological applications like biosensors[116], drug delivery systems[117] or non-fouling surfaces[118].

Reports of light-responsive polymeric membranes are surprisingly rare[222]. As a stimulus, light is very attractive, since it can be applied as an external trigger[119], allowing the remote-controlled actuation of closed systems without risk of chemical contamination (Chapter 1.5). The most commonly used and best investigated photochromic moieties in polymeric materials are azobenzenes[238] and spiropyrans[101, 126] as reversible organic switches. Light-responsive

membranes have found applications in photonic devices[138], photosensitive lenses[239] and have been used for permeability[151, 152], protein adhesion[145] and drug delivery[147-149].

In this article, we demonstrate a facile approach to grafting functional polymer brushes on microporous polymeric substrates. PMAA polymer brushes were grafted from a 30-µm-thick PP membrane to endow it with pH-responsiveness. Further, an established PPM process [240] of the grafted polymer brushes with photochromic spiropyrans (SPs) was used to create light-responsive polymer brushes (PMA-SP). Changes in wettability and in permeability were analysed by means of static water contact angle (CA) and water flux measurements, respectively, upon change in pH and visible and UV-light irradiation. In addition, a switch in color and transmission for photochromic PMA-SP brushes was detected.

4.3   Results and Discussion

4.3.1   Grafting of pH-Responsive PMAA Polymer Brushes on Polymeric Substrates

In this work, we used an argon plasma source to activate a 30-µm-thick microporous polypropylene (PP) membrane and, for comparison, a flat 120-µm-thick PP film. Figure 4.1a illustrates the activation step, as well as the subsequent grafting of pH-responsive poly(methacrylic acid) (PMAA) polymer brushes from the polymeric substrates *via* free-radical polymerization (FRP).

In Figure 4.1, the grafting level (GL) – that is mass uptake of PP membrane samples after grafting of PMAA polymer brushes – is shown in dependence of the activation time with argon plasma. The GL achieved under the same reaction conditions was found to increase linearly with increasing activation time, as a consequence of an increasing radical concentration. It reached a maximum after four minutes and decreased again with longer activation time. This indicates that a very high radical density enhances side reactions in the grafting process, such as recombination of surface-bound or chain-end radicals in immediate vicinity, leading to termination of the polymerization process. Similar behavior was observed by Quing *et al.* [109] when grafting PMAA polymer brushes on PES substrates.

a)

Polypropylene (PP) → Ar Plasma activation → activated PP → MAA / 0.1 M HCl → PMAA Brushes on PP
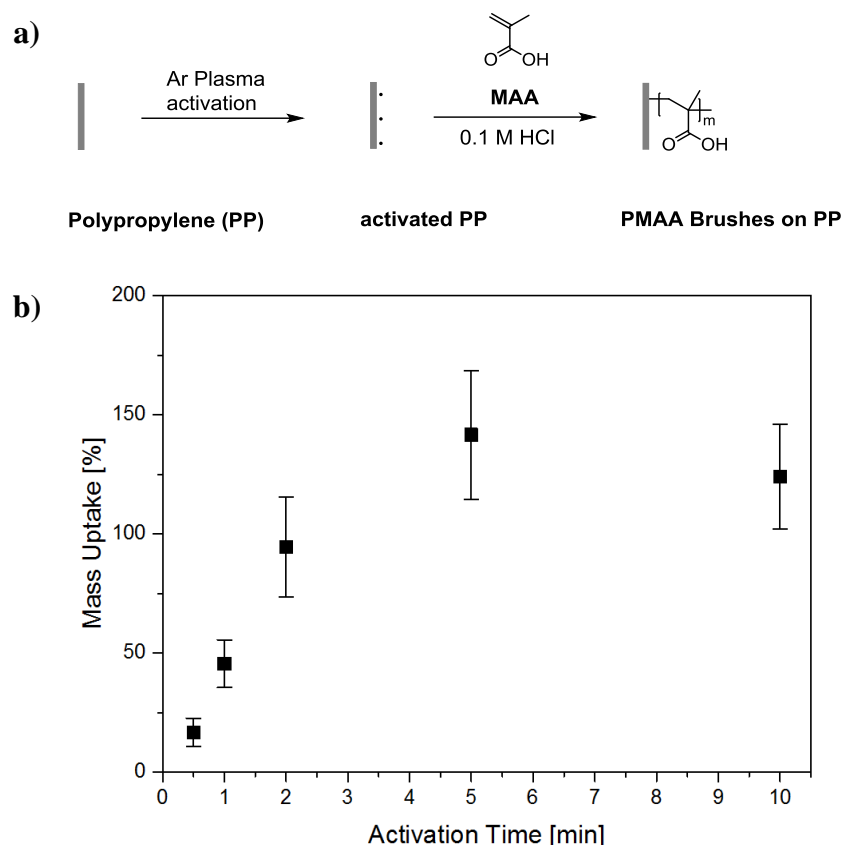
b)

Figure 4.1: Strategy for grafting of PMAA polymer brushes after one-side argon plasma activation from polypropylene (PP) substrates and (b) mass uptake of PP membranes after grafting of PMAA polymer brushes as a function of activation time.

AFM height images of a non-grafted membrane sample, as well as samples grafted under identical conditions with 30 seconds, 1 minute and 2 minute activation time are shown in Figure 4.2. With the applied FRP technique, polymer grafting led to a drastic change in morphology. With increasing GL the fibers of the pristine microporous PP membrane changed from a very delicate microporous network to an increasingly closed and brittle system. Furthermore, samples of higher GL showed optical inhomogeneity and turned opaque-crystalline.

The static water-contact angles (CAs) of grafted PMAA on both PP membrane and flat-pressed PP film samples in dependence of activation time with argon plasma have been determined (Figure A 4.1). After grafting with hydrophilic PMAA, the CA was drastically reduced from 117° to 36° for membrane and from 103° to 57° for film samples, independent of their activation time with argon plasma. The difference in CA between the membrane and film

samples is caused by their different morphology and therefore higher surface roughness of the membrane samples (Cassie-Baxter wetting).
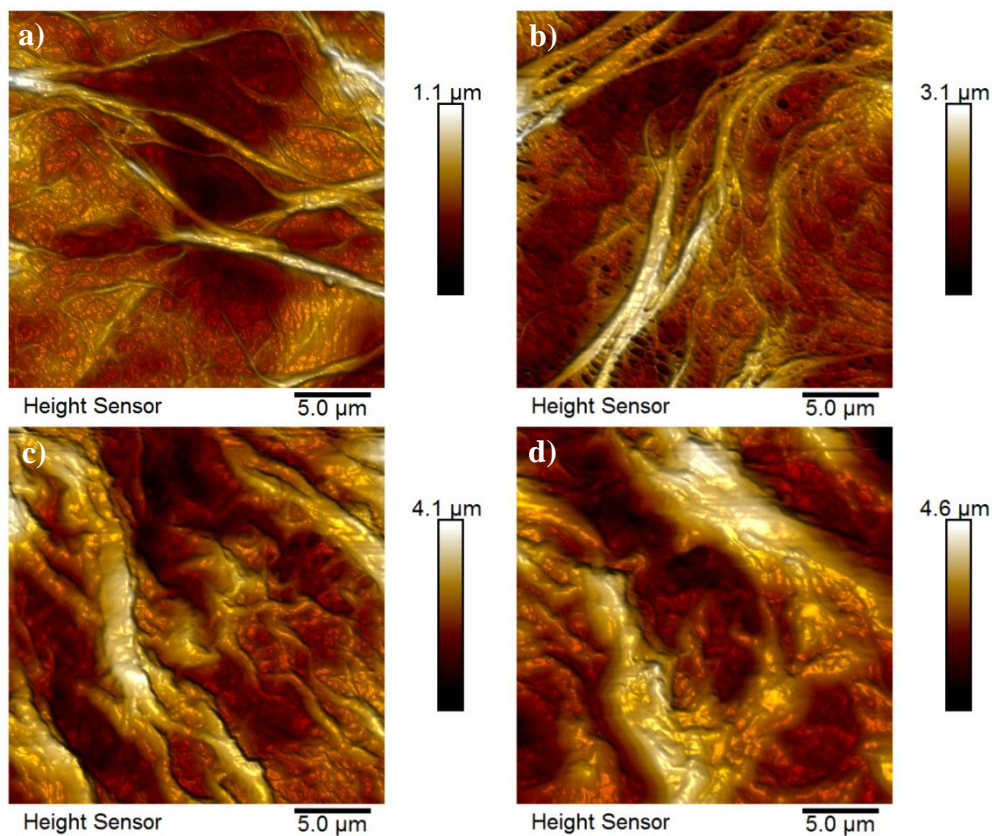

Figure 4.2: AFM images of (a) a pristine, non-grafted PP membrane and PMAA polymer brushes grafted from a PP membrane after (b) 30 seconds, (c) 1 minute and (d) 2 minutes activation time with argon plasma.

4.3.2   Switching Properties of pH-Responsive PMAA Polymer Brushes

The response of PMAA polymer brushes in terms of wettability towards different pH was analyzed by static water contact angle (CA) measurements. Figure 4.3a shows that the CA could be reversibly switched between 59° and < 10° for PP membranes and 68° and 21° for PP films, for alternating acidic and basic conditions. These changes in wettability are caused by a change in surface free energy due to reversible protonation from the more hydrophobic state (PMAA) under acidic conditions (pH 1) and deprotonation of the carboxylic acids to the very hydrophilic polyelectrolyte state (PMA$^-$) under basic conditions (pH 13). Under neutral conditions (pH 7), the

CA in both cases took up a position in between both states (36° for membranes and 58° for film samples), which could be interpreted as a configuration where the brushes are partly deprotonated to a partly charged copolymer P(MAA-*co*-MA⁻) (Figure 4.3b).

The pH-responsiveness in terms of permeability of PMAA-modified PP membranes has been determined by measurement of the flux under neutral, acidic and basic conditions and as a function of the grafting level (GL) caused by different activation times with argon plasma (Table 4.1, Figure 4.4).
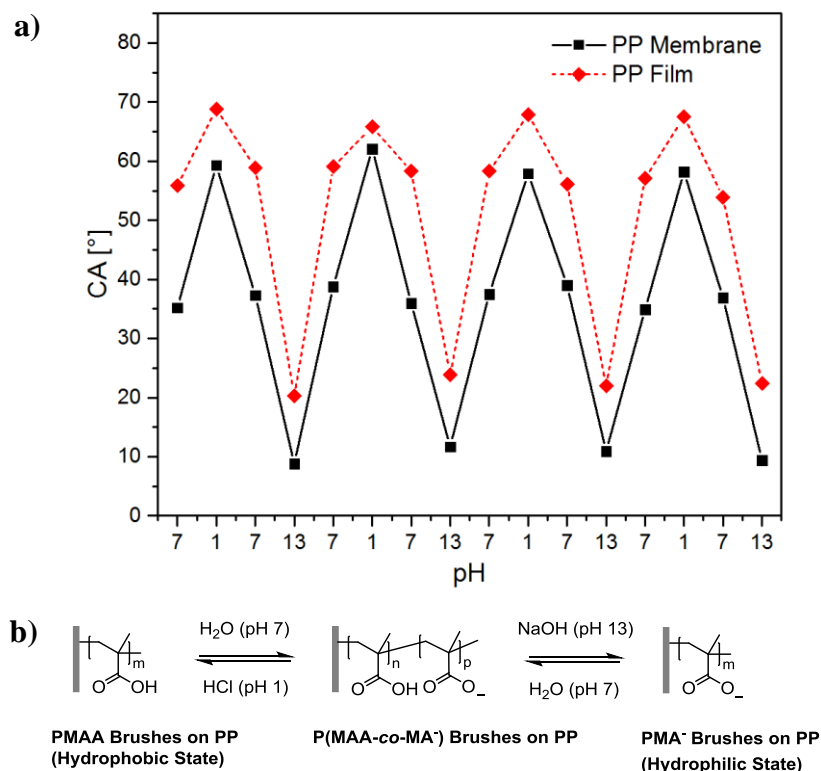

Figure 4.3: Reversible pH-induced switching (a) in static water-contact angles (CA) of PMMA brush-modified PP membrane and film surfaces measured with 3 μL water droplets between (b) the fully protonated hydrophobic state (PMAA) under acidic conditions, a partly charged copolymer state (P(MAA-*co*-MA⁻)) under neutral pH and the fully deprotonated polyelectrolyte configuration (PMA⁻) under basic conditions.

The water flux of a PMAA-grafted PP membrane with 30 seconds plasma activation $(256 \, \text{L} \, \text{m}^{-2} \, \text{h}^{-1})$ was lower compared to that of the pristine PP membrane $(306 \, \text{L} \, \text{m}^{-2} \, \text{h}^{-1})$, indicating a reduced pore size caused by the grafting of PMAA brushes. Under acidic conditions,

the flux is enhanced by roughly 30 % to 331 L m^{-2} h^{-1}, *i.e.* to a value higher than that of the pristine membrane. This effect is interpreted as deswelling of the fully protonated PMAA brushes, leading to an enhanced pore size, combined with the higher wettability of PMAA compared to PP (CA$_{PP}$ = 117 ° vs. CA$_{PMAA}$ = 36 °). Under basic conditions, the flux was strongly reduced by 63 % to 94 L m^{-2} h^{-1}, caused by the full deprotonation of the carboxylic acid moieties, causing a strong swelling of the polymer brushes (Figure 4.4). This switching under alternating pH conditions was reversible for more than 10 cycles.

	Activation time [min]				
Flux [L m^{-2} h^{-1}]	0	0.5	1	2	5
HCl	308	331	183	117	100
Relative to H$_2$O [%]		*+29*	*+23*	*+22*	*+24*
H$_2$O	306	256	149	96	81
NaOH	308	94	68	47	55
relative to H$_2$O [%]		*-63*	*-54*	*-51*	*-32*
pH Switch [%]		252	168	148	81

Table 4.1: Flux of PMMA brush-modified PP membranes in dependence of the grafting level (GL) caused by the activation time with argon plasma under different pH conditions.

With increasing GL, the water flux under neutral conditions reduced significantly, *i.e.* by more than two thirds from 256 L m^{-2} h^{-1} for 30 seconds activation time to 81 L m^{-2} h^{-1} for 5 minutes activation time. Similar trends for swelling and deswelling of the polymer brushes under basic and acidic conditions were observed in the flux for all GLs. The relative flux at low pH was roughly 20 % higher than under aqueous conditions, independent of the GL. This implies a similar deswelling of the polymer brushes, irrespective of their chain length. In contrast, the relative flux under basic conditions is more dependent on the GL. It reduced from 63 % for 30 seconds to 32 % for 5 minutes activation time, since the membrane pores became increasingly blocked. The highest magnitude of flux switching due to pH was seen at the lowest GL (252 % for 30 seconds activation), and the lowest magnitude at highest GL (81% for 5 minutes activation).
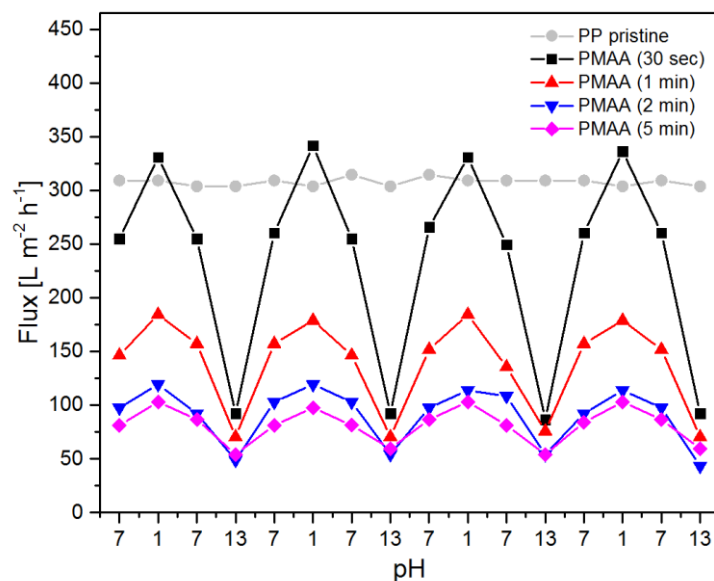
Figure 4.4: Reversible switching of the flux through PMMA brush-modified PP membranes under different pH conditions, in dependence of the grafting level (GL)—in turn a function of the activation time with argon plasma. The most intense switching is observed at a lowest grafting level.

4.3.3   Post-Polymerization of PMAA Polymer Brushes to Create Light-Responsive Substrates

To impart light responsiveness to the PP substrates, a previously established two-step post-polymerization modification (PPM) has been applied to covalently attach photochromic spiropyran (SP) moieties *via* an amine linker to activated PMAA polymer brushes (Scheme 4.1).
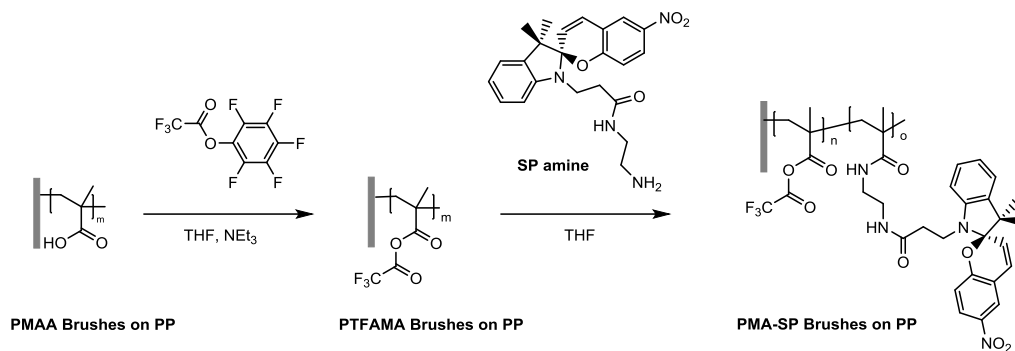
Scheme 4.1: Strategy for synthesis of light-responsive polymer brushes *via* post-polymerization modification of PMAA polymer structures on polypropylene (PP) substrates.

In brief, the carboxylic acid groups of the PMAA brushes are converted in quantitative yields into fluorinated anhydrides (PTFAMA). The activated acids allow covalent attachment of the SP amines *via* an amide formation to modify the polymer brushes up to 40 %. Detailed characterization of the grafted PMAA polymer brushes and their PPM on both PP membranes and films using attenuated total reflectance infrared (ATR-IR) microscopy and CA measurements is given in the supporting information (Figure A 4.2, Table A 4.1 and Table A 4.2).

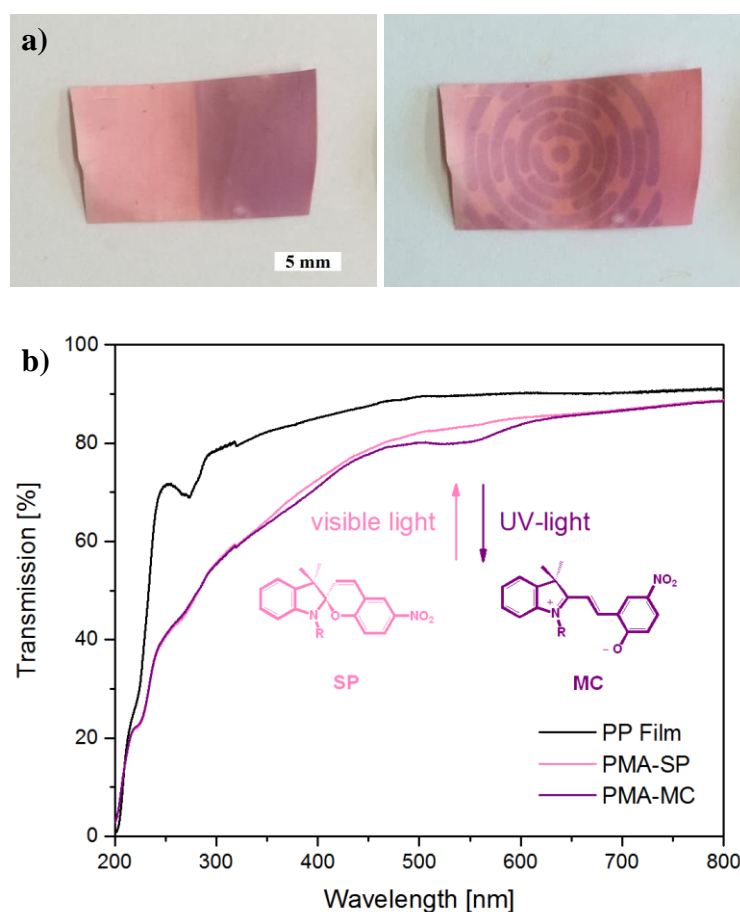### 4.3.4   Switching Properties of Light-Responsive Polymeric Substrates

Figure 4.5: (a) Optical images of consecutive light-induced color switches on a photochromic PP membrane according to the transformation of isomeric structures of ring-closed spiropyran (SP) to the zwitterionic open form of merocyanine (MC). In areas covered by different masks, weakly-pink colored PMA-SP brushes do not switch in color, while in areas exposed to UV-light the membrane appears deep-purple colored due to PMA-MC brushes. (b) Transmission spectra of thick PMA-SP brushes on a PP film, upon exposure to visible (PMA-SP) and UV-light (PMA-MC) showing the reversible switch in absorption around 570 nm.

After the PPM the PP membrane samples appeared weakly pink in color and showed a strong color switch to deep-purple when exposed to UV-light inducing the SP-MP transition (Figure 4.5a). The color change was also detected in transmission spectrometry as an absorbance band around 570 nm (Figure 4.5b).
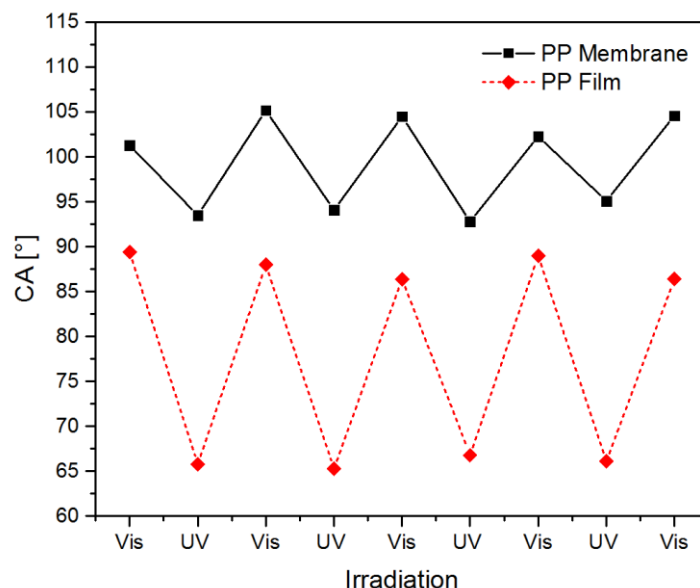

Figure 4.6: Reversible switching in static water-contact angle (CA) on a with PMA-SP-brush-modified PP membrane and film, upon alternating exposure to visible and UV-light, measured with 3 μL water droplets.

Upon alternating exposure to visible and UV-light, the static water CA of SP-modified surfaces could be reversibly switched between 88° (PMMA-SP) and 66° (PMMA-MC) on PP films and between 103° and 93° on PP membranes (Figure 4.6). The surface free energy increases with increasing dipole moment, causing a higher wettability and a lower CA. The switches in CA on both surfaces are within the range for SP-modified surfaces[240, 241]. Again, the difference in CA between the membrane and film samples is presumably an effect of their differing morphologies.

In Figure 4.7, the switching of permeability upon light exposure of photochromic PP membranes is demonstrated using flux measurements under alternating visible and UV-light irradiation. The flux increased by roughly 40 % from $306 \, \text{L m}^{-2} \text{h}^{-1}$ to $424 \, \text{L m}^{-2} \text{h}^{-1}$ after an exposure of 30 seconds with UV-light and relaxed back within 30 minutes under ambient visible

light. In contrast to the pH-dependent switch in flux, the permeability of UV sensitive the membranes appears not to be dominated by the swelling behavior of the brushes, but by the wettability switch induced by the SP-MC transition. The usually short activation time of only 30 seconds with UV-light causes an immediate difference in wetting but not in swelling. The swelling of the zwitterionic brushes would need more time to decoil and to overcome the configurational changes. The pristine and SP-modified PP membranes are very hydrophobic, while the zwitterionic MC isomers formed under UV-light irradiation favor the passage of water through the membrane. Similarly increased permeability caused by UV-light irradiation has been described by Chung *et al.*[152] for grafted SP-containing methacrylates on PTFE.
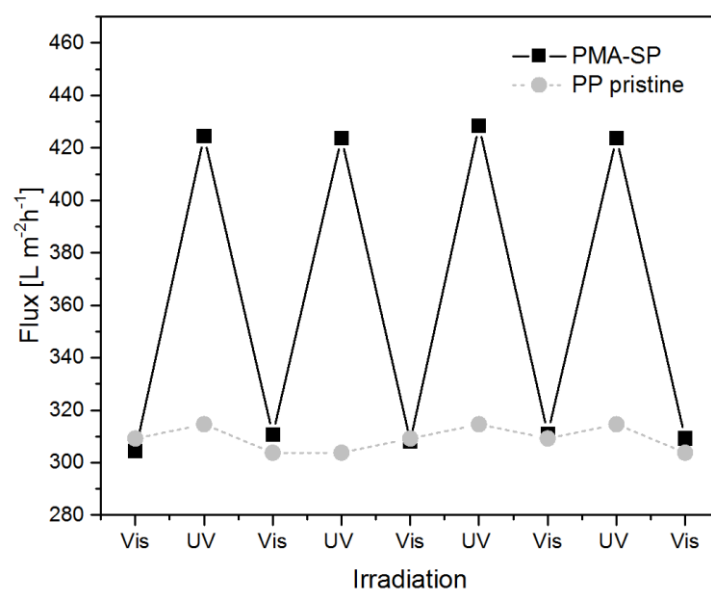

Figure 4.7: Reversible switching in water flux through a pristine and a SP-modified PP membrane under a pressure of 750 mbar upon alternating exposure to visible and UV-light.

4.4   Conclusions

A new method for the fabrication of responsive polymeric membranes has been demonstrated that uses argon-plasma activation and free-radical polymerization to graft pH-responsive PMAA polymer brushes from microporous polypropylene. It was clearly evident from ATR-IR spectra that PMAA polymer brushes had been grafted and functionalized *via* an established two-step post-polymerization modification strategy to generate photochromic

spiropyran-containing PMA-SP polymer brushes. Both PMAA and PMA-SP modified membranes were successfully shown to be smart materials that could switch in wettability and permeability in response to either pH or light as external stimulus. Switching was demonstrated using static water-contact angle and water flux measurements. In addition, photochromic PMA-SP brushes show a reversible switch in color upon alternating visible and UV-light irradiation. The flux properties of pH-switched PMAA-modified membranes were dominated by the swelling of the brushes and little influenced by the hydrophilicity of the surface. In contrast, hydrophilicity changes dominated the photon-induced switching of SP-modified membranes.

The advantage of the presented approach lies in its simplicity and versatility. The application of responsive systems to influence the hydrophilicity or pore size *via* swelling of the material is of great interest for the controlled separation or transport of dissolved species. With this in mind, a detailed understanding of the parameters that determine the reversible responses is very valuable for a wide range of researchers in surface chemistry, materials science and membrane engineering.

4.5   Appendix

4.5.1   Static Water-Contact-Angle (CA) Measurements
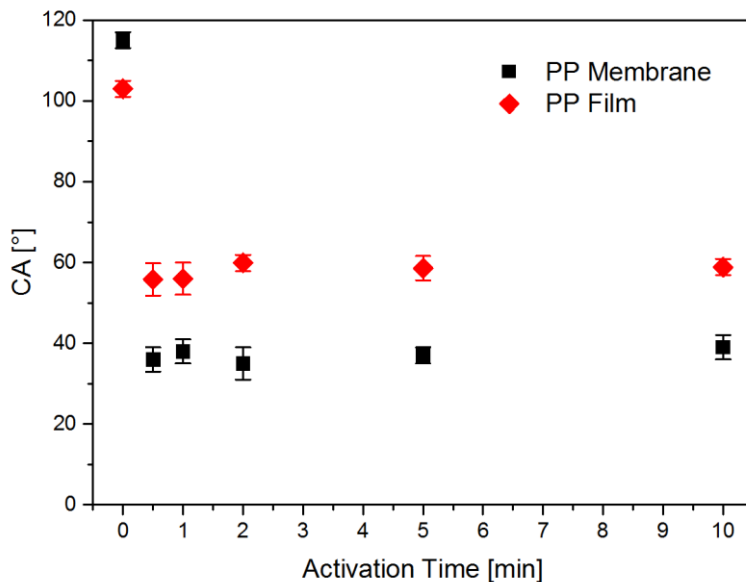

Figure A 4.1: Static water-contact angle (CA) of grafted PMAA polymer brushes on polypropylene (PP) membranes and films in dependence of activation time of the samples with argon plasma.

	static CA [°]* on PP Membranes			static CA [°]* on PP Films		
Substrate	117	±	2	103	±	2
PMAA	36	±	3	56	±	4
PTFAMA	82	±	3	92	±	2
PMA-SP	103	±	2	88	±	3
PMA-MC	93	±	2	66	±	3

*average of five measurements

Table A 4.1: Static water contact angle (CA) of substrate, grafted PMAA, PTFAMA and light-responsive PMA-SP (visible) and PMA-MC (UV-light) brushes on PP membranes and films.

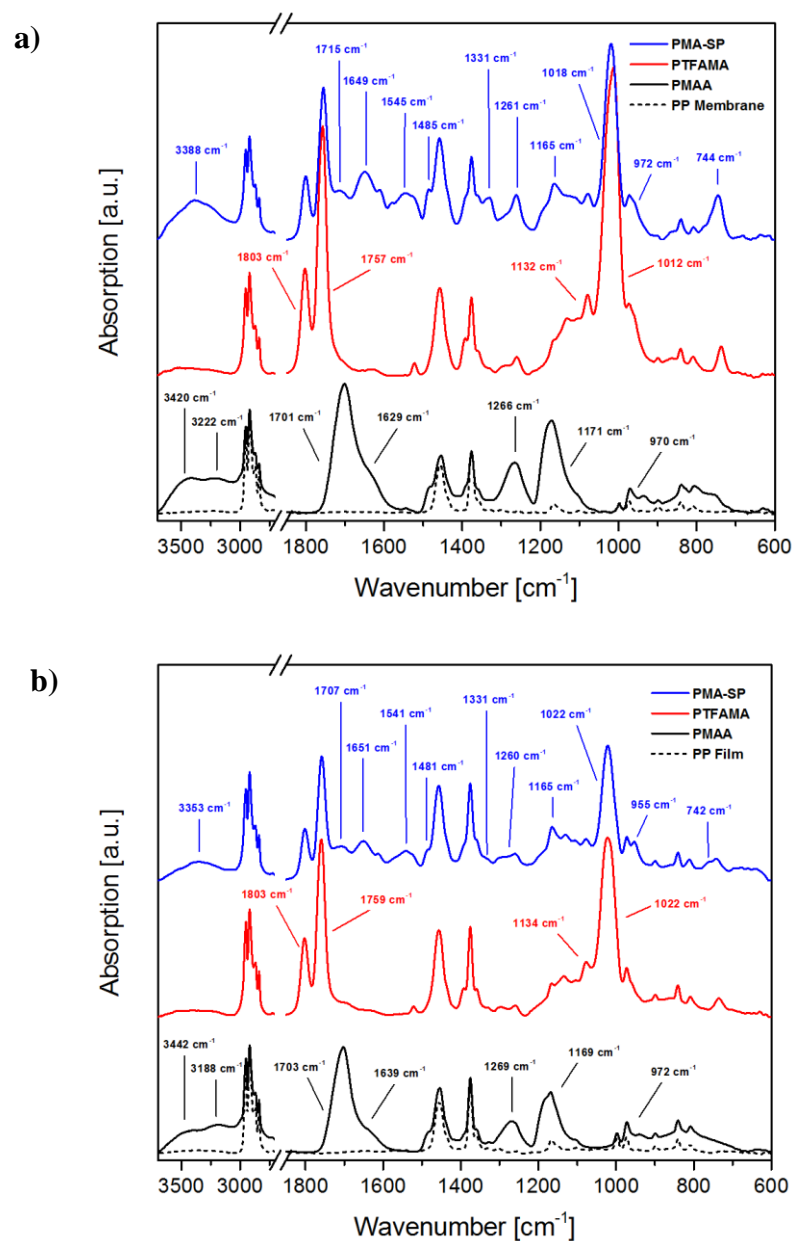4.5.2   Attenuated Total Reflectance – Infrared (ATR–IR) Spectroscopy

Figure A 4.2: ATR-IR spectra of thick PMAA, PTFAMA and spiropyran-carrying PMA-SP brush structures grafted from (a) a PP membrane and (b) a PP film, with the relevant bands marked with arrows.

		Wavenumber [cm^{-1}] PP Membrane	Wavenumber [cm^{-1}] PP Film
PMAA	υ(O-H)$_{COOH^{\cdots}H}$	3420	3442
	υ(O-H)$_{COOH}$	3222	3188
	υ(O-H)$_{COOH}$	970	972
	υ(C=O)$_{COOH}$	1701	1703
	υ(C=O)$_{COO^-}$	1629	1639
	δ(C-H)$_b$	1266	1269
	υ(C-O)$_{acyl}$	1171	1169
PTFAMA	υ(C=O)$_{anhydride}$	1803, 1757	1803, 1759
	υ(C$_{alkoxy}$-O)	1132	1134
	υ(C-F)	1012	1022
PMA-SP	υ(N-H)$_{st}$	3388	3353
	υ(C=O)$_{anhydride}$	1803, 1757	1803, 1759
	υ(C=O)$_{amide}$	1715	1707
	υ(N-H)$_{b, amide}$	1649	1651
	υ(C-H)$_{arom., metasubst.}$	972, 744	955, 742
	υ(N-O)$_{asym}$	1545	1541
	υ(N-O)$_{sym}$	1331	1331
	υ(C=C)$_{st, arom.}$	1485	1481
	υ(C$_{Ph}$-O)	1331	1331
	υ(C$_{alkoxy}$-O)	1165	1165
	υ(C-F)	1018	1022

Table A 4.2: List of signals appearing in ATR-IR spectra of thick PMAA, PTFAMA and spiropyran (SP)-carrying PMA-SP brush structures grafted from a PP membrane and a PP film.

4.5.3   Ultraviolet-visible (UV/vis) Light Spectroscopy
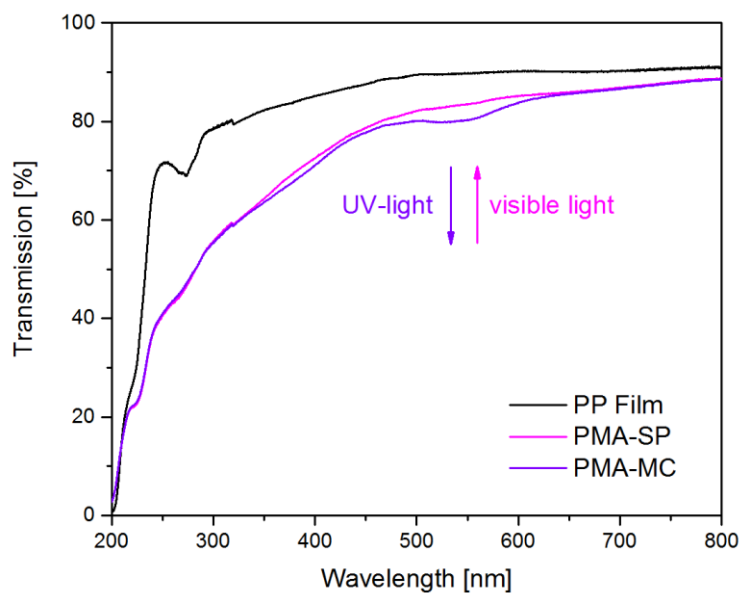

Figure A 4.3: Transmission spectra of thick PMA-SP brushes on a PP film, upon exposure to visible (PMA-SP) and UV-light (PMA-MC) showing the reversible switch in absorption around 570 nm.

5. Fabrication of Thiol-ene 'Clickable' Copolymer-Brush Nanostructures on Polymeric Substrates *via* Extreme Ultraviolet Interference Lithography[3]

5.1   Abstract

We demonstrate a new approach to grafting thiol-reactive nanopatterned copolymer-brush structures on polymeric substrates by means of extreme ultraviolet (EUV) interference lithography. The copolymer brushes were designed to contain maleimide functional groups as thiol-reactive centers. Fluoropolymer films were exposed to EUV radiation at the X-ray interference lithography beamline (XIL-II) at the Swiss Light Source, in order to create radical patterns on their surfaces. The radicals served as initiators for the copolymerization of thiol-ene 'clickable' brushes, composed of a furan-protected maleimide monomer (FuMaMA) and different methacrylates, namely methyl methacrylate (MMA), ethylene glycol methyl ether methacrylate (EGMA) or poly(ethylene glycol) methyl ether methacrylate (PEGMA). Copolymerization with ethylene glycol-containing monomers provides anti-biofouling properties to these surfaces. The number of reactive centers on the grafted brush structures can be tailored by varying the monomer ratios in the feed. Grafted copolymers were characterized by using attenuated total reflectance infrared (ATR-IR) spectroscopy. The reactive maleimide methacrylate (MaMA) units were utilized to conjugate thiol-containing moieties using the nucleophilic Michael-addition reaction, which proceeds at room temperature without the need for any metal-based catalyst. Using this approach, a variety of functionalities was introduced to yield polyelectrolytes, as well as fluorescent and light-responsive polymer-brush structures. Functionalization of the brush structures was demonstrated *via* ATR-IR and UV/vis spectroscopy, fluorescence microscopy, and was also indicated by a color switch. Furthermore, grafted surfaces were generated *via* plasma activation, showing a strongly increased wettability for polyelectrolytes and a reversible switch in static water contact angle (CA) of up to 18° for P(EGMA-*co*-MaMA-SP) brushes, upon exposure to alternating visible and UV-light irradiation.

5.2   Introduction

Patterned functional polymeric surfaces with reactive groups that can be modified under mild conditions without employing any metal catalyst open a broad field of applications and are of particular interest for the bioconjugation of polymeric materials.[164] Such patterns need to be fabricated with properties and characteristics that enable them to interact with their environment in a desired manner. Polymer brushes are ideal candidates for such applications, since polymers can be readily synthesized to be multifunctional by the incorporation of several monomers with different properties and functions.

Highly efficient reactions for post-polymerization modification (PPM) have been discussed in (Chapter 1.4). Among the so-called "click" reactions, the nucleophilic Thiol-Ene reaction is a very robust technique, which benefits from its fast reaction kinetics, usually leading to very high yields, with little or no byproduct, under ambient, non-stringent reaction conditions.[70, 71]

Thiol-reactive polymeric materials that contain maleimide groups for conjugation have been developed recently.[63, 75, 90, 242-244] Maleimides are versatile functional groups for thiol-ene reactions, as they show fast kinetics[70-74] and provide the ability to be reversibly deactivated/activated by means of Diels-Alder (DA) and retro Diels-Alder (rDA) reactions.[75-77] The thiol-maleimide reaction, which is fast, facile, and selective, has been exploited intensively for coupling functional moieties to biomolecules.[245-247] Although many examples of self-assembled monolayers of maleimide conjugates on various metallic and glass surfaces have been described,[248] reports of polymer surfaces functionalized with maleimides are rare.[249]

Maleimide-containing polymer brushes were fabricated on silicon oxide surfaces using copper-mediated atom transfer radical polymerization (ATRP).[250] This approach entails immobilization of specific radical initiators on the silicon-based substrate, followed by metal-mediated polymerization. Needless to say, development of a universal method for fabrication of thiol-reactive brushes on polymeric substrates will expand their versatility. In particular, to date, there are no reports of fabrication of thiol-reactive copolymer brushes on polymeric substrates. The rapid increase in the utilization of polymeric substrates due to their cost-effectiveness for high-throughput usage in a disposable manner necessitates the development of protocols that will allow rapid production of patterned reactive platforms on polymeric substrates, *e.g.* for biological assays.

Precise definition of domain sizes and architectures in soft-material systems provides a basis for controlling interactions of the environment with a surface. A technology for radiation-induced grafting of micro- and nanostructured polymers by free-radical polymerization (FRP) has been established in the past years.[24, 25, 217, 240]

In this approach, nanostructured patterns of polymer brushes were grafted from activated polymeric surfaces such as polyolefins and fluoropolymers. The activation was carried out *via* interference exposure with extreme ultraviolet (EUV) light. Precise control over the creation of radical patterns, down to the nanometer scale, allows grafting of nanostructured brushes in a subsequent polymerization process. The process is very simple compared to controlled radical polymerization (CRP) methods, where initiators need to be immobilized at the surface. Furthermore the FRP-approach yields periodic brush structures, even at short reaction times, with more than an order of magnitude higher thickness compared to brushes produced by CRP.[240]

Here, we demonstrate grafting of patterned copolymer-brush structures on a polymeric substrate, namely poly(ethylene-*alt*-tetrafluoroethylene) (ETFE), which could easily be functionalized at room temperature *via* metal-free thiol-ene reaction. In particular, copolymers containing furan-protected maleimide side chains as reactive groups and different pendant side chains were synthesized. In particular poly(methyl methacrylate), ethylene glycol methyl ether methacrylate and poly(ethylene glycol) methyl ether methacrylate were used as the comonomers yielding the copolymers P(MMA-*co*-FuMaMA), P(EGMA-*co*-FuMaMA) and P(EGMA-*co*-FuMaMA), where the latter two provided anti-biofouling properties to the brushes. Thereafter, activation of masked maleimide groups *via* the rDA reaction, as well as a facile fabrication of reactive surfaces *via* thiol-ene reactions was carried out. Successful modification of the patterned brushes was displayed *via* modification with different thiols generating polyelectrolytes, as well as fluorescent and light-responsive polymer-brushes on a polymeric substrate.

5.3   Results and Discussion

5.3.1   Fabrication of Patterned Copolymer Brushes *via* Interference Lithography

Patterned functional polymeric surfaces with chemoselective groups open up a broad field of applications in various areas, such as diagnostic microarray fabrication. In this work, we used an established process, which has been developed in our institute, to produce nanostructured,

functional polymer brushes showing high reproducibility in terms of achievable height-dose dependence and resolution.[24, 25, 217, 240]
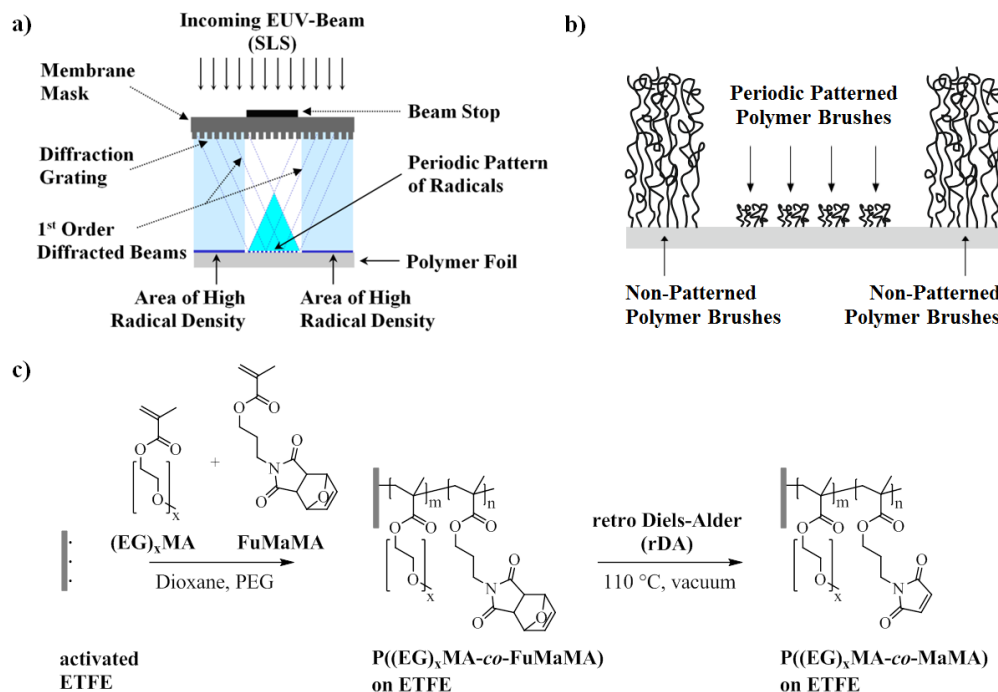

Figure 5.1: (a) Scheme of EUV interference lithography, as performed at SLS. Patterns of radicals were created by interference of photon beams (92.5 eV) diffracted at grating structures. (b)   Cross-section of non-patterned and periodic patterned polymer-brush nanostructures grafted from areas of high radical density and periodic pattern of radicals, respectively. (c) Synthetic strategy for copolymer brushes *via* grafting of P((EG)$_x$MA-*co*-FuMaMA) and the subsequent retro Diels-Alder (rDA) reaction used to activate the maleimide groups.

In Figure 5.1a, a scheme of the EUV lithographic exposure step providing the basis for grafting nanostructured polymer brushes is shown. Undulator light with a wavelength of 13.5 nm (92.5 eV) was used to crack chemical bonds and, as a consequence, to create radicals at polymer surfaces. The interference setup used creates periodic radical patterns on the surface of ETFE foils *via* diffraction at grating structures in the mask. The formed radical were used as initiators in a subsequent polymerization reaction, to graft micro- and nanostructured polymer brushes covalently from substrate polymer surfaces (Figure 5.1b). The masks used here allowed the

production of line and dot arrays or hexagonal patterns with 100 nm to 1.5 µm resolution on areas as large as 200 µm^2 based on two, four or six beam interference, respectively.

The aim of this work was the fabrication of functionalizable maleimide-containing polymer brushes on geometrically well-defined areas and with a defined thickness. For the copolymerization, we have chosen methacrylates with 0, 1 or, on average, 4.5 ethylene glycol units as side groups mixed in different ratios with the protected maleimide monomer (Figure 5.1c). This gave us control over the concentration of reactive centers in the grafted brush structures and provides additional anti-biofouling properties to these patterned surfaces.
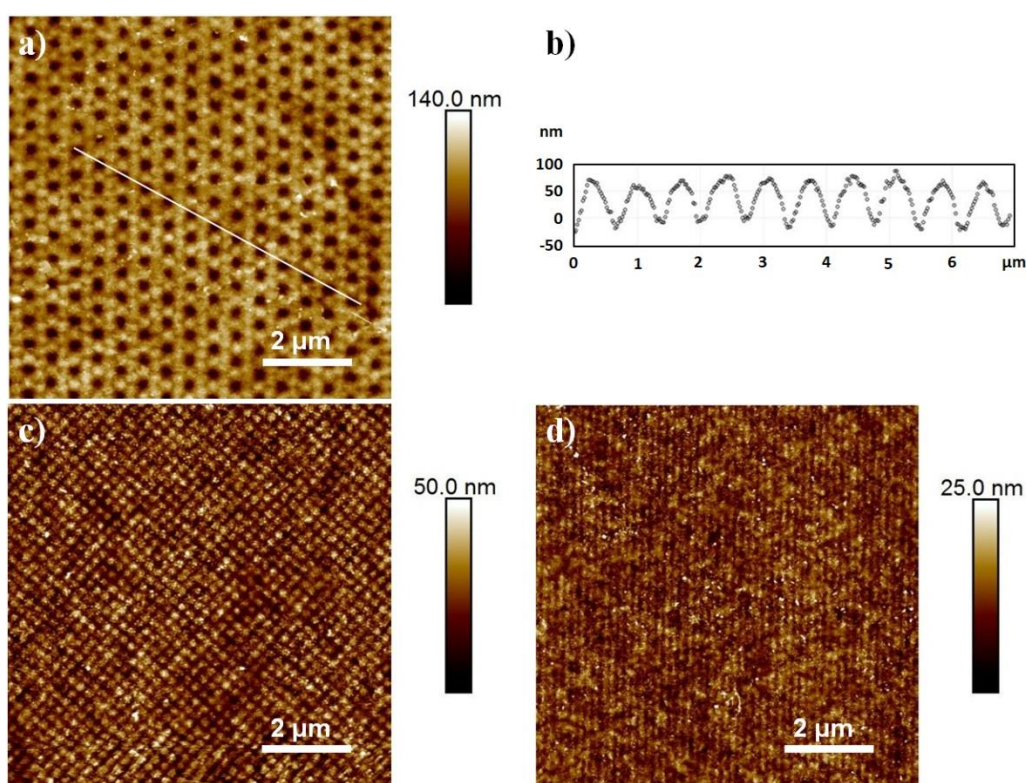

Figure 5.2: AFM images of P(EGMA-*co*-FuMaMA) copolymer nanostructures grafted from ETFE. (a) Structure with hexagonal symmetry defined by six interfering beams and (b) line profile along the line indicated in (a). High resolution structures were achieved using interference of (c) four beams, resulting dots with 280 nm period, and (d) two beams, resulting in 200 nm period lines.

Atomic force microscopy (AFM) images of areas covered with brush nanostructures grafted using free radical polymerization (FRP) are shown in Figure 5.2. Patterns were defined by

two, four or six interfering EUV-beams using the established lithography setup and grafted at an EGMA:FuMaMA-ratio of 2:1. Two interfering EUV-beams led to nanopatterned line structures, four interfering EUV-beams led to dot structures, and six interfering EUV-beam led to hexagonal structures of P(MMA-*co*-FuMaMA), P(EGMA-*co*-FuMaMA) and P(PEGMA-*co*-FuMaMA). Homogeneous copolymer hexagonal nano-patterned structures with a strong contrast could be grafted, as indicated also in the cross-section profile (Figure 5.2b). In this case cavities of 100-200 nm in diameter were formed by dots six hexagonally arranged of 650 nm in width.

Representative of all maleimide-containing copolymer combinations, P(EGMA-*co*-FuMaMA) copolymer brush structures are shown in Figure 5.2a. Furthermore, dot and line nanopatterns with a period down to 280 nm (Figure 5.2c) and down to 200 nm (Figure 5.2b), respectively could be achieved. P(MMA-*co*-FuMaMA), as well as P(PEGMA-*co*-FuMaMA) copolymer nanostructures led to similar dimensions, differing only in their dose dependence and reaction times according to their grafting behavior described before.

To gain a better understanding of the grafting kinetics, homopolymers grafted with each ethylene glycol derivate monomer were analyzed individually. Evaluation of the dry thickness of grafted micropatterns of poly(methyl methacrylate) P(MMA), ethylene glycol methyl ether methacrylate P(EGMA) and poly(ethylene glycol) methyl ether methacrylate P(PEGMA), showed a roughly square-root dependence on dose, consistent with the brush-like configuration for all three polymers (Figure A 5.1). Using FRP conditions, microstructures were accessible that exceeded 1 µm in thickness for MMA, 650 nm for EGMA and 200 nm for PEGMA brushes. These different findings for the different monomers may be explained by the polymerization kinetics, which were influenced by the number of ethylene glycol units on the monomer and therefore its size. This led to a 2 to 5 times faster grafting process for P(MMA), *i.e.* the monomer without ethylene glycol compared to P(EGMA) with one or P(PEGMA) with 4.5 ethylene glycol groups, respectively. Another aspect that may influence the grafting kinetics is the occurrence of side reactions such as hydrogen-abstraction reactions. (Oligo) ethylene glycol-based monomers bear abstractable hydrogens, which can reduce the reaction rates and yields drastically by the formation of radicals of low reactivity in the glycol side chains, leading to termination reactions[251].

5.3.2   Copolymerization of Different Methacrylates with Maleimide-Containing Monomer

The furan-protected maleimide-containing monomer (FuMaMA) was copolymerized with MMA, EGMA or PEGMA (Figure 5.1c). Polymerization temperature needed to be kept moderate (typically below 90°C) in this case in order prevent rDA reactions and to avoid *in situ* crosslinking which would result in gelation.[32]
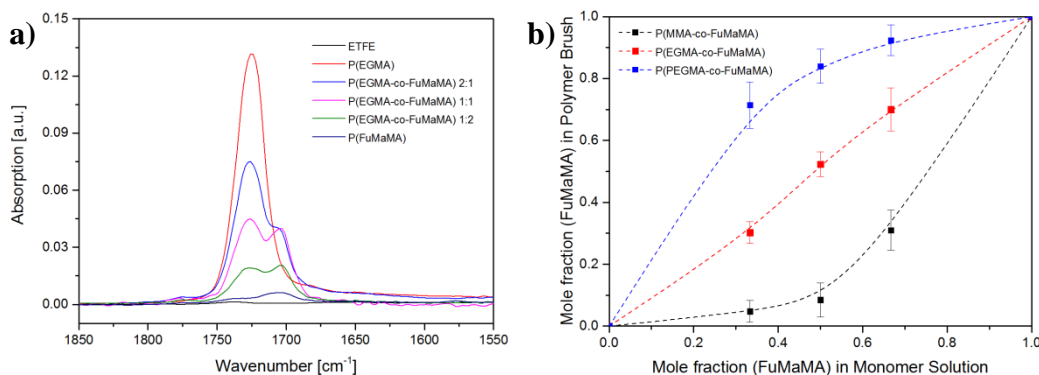

Figure 5.3: (a) ATR-IR spectra of P(EGMA), P(EGMA-*co*-FuMaMA) and P(FuMaMA) brush microstructures grafted from ETFE. (b) Mole fraction of FuMaMA in MMA, EGMA and PEGMA copolymer-brush structures grafted from ETFE in dependence of the mole fraction of FuMaMA in the comonomer solution. Determination was performed *via* the relative ratios of the carbonyl vibrations of the ester and imide groups in ATR-IR spectra.

We quantified the monomer compositions on the copolymer-brush structures *via* the intensity ratios of the carbonyl vibrations at 1726 and 1705 cm^{-1} for the ester and imide groups appearing in the ATR-IR spectra of the individual copolymers (Figure 5.3a, Figure A 5.2 and Figure A 5.3). Their relative intensities of P(MMA), P(EGMA), P(PEGMA) and P(FuMaMA) homopolymers were used to define the mole fractions of FuMaMA for having no FuMaMA on the ethylene glycol or full FuMaMA homopolymer brushes, respectively. The relative intensities for copolymers were fitted in terms of the carbonylic vibrations for esters from the backbone of the FuMaMA fraction. With increasing content of FuMaMA in the brush, the C=O vibration for esters was reduced, while that for imides was enhanced. The experimentally obtained monomer compositions of the copolymer-brush structures showed that the incorporation of the masked monomer was not equal to its mole fraction in solution. This discrepancy can be assigned to the steric hindrance of the pendant bicyclic group in the monomer. Thus, again, size appeared to

determine the stoichiometry, as two different monomer types always compete for the free radicals on the surface or in the growing chains. As a result of this, the mole fraction of FuMaMA was much lower on the P(MMA-*co*-FuMaMA) and much higher on the P(PEGMA-*co*-FuMaMA) brush structures than its mole fraction in the monomer solution (Figure 5.3b). Interestingly, when grafted in a copolymer with EGMA, the stoichiometry was almost identical to that in the monomer solution.

5.3.3   Deprotection of the Maleimides

The deprotection of the maleimide groups was achieved using a heat treatment under vacuum to remove the furan moiety *via* the retro Diels-Alder (rDA) reaction (Figure 5.1c). This reaction step is expected to be nearly quantitative.[250] It could be detected as a minor shift in the ATR-IR spectra of the imide C=O vibration of the conjugated amide rDA product (Figure A 5.4) and the appearance of strong bands at 830 and 696 cm^{-1} for cis-conjugated sp^2 C-H vibrations, respectively (Figure A 5.5).

5.3.4   Thiol-ene Functionalization of Copolymer Brushes

Our strategy was to create functionalized polymer-brush structures *via* covalent binding of different thiols to surface grafted maleimide-containing brushes *via* the thiol-ene reaction (Scheme 5.1). Effective functionalization was demonstrated by the coupling of a thiol-containing coumarin, resulting in fluorescent brushes (Figure 5.4), as well as coupling of sulfonated thiols resulting in polyelectrolytes (Figure 5.5).

Figure 5.4 shows the fluorescence images for patterned surfaces after rDA and Michael addition with blue fluorescent coumarin-thiol dye. The effective thioether formation was demonstrated *via* the strong blue fluorescence detected only on the patterns of grafted brushes, indicating a covalent attachment of the dye and the absence of physisorption on the unmodified ETFE surface. The control experiment using protected FuMaMA brush structures resulted in negligible fluorescence intensity in the structured areas (Figure 5.4b).
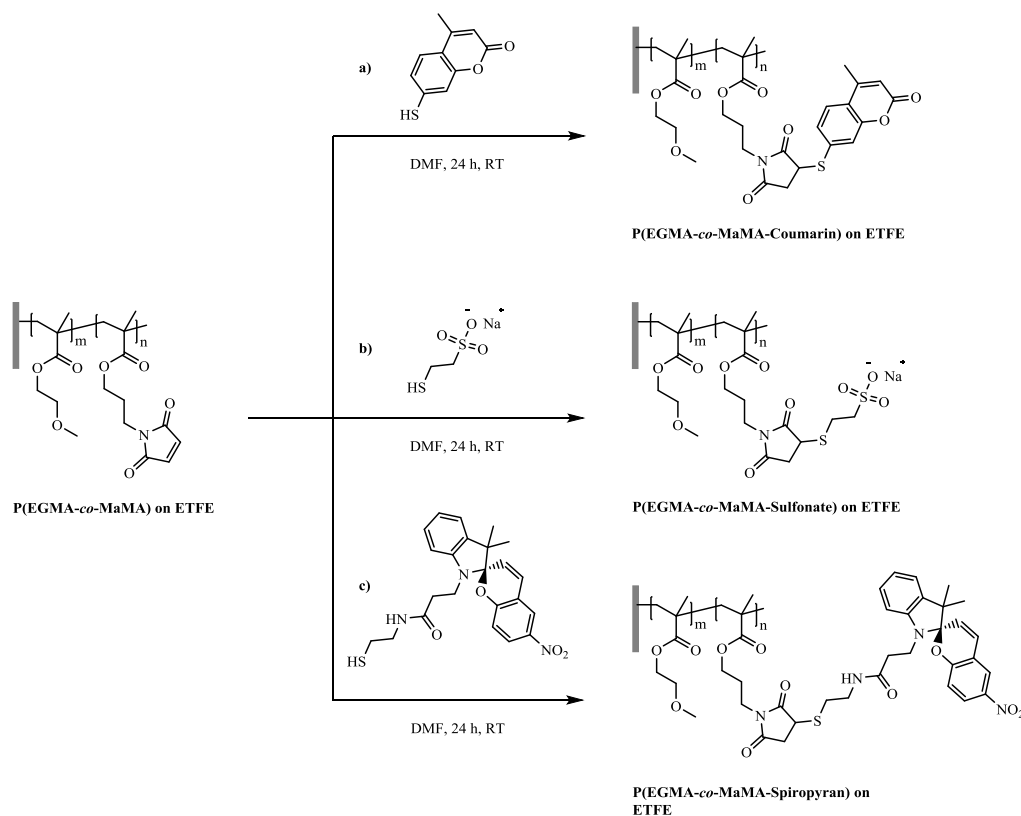
Scheme 5.1: Examples for thiol-ene post-polymerization modification of grafted P(EGMA-*co*-FuMaMA) on ETFE: (a) coumarin-containing fluorescent brushes, (b) sulfonate-containing polyelectrolytes and (c) spiropyran-containing light-responsive brushes.

In order to analyze macroscopic properties, such as the wetting behavior of mercaptoethane sulfonate (MES)-containing polyelectrolyte surfaces, ETFE foils were activated in argon plasma to create cm^2-scale areas of radicals suitable to initiate graft polymerization of P(EGMA-*co*-FuMaMA) . After modification of the maleimide-containing brushes with MES, a substantial increase in surface wettability was evident since the water contact angle decreased from 73 $^{\circ}$ to 31 $^{\circ}$, as expected from the transformation of the neutral polymer into a negatively charged polyelectrolyte brush. On the protected brush, no reaction with MES was observed (Figure 5.5). The Michael-addition of the thiols to the unprotected maleimide could also be detected *via* ATR-IR microscopy. The appearance of strong characteristic bands for the C=O, C=C and C-H vibrations of the aromatic coumarin (Figure A 5.6), as well as SO_3^- vibrations for the sulfonate (Figure A 5.7) after the thiol-ene reaction showed covalent attachment to the brush structures. Furthermore, the disappearance of the characteristic peaks at 830 and 696 cm^{-1} for cis-

conjugated sp^2 C-H vibrations demonstrated very high to quantitative yields for the hydrothiolation reactions. A detailed analysis of the IR bands is listed in Table A 5.1. In summary, the nucleophilic thiol-ene reaction offers a highly efficient and specific methodology for modification of polymeric surfaces coated with maleimide-containing polymer brushes.
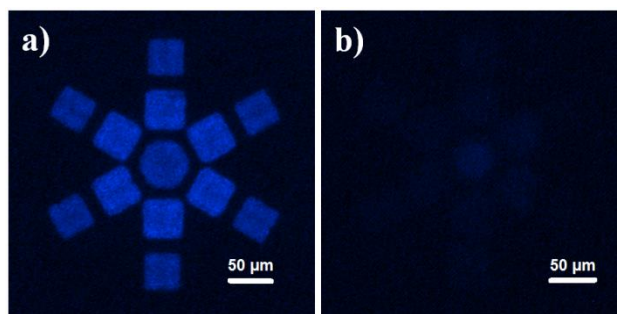

Figure 5.4: Fluorescence emission (λ_{Em} = 390 nm) of (a) coumarin-containing P(EGMA-*co*-MaMA-Coumarin) and (b) negative control of non coumarin-containing P(EGMA-*co*-FuMaMA/Coumarin) brush structures grafted from ETFE under an excitation with UV-light (λ_{Ex} = 360 nm).
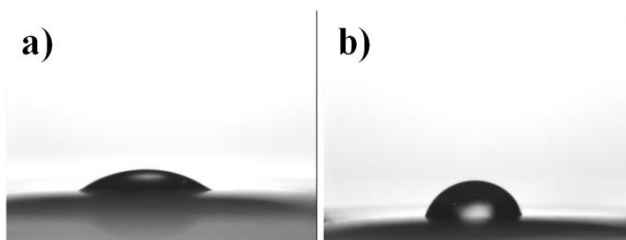

Figure 5.5: Static water contact-angle (CA) measurements on large-area brush structures of (a) sulfonate on P(EGMA-*co*-MaMA-Sulfonate) polyelectrolytes and (b) negative control of sulfonate on P(EGMA-*co*-FuMaMA/Sulfonate) brushes grafted from plasma activated 100-µm-thick ETFE foil.

To demonstrate that the copolymer brushes on a polymeric substrate can be used as a platform to fabricate a stimuli-responsive system, light-responsive spiropyran (SP)-containing polymer brush structures for smart surface applications have been created *via* conjugation of a newly synthesized thiol-containing SP to the reactive maleimide groups along the polymeric backbone (Scheme 5.1). For this purpose, ETFE foils have been irradiated on a large area with

EUV-light (92.5 eV) in an exposure without an interference mask, to achieve sufficiently thick areas to detect a visible color change (Figure 5.6).

The almost transparent SP-containing P(EGMA-*co*-MaMA-SP) brushes switched to a deeply purple color when exposed to UV-light (Figure 5.6a). The color switch could also be detected in the appearance of a strong absorbance band in the transmission spectra around 570 nm, which is in the typical range for spiropyrans (Figure 5.6b).[240] The heterocyclic spiropyrans carry a chromene moiety, which is orthogonally linked through a spiro-carbon atom. UV-light causes the reversible heterolytic cleavage of the sp^3 carbon-oxygen bond, forming the planar zwitterionic open form of the deeply colored merocyanine.[130-132]
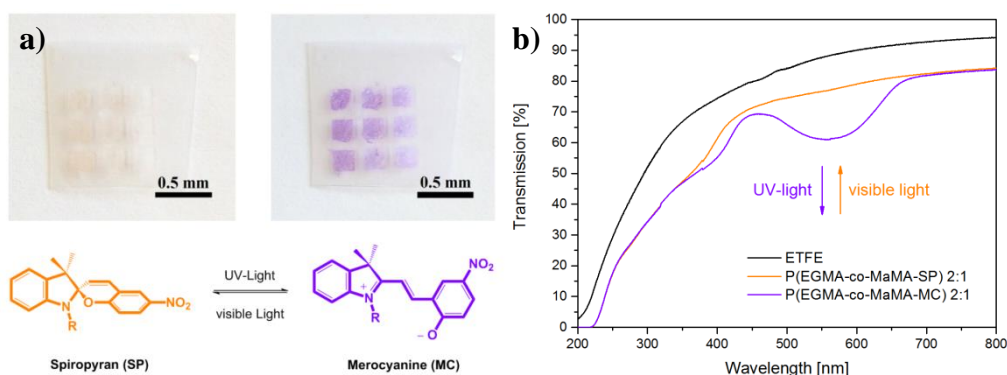

Figure 5.6: (a) Reversible color switching and (b) transmission spectra of thick micro-structured P(EGMA-*co*-MaMA-SP) brushes on ETFE upon exposure to visible and UV-light showing the reversible switch in absorption around 570 nm. The switch in color and transmission was originating from the transition of colorless spiropyran (SP) to zwitterionic merocyanine (MC).

Furthermore, sample spectra of P(EGMA-*co*-MaMA) and spiropyran-functionalized P(EGMA-*co*-MaMA-SP) brush structures acquired with ATR-IR and the listed appearing peaks with assignments can be found in the supplementary information (Figure A 5.8 and Table A 5.1). After the post-polymerization modification (PPM), strong characteristic bands for N-H and NO$_2$-stretching, as well as C-H, C=C and C-O vibrations from the aromatic skeleton of the SP could be detected. The complete disappearance of the peaks for cis-conjugated sp^2 C-H vibrations, which are characteristic for maleimides, indicated a highly efficient PPM (> 95 % yield).

In the next step, argon-plasma activation was used to graft large areas of P(EGMA-*co*-FuMaMA) brushes from ETFE foils for analyzing the switching of wettability of photoresponsive

polymer brushes. The grafting process led to an enhanced surface free energy and therefore to a more hydrophilic surface as indicated by a water-contact-angle reduction from 104° to 60° (Table A 5.2).
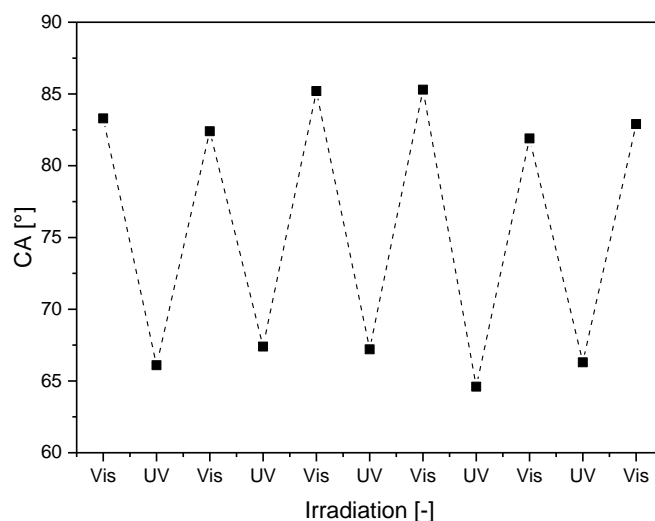

Figure 5.7: UV- and visible light- induced switching of the static contact angles of P(EGMA-*co*-MaMA-SP) brush surfaces measured with 3 μL water droplets.

The deprotection *via* the rDA to the maleimide-containing P(EGMA-*co*-MaMA) resulted in an increase of the CA to 73°, explicable by the more hydrophobic nature of the conjugated maleimide. After the binding of the spiropyran moieties yielding P(EGMA-*co*-MaMA-SP) brushes, a static contact angle of 84° was reached. The static contact angle of these modified surfaces could now reversibly be switched between 84° (P(EGMA-*co*-MaMA-SP)) and 66° (P(EGMA-*co*-MaMA-MC)) by alternating irradiation with UV and visible light. (Figure 5.7) The reversible change of up 18° was close to values observed for non-polymeric spiropyran-containing surfaces[33, 39, 219]. Switching was reversible for at least 10 cycles.

The abovementioned functionalization was carried out to demonstrate how polymeric substrates could be modified in nano-structured as well as in large-area form by using maleimide-containing copolymer brushes. The benign, metal-free polymerization and post-polymerization modification steps allowed preservation of properties of the appended functional molecules

without the threat of any metal-ion contamination. The effective functionalization in a facile manner demonstrates the versatility of this approach.

5.4   Conclusions

A method for functionalization of polymeric substrates with thiol-reactive copolymer brushes *via* extreme ultra-violet (EUV) radiation and their subsequent functionalization using nucleophilic thiol-ene conjugation was demonstrated. In particular, free-radical polymerization of masked maleimide monomers from initiator patterns created with EUV interference was used to grow brush structures, which could be deprotected and modified *via* thiol-ene coupling, to yield fluorescent, polyelectrolytic and light-responsive polymer brushes on fluoropolymer surfaces. A successful copolymerization was carried out with short (MMA), medium (EGMA) and long (PEGMA) comonomers. Grafting of furan-protected maleimide-containing copolymer brush structures of P(MMA), P(EGMA) and P(PEGMA) was clearly evident from ATR-IR spectra.

Attachment of thiols *via* thiol-ene reactions to the deprotected maleimide side chains was chemoselective and specific. Additionally, patterned, spiropyran-containing polymer brushes were demonstrated to behave as smart surfaces reacting to light as an external stimulus by switching of contact angle, fluorescence and color. The UV-light-induced wettability switch of 18° caused by spiropyran-merocyanine isomerization was in the characteristic range for spiropyran-modified surfaces.

The three presented examples of functionalization of maleimide-containing copolymer brushes on polymeric substrates demonstrate the versatility of this approach. Further expansion of the concept towards multi-functional and multi-responsive systems may for instance be achieved by copolymerization of two reactive monomers that will allow to orthogonal modification with different functional moieties.

Different activation methods have been used to control the creation of radicals on the surface, taking advantage of plasma activation for large-area activation and of the EUV interference lithography setup at the Swiss Light Source to access micro- and nanopatterns. Exposure and grafting parameters allowed us to control the grafting density and thickness of the brush structures. Furthermore, copolymerization regulated the density of the attached functional centers on the structures to help controlling other additional properties to the brushes such as hydrophobicity or hydrophilicity by varying the number of ethylene glycol moieties in the side

chains of the comonomer. Especially hydrophilic PEG-containing functional brushes will be interesting in future projects as they provide anti-biofouling properties along with the potential for selective bioconjugation.

5.5   Appendix

5.5.1   Organic Synthesis
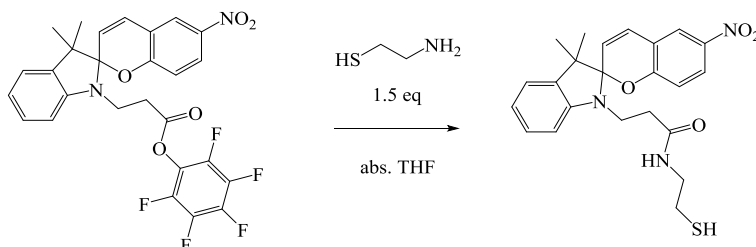
Scheme A 5.1: Synthetic route to spiropyran (SP) with thiol linker, which can be covalently bound to previously grafted maleimide-containing polymer-brush structures.

Spiropyran thiol (SP-SH): The precursor molecule SP PFP-ester (perfluorophenyl 3-(3',3'-dimethyl-6-nitrospiro[chromene-2,2'-indolin]-1'-yl)propanoate) was prepared as reported before. For the SP-SH, SP-PFP (1.50 g, 2.72 mmol) and cysteamine (0.32 g, 4.08 mmol) were diluted in 25 mL abs. THF. The reaction mixture was stirred for 2 h under argon at RT. DCM (50 mL) was added to the reaction mixture and washed five times with 50 mL H_2O. The organic layer was dried over $MgSO_4$ and the solvent removed at high vacuum receiving spiropyran thiol as yellow solid in a 94 % yield (1.12 g, 2.55 mmol). ^{1}H-NMR (300 MHz, DMSO-d_6, δ, ppm): 1.08 (s, 3 H, CH_3), 1.19 (s, 3 H, CH_3), 1.53 (s, 1 H, SH), 2.25-2.47 (m, 2 H, $NCH_2C\underline{H}_2$), 3.13 (q, 2 H, $^3J_{H,H}$ = 6.50 Hz, $SHC\underline{H}_2$), 3.19-3.38 (m, 2 H, $SHCH_2C\underline{H}_2$), 3.31-3.53 (m, 2 H, $NC\underline{H}_2CH_2$), 5.99 (d, 1 H, $^3J_{H,H}$ = 10.21 Hz, $C_q\underline{H}C$=CHPh), 6.67 (d, 1 H, $^3J_{H,H}$ = 7.51 Hz, CH_{arom}), 6.80 (t, 1 H, $^3J_{H,H}$ = 7.21 Hz, CH_{arom}), 6.86 (d, 1 H, $^3J_{H,H}$ = 9.01 Hz, CH_{arom}), 7.11 (m, 2 H, CH_{arom}), 7.20 (d, 1 H, $^3J_{H,H}$ = 10.51 Hz, C_qHC=C$\underline{H}$Ph), 7.97 (s, 1 H, NH), 8.00 (dd, 1 H, $^3J_{H,H}$ = 9.01 Hz, $^4J_{H,H}$ = 2.70 Hz, CH_{arom}), 8.22 (d, 1 H, $^4J_{H,H}$ = 2.70 Hz, CH_{arom}).; ^{13}C-NMR (300 MHz, DMSO-d_6, δ, ppm): 171.0, 159.7, 146.8, 141.0, 136.1, 128.5, 128.0, 126.1, 123.2, 122.4, 122.1, 119.6, 119.4, 115.9, 107.1, 107.0, 52.9, 42.6, 35.3, 28.4, 26.1, 23.9, 19.9;

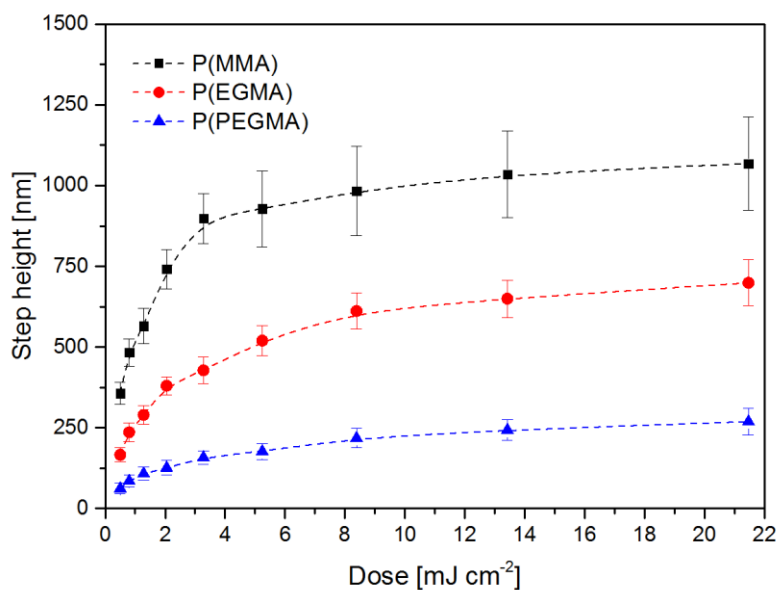## 5.5.2   Atomic Force Microscopy (AFM)

Figure A 5.1: Thickness of dry P(MMA), P(EGMA) and P(PEGMA) brush microstructures grafted from ETFE surfaces, as a function of the EUV-light (92.5 eV) irradiation dose. Step heights have been derived from AFM images in non-patterned areas of high radical density.

5.5.3   Attenuated Total Reflectance – Infrared (ATR–IR) Spectroscopy

Figure A 5.2: ATR-IR spectra of thick dry P(MMA-*co*-FuMaMA) brush microstructures grafted from ETFE.
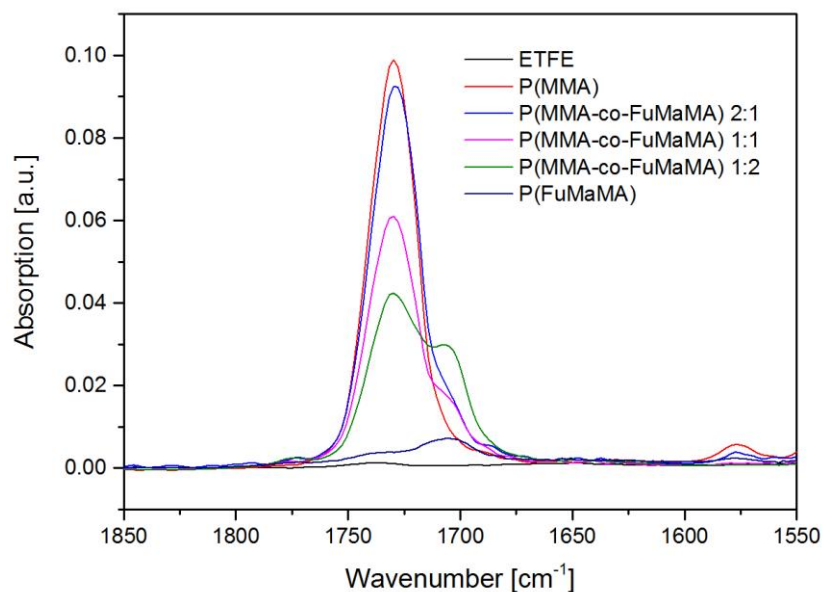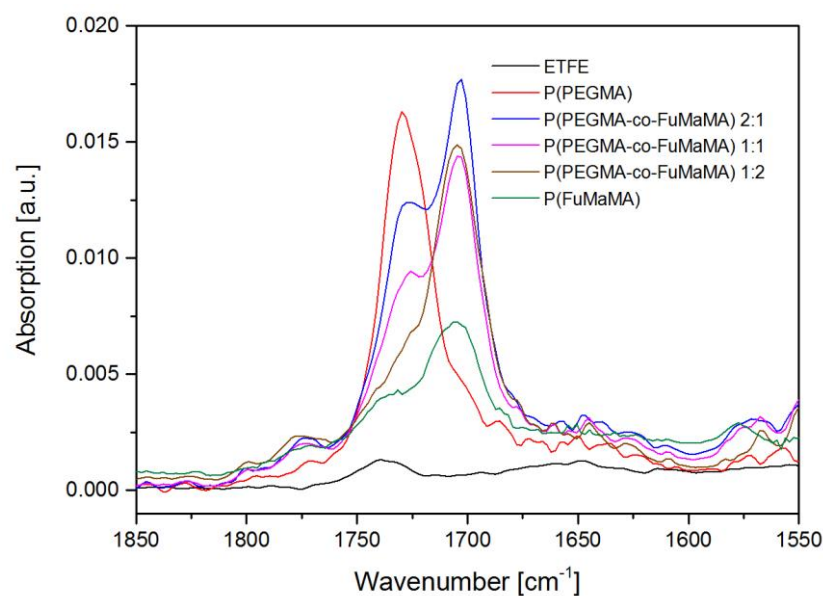

Figure A 5.3: ATR-IR spectra of thick dry P(PEGMA-*co*-FuMaMA) brush microstructures grafted from ETFE.

Figure A 5.4: ATR-IR spectra of thick dry P(EGMA-*co*-FuMaMA) (1:9) structures grafted from ETFE and the rDA product P(EGMA-*co*-MaMA) (1:9).
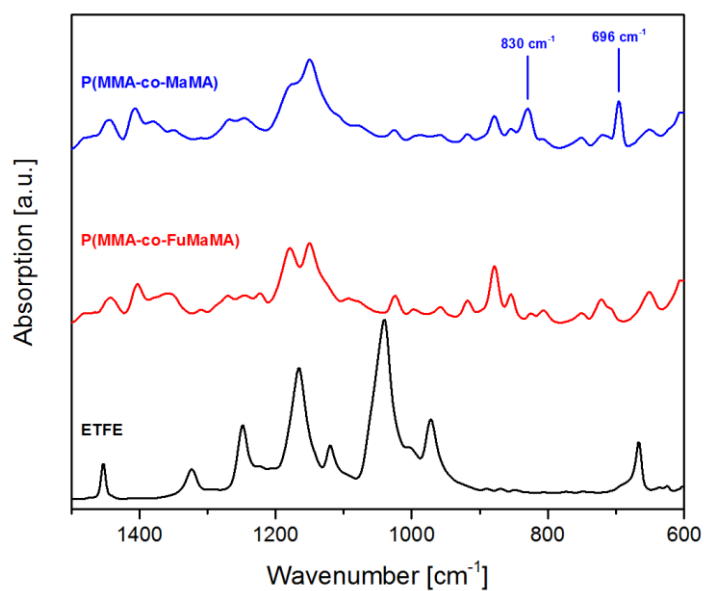
Figure A 5.5: ATR-IR spectra of thick dry P(MMA-*co*-FuMaMA) (1:9) structures grafted from ETFE and the rDA product P(MMA-*co*-MaMA) (1:9).
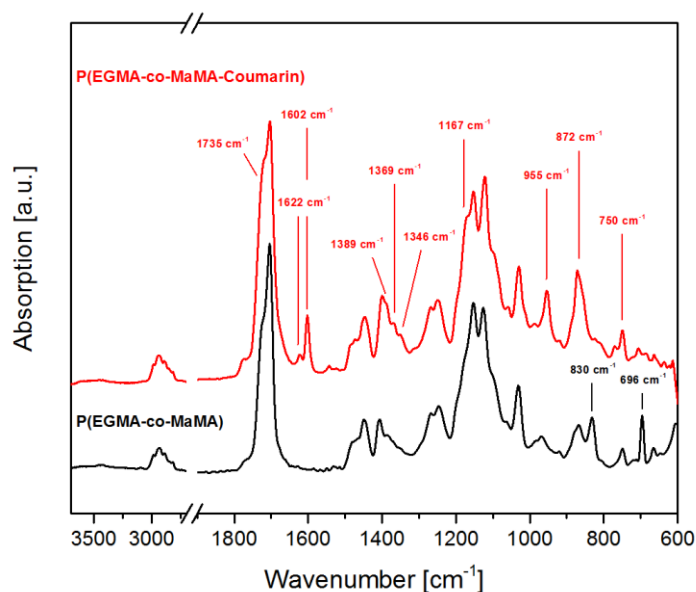
Figure A 5.6: ATR-IR spectra of thick dry P(EGMA-*co*-MaMA) (1:9) structures grafted from ETFE and the thiol-ene product P(EGMA-*co*-MaMA-Coumarin) (1:9).

Figure A 5.7: ATR-IR spectra of thick dry P(EGMA-*co*-MaMA) (1:9) structures grafted from ETFE and the thiol-ene product P(EGMA-*co*-MaMA-Sulfonate) (1:9).
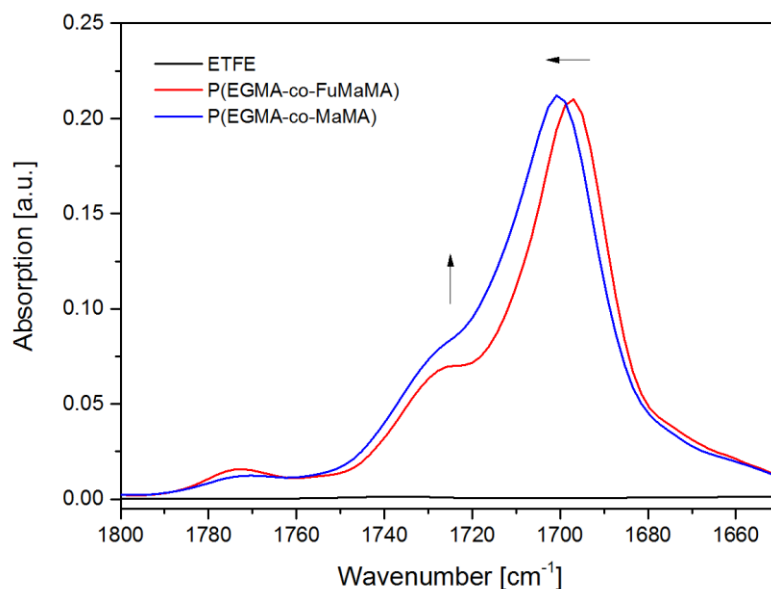
Figure A 5.8: ATR-IR spectra of thick dry P(EGMA-*co*-MaMA) (1:9) structures grafted from ETFE and the thiol-ene product P(EGMA-*co*-MaMA-SP) (1:9).
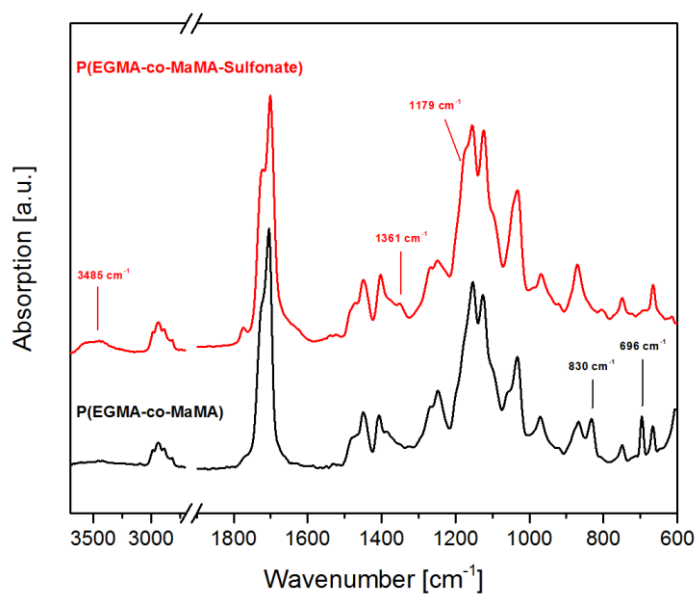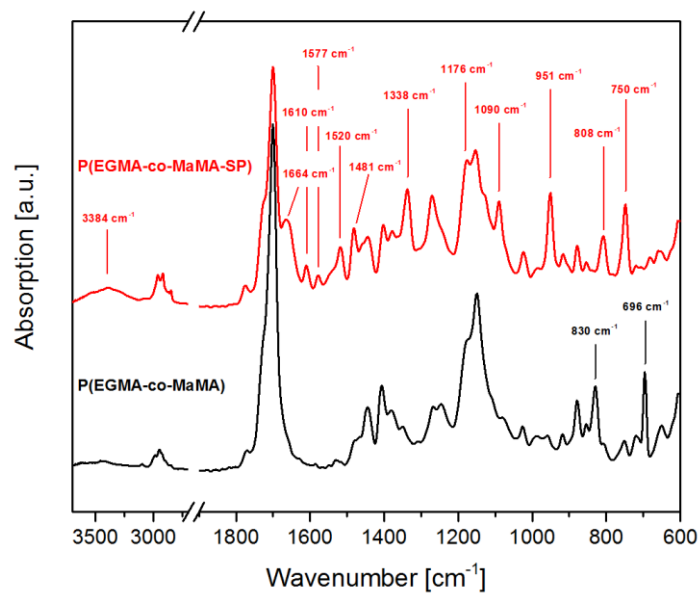
		Wavenumber [cm^{-1}]
P(EGMA-*co*-MaMA)	$\upsilon(\text{sp}^2 \text{ C-H})$	830, 696
P(EGMA-*co*-MaMA-Coumarin)	$\upsilon(\text{C-H})_{\text{st.}}$	3100 - 2800
	$\upsilon(\text{C-H})_{\text{arom.}}$	955, 872, 750
	$\upsilon(\text{C=O})_{\text{arom. ester}}$	1735
	$\upsilon(\text{C=O})_{\text{ester}}$	1726
	$\upsilon(\text{C=O})_{\text{amide}}$	1705
	$\upsilon(\text{C=C})_{\text{st. arom.}}$	1622, 1602
	$\delta(\text{C-H})$	1389, 1369, 1346
	$\upsilon(\text{C-O})_{\text{arom.}}$	1167
P(EGMA-*co*-MaMA-Sulfonate)	$\upsilon(\text{OH})_{\text{st.}}$	3485
	$\upsilon(\text{SO}_3\text{Na})_{\text{st. asym. + sym.}}$	1361, 1179
P(EGMA-*co*-MaMA-SP)	$\upsilon(\text{N-H})_{\text{st.}}$	3384
	$\upsilon(\text{C=O})_{\text{ester}}$	1726
	$\upsilon(\text{C=O})_{\text{amide}}$	1705
	$\upsilon(\text{N-H})_{\text{b. amide}}$	1664
	$\upsilon(\text{C-H})_{\text{st.}}$	2330 - 2850
	$\upsilon(\text{C-H})_{\text{arom., metasubst.}}$	951, 838, 750
	$\upsilon(\text{N-O})_{\text{st. asym. + sym.}}$	1520, 1338
	$\upsilon(\text{C=C})_{\text{st. arom.}}$	1481
	$\upsilon(\text{C}_{\text{Ph}}\text{-O})$	1176
	$\upsilon(\text{C}_{\text{alkoxy-}}\text{O})$	1090

Table A 5.1: List of signals appearing in ATR-IR spectra of thick P(EGMA-*co*-MaMA), coumarin-carrying P(EGMA-*co*-MaMA-Coumarin), sulfonate-carrying P(EGMA-*co*-MaMA-Sulfonate) and spiropyran-carrying P(EGMA-*co*-MaMA-SP) brush structures grafted from ETFE.

5.5.4   Static Water-Contact-Angle (CA) Measurements

	static CA [°]* on ETFE		
Substrate	104	±	2
P(EGMA-*co*-FuMaMA)	60	±	2
P(EGMA-*co*-MaMA)	73	±	3
P(EGMA-*co*-MaMA-SP)	84	±	3
P(EGMA-*co*-MaMA-MC)	66	±	3

*average of five measurements

Table A 5.2: Static water contact-angle (CA) measurements of 100 µm thick ETFE foils, without polymer structures, and with grafted dry P(EGMA-*co*-FuMaMA), P(EGMA-*co*-MaMA) and spiropyran-carrying P(EGMA-*co*-MaMA-SP) structures under visible light (MaMA-SP) and UV-light (MaMA-MC).

6.   Light-Switching of Enzymatic Activity on Orthogonally Functionalized Polymer Brushes[4]

6.1   Abstract

We demonstrate light-controlled enzymatic activity on orthogonally functionalized polymer brushes. A new approach has been used to graft amine- and thiol-reactive copolymer-brush structures on polymeric substrates. The copolymer brushes were designed to incorporate epoxide and maleimide functional groups as amine- and thiol-reactive centers, respectively. ETFE films were exposed to extreme ultraviolet (EUV) light, in order to create radical patterns on their surfaces. The radicals served as initiators for the copolymerization of orthogonally functionalizable brushes, composed of glycidyl methacrylate (GMA) and furan-protected maleimide (FuMaMA) monomers in different ratios. The epoxides were utilized for chemoselective bio-conjugation of microperoxidase-11 (MP-11) *via* an amine linker and activated maleimides to conjugate photochromic spiropyran (SP) thiols using the nucleophilic Michael-addition reaction. The grafted copolymer synthesis and their post-polymerization modifications were demonstrated *via* ATR-IR and UV/vis spectroscopy, as well as with static water-contact-angle measurements. Enzymatic activity was illustrated *via* a MP-11-catalyzed oxidation of colorless 3,3',5,5'-tetramethylbenzidine (TMB) diamine to deep-blue colored TMB diimine. A light-induced switch in the enzymatic turn-over of TMB was detected and quantified by means of UV/vis spectroscopy. A dramatic change according to exposure to either visible or UV-light allowed us to control the enzymatic activity of fabricated photochromic bio-conjugated P(GMA-MP-11-*co*-MaMA-SP) copolymer brushes grafted from polymeric substrates.

6.2   Introduction

Smart, bio-conjugated surfaces are of great interest, as they allow stimulus-induced switching of bio-functionality on demand, based on their responsiveness to a certain trigger, such

---

[4] This chapter is the basis for a manuscript to be submitted to Nature Materials. The experimental part has been integrated in Chapter 2. The supplementary information has been added as an appendix at the end of this chapter.

as temperature[252], pH[253], magnetic fields[254], enzymatic activity[255] or light[240]. Reports of stimuli-responsive bio-conjugated systems have been summarized in Chapter 1.6. Most often, control over bioactivity has been achieved by means of changes in pH or temperature. Reports of light as the remote-control element, on the other hand, have been surprisingly rare. Light as an external stimulus has the advantages of spatial and temporal control without suffering from diffusion effects, as it can be directed and delivered to distant locations and applied instantaneously under specific conditions with high accuracy (Chapter 1.5). Light can reversibly be switched on and off and allows tuning of the response *via* its wavelength and intensity.[256]

The first example of actual control over enzymatic activity on surfaces with light was described by Poloni *et al.*[206], who used UV-light to deactivate lipase, which was immobilized on an azobenzene-containing SAM-modified quartz surface. However, the lack of flexibility of the SAM and the direct connection of the chromophore to the enzyme limited the reversibility of the process due to deformation of the active center of the lipase and, as a consequence, irreversible deactivation of the enzyme.

Here we report the grafting on polymeric substrates of copolymer-brush structures that provide both amine- and thiol-reactive units suitable for chemoselective orthogonal PPM. Patterns of radicals serving as initiators were created by exposure of ETFE films to extreme ultraviolet light using the X-ray interference lithography beamline at the Swiss Light Source. EUV-light was chosen as an activation method as it generates very high radical densities and consequently very homogenously grafted polymer-brush structures. Furthermore, high-resolution patterns may be generated using interference exposures with EUV light. However, in principle other radical-formation methods, such as argon and helium plasma-activation, or exposure to less-powerful UV-light sources could be applied in this process.

Free-radical polymerization (FRP) was used to graft orthogonally functionalizable copolymers containing epoxide (glycidyl methacrylate, GMA) and furan-protected maleimide (FuMaMA) groups as side chains. The removal of the furan protecting group after polymerization *via* a retro Diels-Alder (rDA) reaction yields chemoselective thiol-reactive maleimide groups.

Multifunctional smart surfaces were fabricated in an orthogonal two-step PPM using, first, the amine-epoxide reaction for bio-conjugation of microperoxidase-11 (MP-11) chemoselectively to GMA and, second, the nucleophilic thiol-ene reaction to covalently attach photochromic spiropyran (SP) moieties to activated maleimides. Microperoxidase-11 (MP-11) is a fragment of ferric heme enzyme cytochrome c (CytC) with the heme group covalently bound

via two thioether bonds to the amino acid residues 11-21. It catalyzes the oxidation of a variety of substrates by hydrogen peroxide.[257] Though the peroxidase activity of a heme peptide is lower than that of intact peroxidase[258], MP-11 is much smaller in size (1.9 kDa), allowing us to bind a much higher density of catalytic active centers onto grafted brushes.

A reversible light-induced switch in enzymatic activity of P(GMA-MP-11-*co*-MaMA-SP) copolymer brushes was demonstrated *via* MP-11-catalyzed oxidation of colorless 3,3'5,5'-tetramethylbenzidine (TMB) diamine to deep-blue-colored TMB diimine.

6.3   Results and Discussion

6.3.1   Fabrication of Orthogonally Functionalizable Copolymer Brushes

Extreme ultraviolet (EUV) lithography was used for activating polymeric surfaces. Chemical bonds in the parent material were cracked using undulator light with a wavelength of 13.5 nm (92.5 eV), causing radical formation near the polymer surfaces, which allowed grafting of orthogonally functionalizable copolymer brushes in a subsequent free-radical polymerization (FRP) process. This process has been established in our institute in recent years[24, 25, 217, 240, 241].

To fabricate orthogonally functionalizable polymer brushes, it was necessary to copolymerize two functional monomers, which allowed chemoselective post-polymerization modification (PPM) of the brush structures. As monomers, we chose glycidyl methacrylate (GMA) in different ratios with a furan-protected maleimide monomer (FuMaMA) (Figure 6.1a). In order to prevent retro Diels-Alder (rDA) reactions of the furan-protected maleimides and to avoid *in situ* crosslinking (gelation)[244] during the polymerization process, the temperature needed to be maintained below 90 °C. The grafting level was analyzed by varying the monomer ratios of GMA to FuMaMA in the grafting solution. The dry thickness of grafted brush patterns of homopolymers P(GMA) and P(FuMaMA), as well as for P(GMA-*co*-FuMaMA) copolymers showed a square-root dependence on dose, as assessed by means of atomic force microscopy (AFM) (Figure 6.1b). The dry thickness of P(GMA) exceeded 2 μm and reduced with increasing concentration of FuMaMA in the monomer feed, resulting in only 100 nm thickness for P(FuMaMA) homopolymer brushes. This grafting behavior was dominated by the grafting kinetics of the two different monomers and is in good agreement with our previous findings for ethylene-containing copolymer brush structures[241].
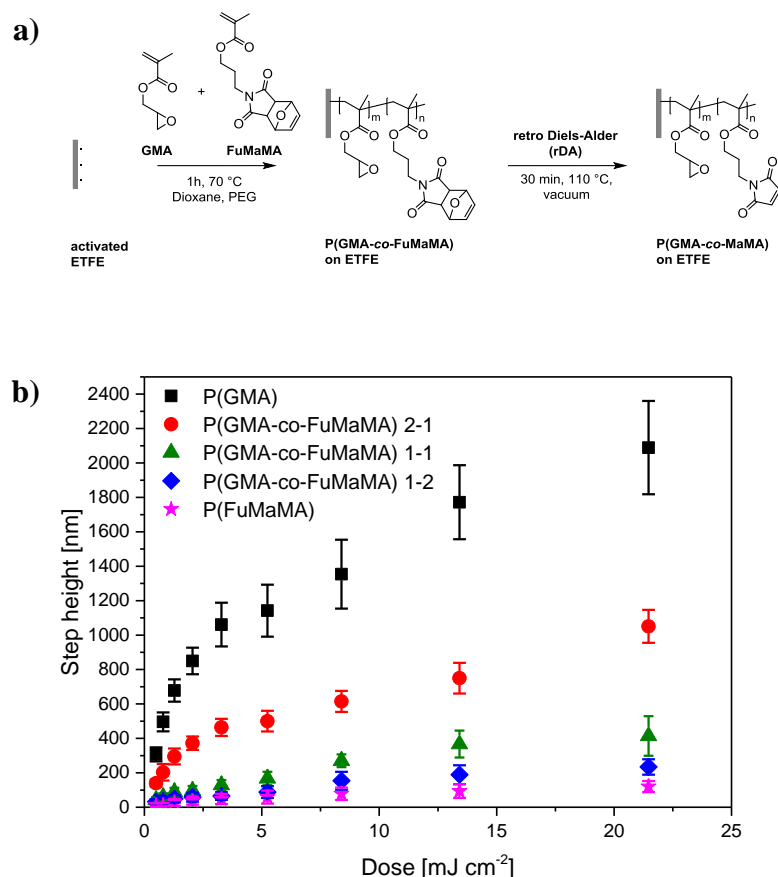
Figure 6.1: (a) Synthetic strategy for orthogonally functionalizable copolymer brushes *via* grafting of P(GMA-*co*-FuMaMA), with a subsequent retro Diels-Alder (rDA) reaction used to activate the maleimide groups. (b) Thickness of dry P(GMA), P(GMA-*co*-FuMaMA) and P(FuMaMA) brush microstructures grafted from ETFE surfaces, as a function of the EUV-light (92.5 eV) irradiation dose.

For quantification of the monomer compositions on the copolymer-brush structures, the intensity ratios of the carbonyl vibrations for the ester and imide groups, appearing in the IR spectra at 1728 and 1704 cm^{-1}, respectively, were analyzed using the relative intensities of P(GMA) and P(FuMaMA) homopolymers as reference values (Figure 6.2a). The experimentally obtained stoichiometry of the copolymer-brush structures showed that the incorporation of the masked monomer was almost equal to its mole fraction in solution (Figure 6.2b).

The deprotection of the maleimide groups was achieved using a heat treatment under vacuum to remove the furan moiety *via* the retro Diels-Alder (rDA) reaction (Figure 6.1a). This reaction step is expected to be nearly quantitative[250]. The activation led to a minor shift of the

imide C=O vibration of the conjugated amide rDA product in the IR spectra characteristic for FuMaMA/MaMA transformations[241] (Figure A 6.1), as well as to a change in wettability as the static water contact angle (CA) changed from 68° to 83° (Table 6.1). In order to ascertain that this treatment was not causing a ring-opening reaction of the epoxides of GMA, P(GMA) homopolymers were analyzed before and after the same treatment (Figure A 6.2). The IR spectra of P(GMA) showed no significant difference in a reduction of C-O-C vibrations or additional vibrational bands for newly formed OH groups, indicating the stability of these repeat units for the employed rDA conditions.
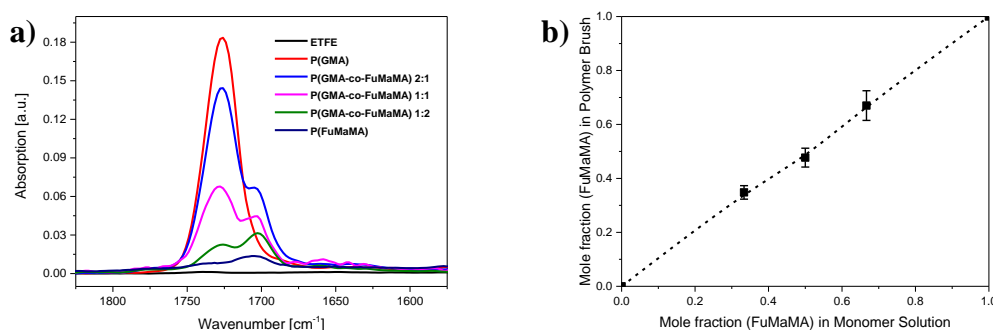

Figure 6.2: (a) ATR-IR spectra of P(GMA-*co*-FuMaMA) brush microstructures grafted from ETFE and (b) the mole fraction of FuMaMA in GMA copolymer-brush structures grafted from ETFE in dependence of the mole fraction of FuMaMA in the comonomer solution. The data were obtained from the relative areas of the carbonyl peaks of the ester and imide groups in the ATR-IR spectra.

6.3.2   Orthogonal Functionalization

Our strategy was to create multi-functionalized polymer-brush structures *via* chemoselective covalent conjugation of microperoxidase-11 (MP-11) and spiropyran (SP) to grafted P(GMA-*co*-MaMA) copolymer brushes (Scheme 6.1a). The lysine residue in the peptide chain of MP-11 was used as flexible linker (Scheme 6.1b) for chemoselective binding to epoxides of GMA in an initial PPM step – note that that the amine-epoxide reaction was carried out in presence of de-protected maleimides. The very high efficiency of this PPM step was demonstrated *via* the disappearance of the C-O-C vibration from the ether-like epoxides and the

appearance of strong vibrations for OH, as well as for NH and C=O for amides in the IR spectrum corresponding to the ring-opened epoxides and surface-bound MP-11 (Figure A 6.3, Table A 6.1). High chemoselectivity for the amine-epoxide vs the amine-maleimide reaction was achieved by short reaction times, moderate reaction temperatures and low concentration of the amine, reducing side reactions of MP-11 with the activated MaMA (Figure A 6.4).
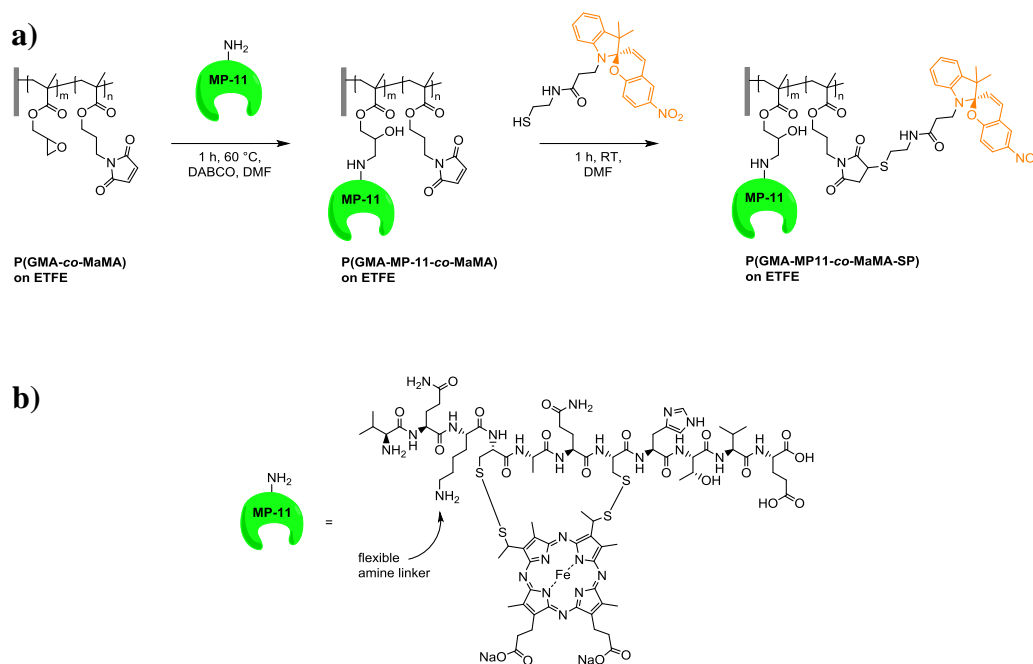
Scheme 6.1: (a) Synthetic strategy for chemoselective post-polymerization modification of orthogonally functionalizable copolymer brushes to covalently attach microperoxidase-11 (MP-11) *via* epoxide-amine and photochromic spiropyran (SP) *via* thiol-ene reactions to P(GMA-*co*-MaMA) brush structures. (b) Chemical structure of MP-11 with the flexible amine linker, allowing conjugation to epoxides.

The low reactivity of maleimides towards MP-11 lysine residues was confirmed in a control experiment. A grafted P(EGMA-*co*-MaMA) copolymer, carrying unreactive ethylene glycol side chains instead of epoxide moieties, was treated under the same reaction conditions. The absence of significant changes in color or in the IR spectra indicated no covalent attachment to the maleimide groups under these reaction conditions. The ethylene glycol-containing copolymer brushes were chosen, as they exhibit a chemical similarity and identical brush dry

thickness to the epoxide-containing brushes, providing a comparable environment for MP-11 to diffuse through the polymeric system.

	static water CA [°]*		
Substrate	104	±	2
P(GMA-*co*-FuMaMA)	68	±	2
P(GMA-*co*-MaMA)	83	±	3
P(GMA-MP-11-*co*-MaMA)	72	±	4
P(GMA-MP-11-*co*-MaMA-SP)	86	±	2

*average of five measurements

Table 6.1: Static water contact angle (CA) of the pristine substrate, grafted P(GMA-*co*-FuMaMA), activated P(GMA-*co*-MaMA), enzyme-carrying P(GMA-MP-11-*co*-MaMA), and light-responsive P(GMA-MP-11-*co*-MaMA-SP) brushes on 100-µm-thick ETFE films.

In a second chemoselective PPM step, SP-thiol was bound to the unreacted maleimides on MP-11-containing P(GMA-MP-11-*co*-MaMA) brushes using the thiol-ene reaction under ambient conditions. Under these reaction conditions, thiols usually do not react with epoxides, as demonstrated in the IR spectra of P(GMA)/SP (Figure A 6.5), which show no significant change after the SP-thiol treatment. This indicates that no covalent attachment of SP-SH to epoxides has occurred, and therefore implies chemoselective attachment of SP-SH to maleimide and not to unreacted epoxide groups in P(GMA-MP-11-*co*-MaMA) copolymers under these reaction conditions. The effectiveness of the nucleophilic thiol-ene reaction was shown in a previous publication[241]. An earlier approach, in which we tried to bind SP-thiols first to P(GMA-*co*-MaMA) and MP-11 in a subsequent PPM step did not provide multifunctionality on the copolymer brushes, as SP moieties seemed be cleaved off by the MP-11 in solution.

Additionally, in order to verify the efficient orthogonal PPM of the grafted polymer brushes, macroscopic properties – such as the wetting behavior – were analyzed using static water-contact-angle (CA) measurements. Table 6.1 shows the corresponding CA changes upon grafting of P(GMA-*co*-FuMaMA) brushes, as well as for activation and for each PPM step of the polymer-brush structures. The changes are well in line with grafting the copolymer to a very hydrophobic substrate (-36°), detachment of the polar furanyl unit (+15°), binding of hydrophilic MP-11 (-11°) and of only slightly polar SP (+14°). In summary, the amine-epoxide and

nucleophilic thiol-ene reactions offer an elegant and simple orthogonal modification platform for copolymer brushes, contributing to a highly efficient and chemospecific methodology for the modification of polymeric surfaces.

6.3.3   Enzymatic activity

The enzymatic activity of surface-bound MP-11 was analyzed by a test reaction using a 3,3',5,5'-tetramethylbenzidine (TMB) analyte solution (Chapter 2.1). MP-11 catalyzes the oxidation of TMB from its colorless diamine to the deep-blue-colored diimine configuration in a buffered hydrogen peroxide (H_2O_2) solution (Figure 6.3a).
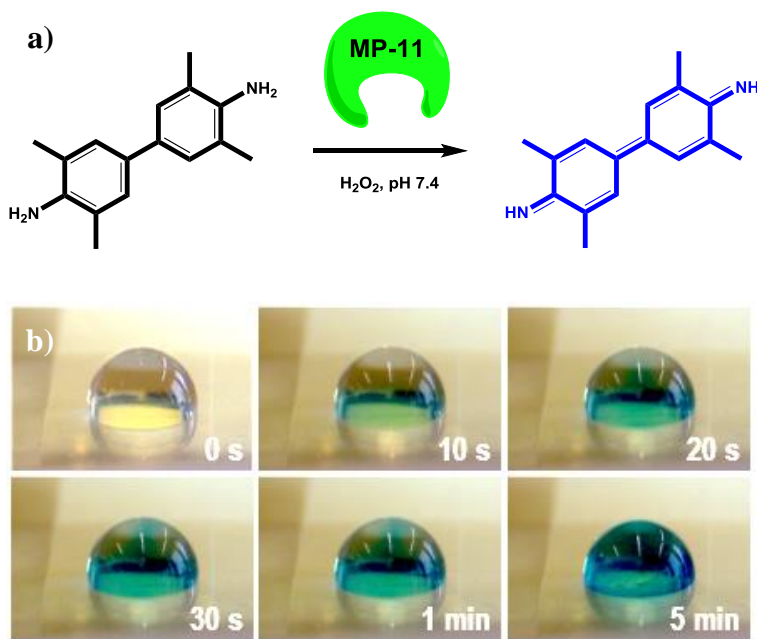
Figure 6.3: (a) MP-11-catalyzed TMB reaction from the colorless diamine to the deep-blue colored diimine configuration causing (b) a color change of a 3 µL droplet of TMB analyte solution on P(GMA-MP-11-*co*-MaMA-SP) polymer brushes grafted from ETFE.

A 3 µL droplet of TMB analyte solution was placed on P(GMA-MP-11-*co*-MaMA-SP) polymer brushes grafted from ETFE. The initially colorless solution showed an immediately appearing blue color close to the grafted surface, while the rest of the droplet remained colorless

(Figure 6.3b). With increasing reaction time the blue color started to diffuse into the droplet until the entire droplet appeared dark blue after 5 minutes.

6.3.4   Light-Responsiveness

The light-responsiveness of P(GMA-MP-11-*co*-MaMA-SP) polymer brushes was demonstrated *via* UV/vis-spectroscopy (Figure 6.4) and contact-angle measurements (Figure 6.5).
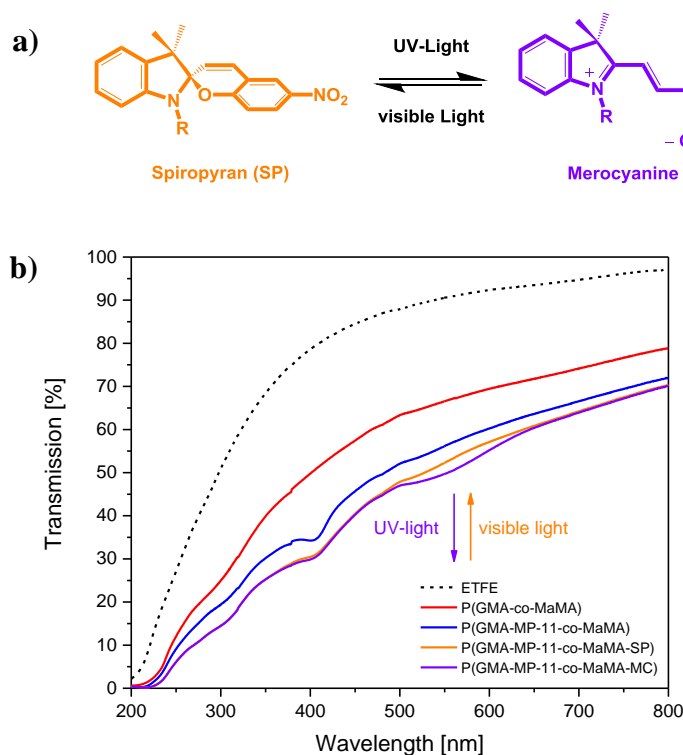
Figure 6.4: (a) Reversible UV- and visible light-induced switching between uncharged colorless spiropyran (SP) and zwitterionic deep-purple colored merocyanine (MC) causing (b) a reversible switch in transmission spectra of thick P(GMA-MP-11-*co*-MaMA-SP) brushes on an ETFE film.

The double-functionalized substrate showed an absorption band at 410 nm, characteristic of the aromatic porphyrin ring of MP-11. After an initial irradiation with UV-light (366 nm) for 30 seconds, an additional band appeared around 570 nm, characteristic of the deep-purple-colored merocyanine (MC) formed from the colorless spiropyran (SP). The system relaxed back under

visible light exposure. The switch in dipole moment was demonstrated *via* reversible, light-induced switching of the static water CA from 86° for P(GMA-MP-11-*co*-MaMA-SP) under visible light to 66° for P(GMA-MP-11-*co*-MaMA-MC) under UV-light irradiation (Figure 6.5).
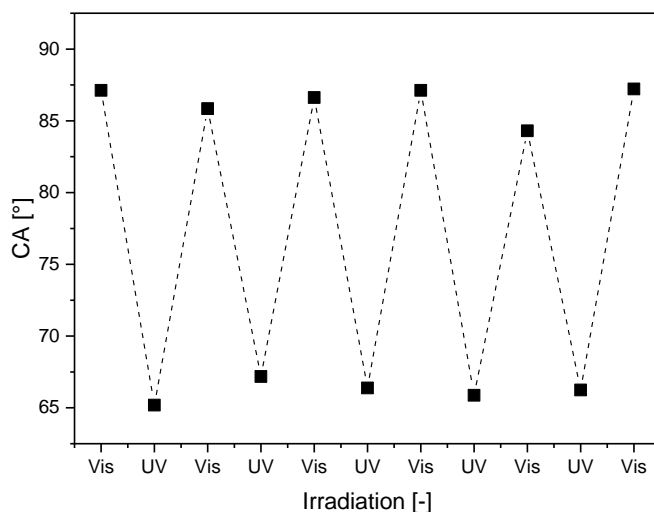

Figure 6.5: Switching of the static contact angle of 3 µL water droplet on P(GMA-MP-11-*co*-MaMA-SP) brush surfaces upon alternating visible and UV-light irradiation.

6.3.5   Light-Controlled Enzymatic Activity

For determination of the influence of the polarity change of photochromic MP-11-containing P(GMA-MP-11-*co*-MaMA-SP) polymer brushes, a surface-modified ETFE sample (18 mm^2) – previously exposed to either visible or UV-light – was dipped into a TMB reaction solution and the absorbance spectra of the solution were measured using UV/vis-spectroscopy in the dark at room temperature.

In the presence of MP-11-containing (P(GMA-MP-11-*co*-MaMA-SP)), *i.e.* following visible-light exposure, two strong absorption bands appeared around 655 and 370 nm, indicating the formation of planar TMB diimine (Figure 6.6a). The intensity at 655 nm increased slowly over time, reaching a maximum of 0.09 a.u. after 27 minutes, after which it remained constant for > 1 hour (Figure 6.7a). In contrast, an initial 30 seconds exposure of the grafted sample to UV-light to form the P(GMA-MP-11-*co*-MaMA-MC) changed the kinetics of the TMB

transformation drastically. Both absorbance bands increased ~ 80x more rapidly than in the prior case, *i.e.* an absorbance value of 0.09 a.u. at 655 nm was reached after only 20 seconds (~ 80-fold faster) (Figure 6.7a).
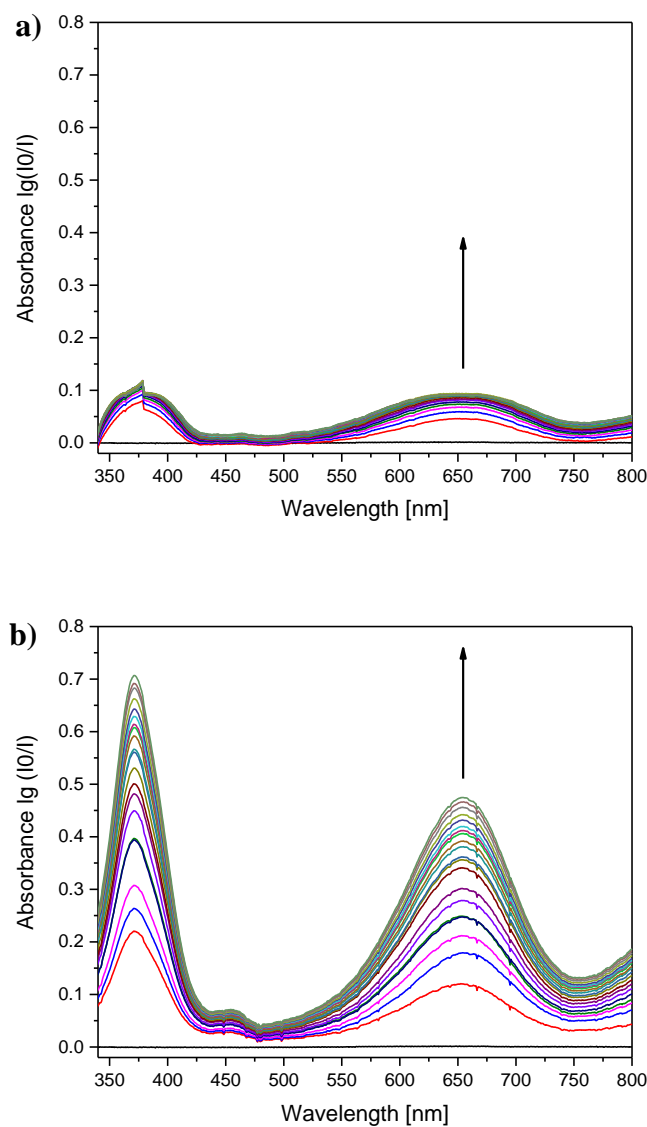

Figure 6.6: Sequences of absorbance spectra acquired at 90 second time intervals of TMB analyte solution in the presence of (a) P(GMA-MP-11-*co*-MaMA-SP) and (b) P(GMA-MP-11-*co*-MaMA-MC), obtained by an initial 30 seconds activation time with UV-light. The absorption bands are characteristic for the diimine oxidation product of TMB.

Additionally, the intensity of the absorbance band increased substantially to 0.48 a.u. after only 30 minutes, even stronger to 0.56 a.u. after 1 hour reaction time (Figure 6.6b). A negative control, consisting of a photochromic but not MP-11-containing P(GMA-*co*-MaMA-SP) grafted sample did not show any significant change in the transmission spectra over time, demonstrating the need for MP-11 to initiate the TMB transformation.

It appears likely that the dramatic, light-induced increase in the TMB transformation rate is caused by the increased wettability of the merocyanine (MC)-containing brushes – as demonstrated with CA measurements (Figure 6.5) – which allowed the aqueous solution to better penetrate into the polymeric system and the TMB diamine to diffuse to the catalytically active centers of the MP-11 attached to the grafted polymer brushes. The overall enhanced TMB oxidation rate is interpreted as a consequence of the swelling of the zwitterionic MC-containing P(GMA-MP-11-*co*-MaMA-MC) brushes. While wetting effects are detected immediately, swelling of polymer brushes usually occurs on a timescale of minutes to hours. Upon UV-light exposure, the catalytic-active centers of MP-11 have much better accessibility within the grafted copolymer brushes than after visible light exposure.

In addition, a switch in absorbance kinetics after *in situ* activation with UV-light was demonstrated (Figure 6.7b, Figure A 6.6). Analogously to the previous measurements, absorbance was determined in the presence of P(GMA-MP-11-*co*-MaMA-SP)). The enzymatic activity (absorbance = 0.05 a.u.) leveled off after 15 minutes, but could be significantly amplified by means of UV-light exposure for 30 seconds, leading to an increase in absorbance to 0.13 a.u.. After a one hour washing in buffer under ambient light to reconstitute the SP moieties, the procedure was repeated in a second cycle of 30 minutes overall reaction time starting from a new TMB solution. The second cycle showed very similar reaction kinetics with slightly reduced intensity.
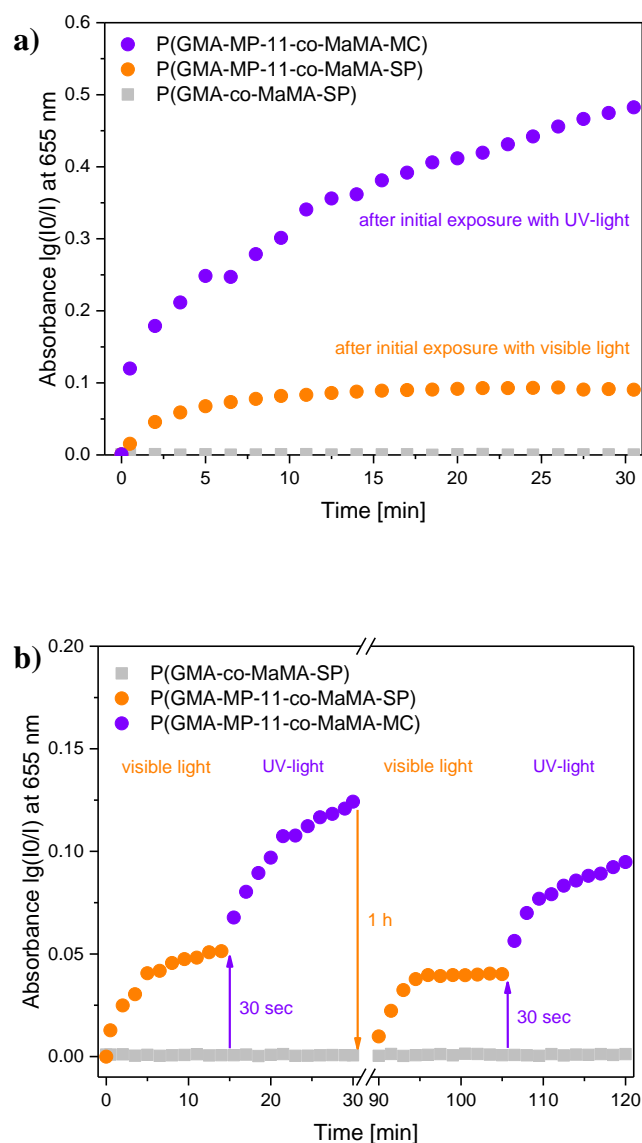
Figure 6.7: Absorbance at 655 nm of TMB analyte solution. (a) Measurements in the presence of P(GMA-MP-11-*co*-MaMA-SP) (orange) and P(GMA-MP-11-*co*-MaMA-MC) (purple) obtained by 30 seconds activation with UV-light. (b) The reaction was started in the presence of P(GMA-MP-11-*co*-MaMA-SP). After 15 minutes the sample was activated after for 30 seconds *in situ* with UV-light. This cycle was repeated after a washing step in between. The exposure changed the kinetics drastically and was reversible after a relaxation after 1 hour under visible light. In both cases P(GMA-*co*-MaMA-SP) (grey) was used as a negative control.

6.4   Conclusions

A new method for the orthogonal functionalization of polymeric substrates with amine- and thiol-reactive copolymer brushes and their subsequent post-polymerization modification (PPM) using amine-epoxide and thiol-ene conjugation was demonstrated. In particular, free-radical polymerization of glycidyl methacrylate and a furan-protected maleimide monomer from initiator patterns was used to grow copolymer brush structures. Simple deprotection of the maleimides allowed us to create dual-reactive copolymer brushes, which were used to conjugate microperoxidase-11 (MP-11) and photochromic spiropyran (SP) to the glycidyl- and maleimide residues, respectively. The orthogonal PPM was proven to be chemoselective and specific using ATR-IR and UV/vis spectroscopy, supported by contact angle measurements.

MP-11-modified surfaces were demonstrated to be enzymatically active by triggering the oxidation of colorless TMB diamine to its deep-blue-colored diimine form. Additionally, SP-containing polymer brushes were demonstrated to behave as responsive surfaces by the reversible light-induced switching of water contact angle and color. The combination of both functionalities in one brush allowed us to control the enzymatic activity of photochromic bio-conjugated polymer brushes using light as an external stimulus, leading to a dramatic, but reversible, change in enzymatic activity on grafted polymer brushes.

These results represent a significant step forward in responsive bio-conjugated polymeric surfaces, as they combine chemospecific highly efficient PPM in an orthogonal fashion with the ability to implement multifunctionality on a single brush. These well-controlled brush structures potentially open up a wide variety of applications for responsive bio-conjugated polymer brushes in, for example, all-polymeric diagnostic microarrays and lab-on-a-chip devices.

6.5   Appendix

6.5.1   Attenuated Total Reflectance – Infrared (ATR–IR) Spectroscopy
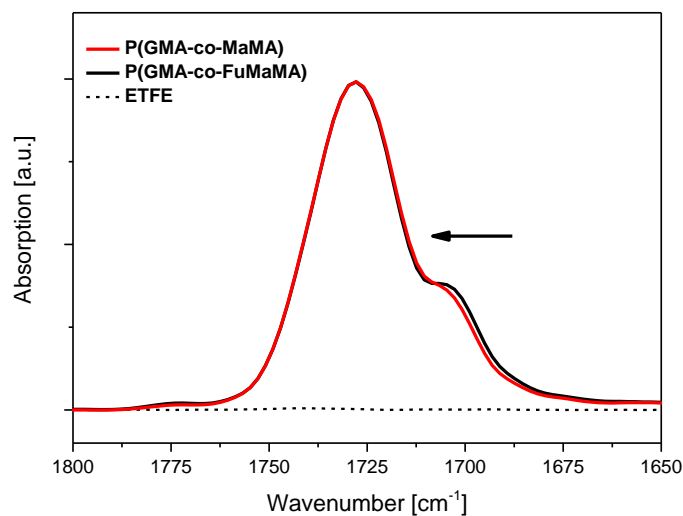

Figure A 6.1: ATR-IR spectra of thick dry P(GMA-*co*-FuMaMA) (2:1) structures grafted from ETFE and the rDA product P(GMA-*co*-MaMA) (2:1).
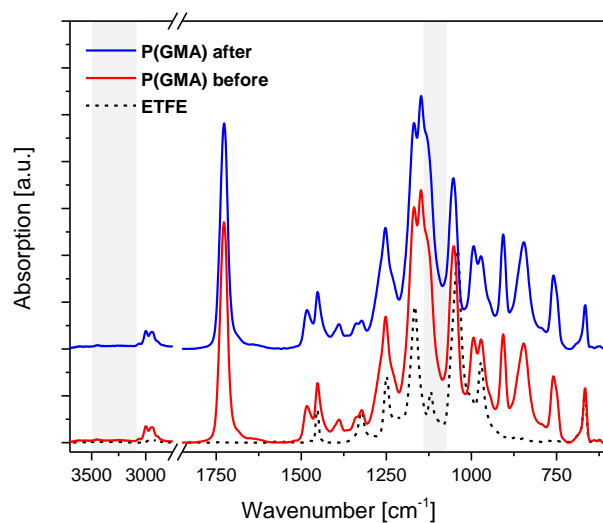
Figure A 6.2: ATR-IR spectra of thick P(GMA) grafted from ETFE before and after treatment for 30 min under vacuum at 110 °C, confirming the stability of the epoxides under rDA conditions.
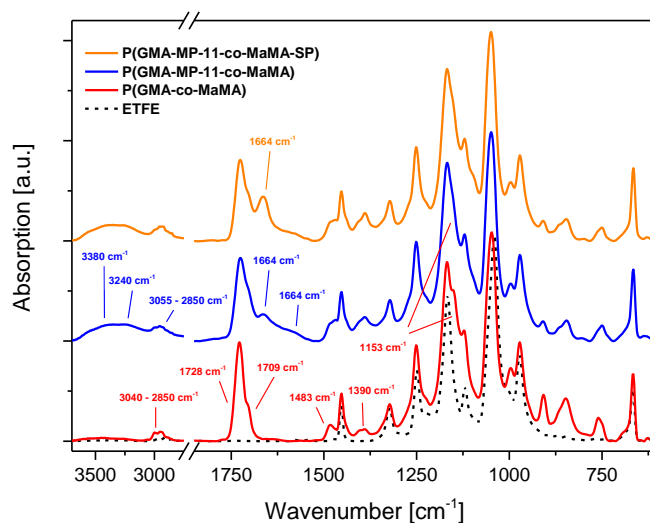
Figure A 6.3: ATR-IR spectra of thick P(GMA-*co*-MaMA), as prepared and after sequential binding of MP-11 and SP.

		Wavenumber [cm^{-1}] on ETFE
P(GMA-*co*-MaMA)	υ(C-H)$_{st}$	3040 – 2850
	δ(C-H)$_{b}$	1483, 1390
	υ(C=O)$_{ester}$	1728
	υ(C=O)$_{imide}$	1709
	υ(C$_{alkoxy}$-H)$_{ether}$	1153
P(GMA-MP-11-*co*-MaMA)	υ(N-H)$_{st}$	3380
	υ(N-H)$_{b, amide}$	1664
	υ(N-H)$_{b, amine}$	1580
	υ(C-H)$_{st}$	3055 – 2850
	υ(O-H)$_{st}$	3240
	υ(C$_{alkoxy}$-O)$_{alcohol}$	1059
P(GMA-MP-11-*co*-MaMA-SP)	υ(N-H)$_{b, amide+imide}$	1664

Table A 6.1: List of peaks in ATR-IR spectra of thick P(GMA-*co*-MaMA) brushes grafted from ETFE, as prepared and after sequential binding of MP-11 and SP.
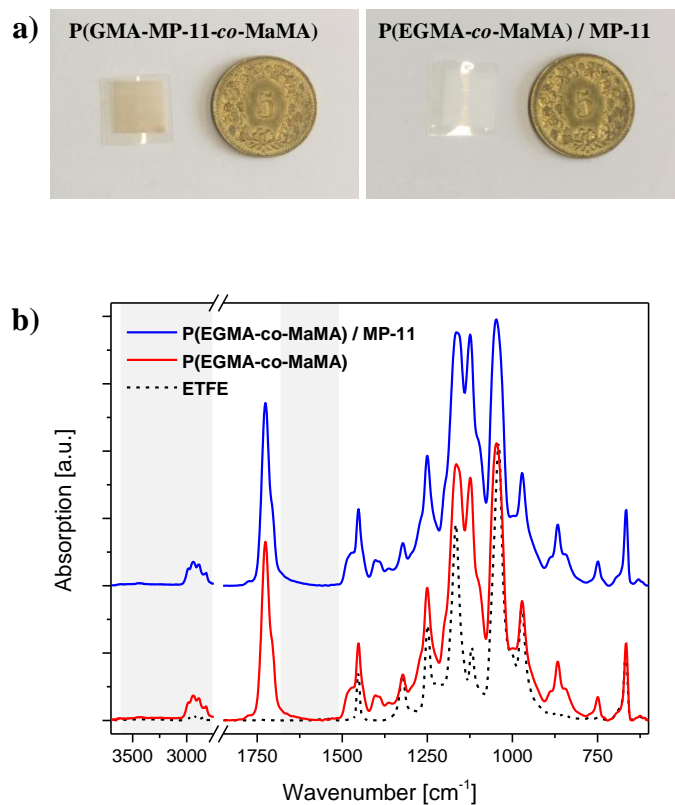
Figure A 6.4: (a) Optical images of a MP-11-functionalized P(GMA-MP-11-*co*-MaMA) and a negative control P(EGMA-*co*-MaMA) / MP-11. The negative control does not show any brown color in the grafted areas, which is characteristic for bound MP-11. (b) ATR-IR spectra of thick P(EGMA-*co*-MaMA) homopolymer brushes grafted from ETFE as a negative control before and after treatment with MP-11 for 1 h at 60 °C.
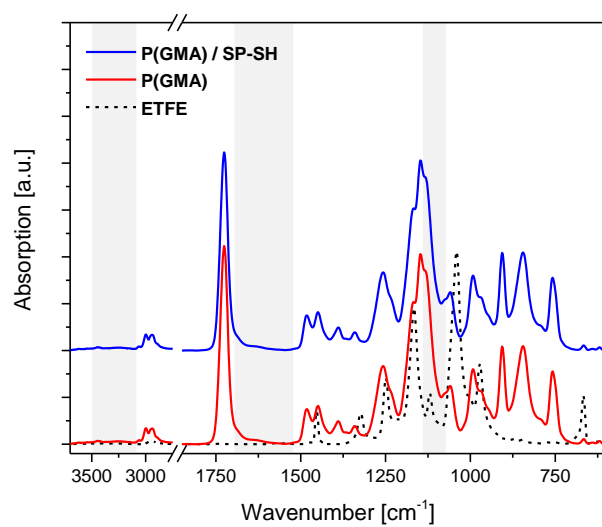
Figure A 6.5: ATR-IR spectra of thick P(GMA) grafted from ETFE before and after coupling attempt with spiropyran thiol (SP-SH) under thiol-ene reaction conditions.

6.5.2   Ultraviolet-visible (UV/vis) Spectroscopy
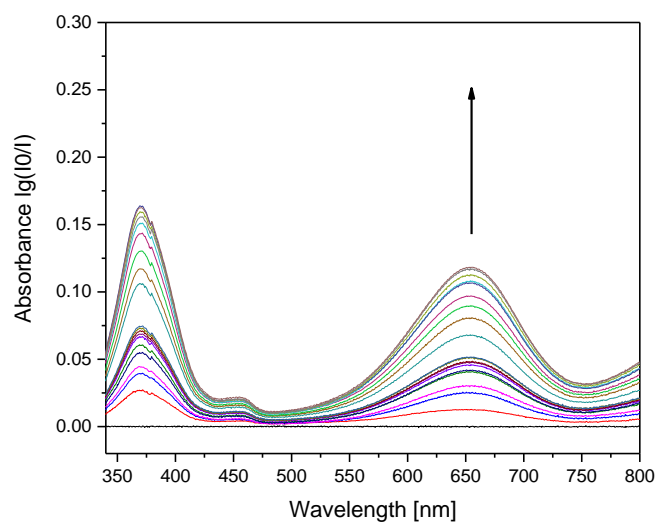
Figure A 6.6: Absorbance spectra of TMB analyte solution over time in the presence of P(GMA-MP-11-*co*-MaMA-SP) for 15 minutes. After the TMB oxidation leveled, the sample was activated *in situ* for 30 seconds with UV-light to form P(GMA-MP-11-*co*-MaMA-MC). The negative control (P(GMA-*co*-MaMA-SP) without MP-11 attached showed no enzymatic activity.

7.   Conclusions and Outlook

The aim of this thesis was the fabrication of light-responsive polymeric surfaces by means of grafting of polymer brushes. Free-radical polymerization (FRP) and different post-polymerization modification (PPM) strategies were used for the generation of photochromic and multifunctional polymer brushes on polymeric substrates. The light-responsive brushes carried covalently attached spiropyran (SP) as pendant groups.

Different activation methods have been used to control the creation of initiator radicals on the surface, taking advantage either of plasma activation for large-area activation or of the unique possibilities at the XIL-beamline at the Swiss Light Source using extreme ultra-violet interference lithography (EUV-IL) which allowed us to reproducibly grow polymer brushes from interference patterns on a micrometer to nanometer scale. Exposure and grafting parameters allowed us to control the grafting density and thickness of the brush structures. The patterned SP-containing polymer brushes were successfully shown to behave as smart surfaces that switch in color, in their fluorescence behavior, and in wettability, using light as external stimulus. The fluorescence half-life ($T_{1/2}$) of the photochromic brushes was determined and demonstrated the importance of the brush chemistry, as well as the solvent environment for the spiropyran-merocyanine isomerization. Non-polar solvents lower $T_{1/2}$, while polar solvents enhance the emission life-time. The gained detailed understanding of the parameters that determine the photoresponsiveness of these engineered brush structures was valuable for the development of further, more complex responsive systems.

In addition, responsive polymeric membranes have been fabricated from microporous polypropylene (PP) by means of argon-plasma activation and free-radical polymerization to graft pH-responsive polymer brushes. The grafted membranes were then modified with the established PPM to implement light-responsiveness. Modified membranes were showed smart properties in that they switched in wettability and permeability in response to either pH or light as external stimulus. The flux properties of pH-switched PMAA-modified membranes were dominated by the swelling of the brushes and much less influenced by the hydrophilicity of the surface. In contrast, hydrophilicity changes dominated the photon-induced switching of SP-modified PP membranes. The simplicity and versatility of the described approach for the fabrication of responsive systems to influence the hydrophilicity or pore size *via* swelling of the material is of

great interest for the controlled separation or transport of dissolved species and could easily be expanded to other functionalities.

In the following, polymeric substrates were modified with thiol-reactive copolymer brushes and subsequent functionalization using nucleophilic thiol-ene conjugation. Chemoselective and specific PPM of grafted brush structures yielded polyelectrolyte brushes, and fluorescent and light-responsive polymer brushes on fluoropolymer surfaces. A successful copolymerization was carried out with different ethylene glycol containing methacrylates comonomers with a furan-protected maleimide methacrylate (FuMaMA). The copolymerization regulated the density of the attached functional centers on the structures to help controlling other additional properties to the brushes such as hydrophobicity or hydrophilicity by varying the number of ethylene glycol moieties in the side chains of the comonomer. Especially hydrophilic PEG-containing functional brushes will be interesting in future projects as they provide anti-biofouling properties along with the potential for selective bioconjugation. Attachment of thiols *via* thiol-ene reactions to the deprotected maleimide side chains was chemoselective and specific, yielding different patterned, functional polymer brushes. These were demonstrated to behave as smart surfaces reacting to light as an external stimulus by switching of contact angle, fluorescence and color. The presented examples for functionalization of such thiol-reactive copolymer brushes on polymeric substrates demonstrate the versatility of this approach.

This approach was continued to graft amine- and thiol-reactive copolymer-brushes allowing chemospecific orthogonal PPM of the grafted structures. The amine-epoxide reaction was utilized for chemoselective bio-conjugation of microperoxidase-11 (MP-11) and the nucleophilic Michael-addition reaction for coupling of photochromic SP thiols to activated maleimides. Enzymatic activity of photochromic bio-conjugated polymer brushes was illustrated *via* a MP-11-catalyzed oxidation of colorless 3,3',5,5'-tetramethylbenzidine (TMB) diamine to deep-blue colored TMB diimine. A dramatic switch in the enzymatic turn-over of TMB according to exposure to either visible or UV-light allowed controlling the enzymatic activity of grafted polymeric substrates. The combination of chemospecific highly efficient PPM in an orthogonal fashion with the ability to implement multifunctionality on a single brush represent a significant step forward in responsive bio-conjugated polymeric surfaces.

Such highly-engineered brush structures potentially open up a wide variety of applications for responsive bio-conjugated polymer brushes in, for example, all-polymeric diagnostic microarrays and lab-on-a-chip devices. Utilizing such microfluidic systems would be another step

forward in terms of analyzing continuously the enzymatic turn-over of catalyzed reactions of *i.e.* photochromic bio-conjugated grafted surfaces.

An optical output signal with a wavelength similar to the absorption maximum of TMB would allow quantification of the enzymatic activity of copolymer brush-bound MP-11 not just in a static but also in a dynamic fashion. In academia, microfluidic chip devices are usually formed into poly(dimethyl siloxane) (PDMS) as PDMS is a cheap, flexible and transparent polymer, making it the ideal candidate for optofluidic biosensor systems. Due to its transparency to visible and UV-light, *in situ* excitation of covalently attached SP moieties would give access to light-induced remote-controlled switching in bio-catalyzed reactions in the microfluidic device. Needless to say, that such microfluidic device allow fast cleaning of test reactors by simply washing out non-bound oxidation products from the grafted copolymer brushes with buffer solutions. In this manner, several cycles of enzymatic activity and in particular the life-time of surface-bound MP-11 can be quantified upon alternating visible and UV-light irradiation.

Unfortunately, polymer brushes cannot be radiation-grafted from PDMS because of radical recombination within this particular polymer after activation with either plasma or EUV light. This drawback could be overcome by bonding of grafted flexible and transparent ETFE foils with formed microfluidic PDMS chip devices creating a closed channel system.

This is only one example of how to implement polymer brushed into microfluidic channels. Alternatively, other activation methods could be used such as electron-beam lithography (EBL), allowing to continuously write spatially controlled large-area initiator patterns. Further, extending the library of grafted monomers would be of particular interest for multi-responsive polymer systems by copolymerization of poly(methacrylic acid) (PMAA) for pH-responsiveness, poly(*N*-isopropyl acrylamide) (PNIPAAM) for thermo-responsiveness or poly(2-(acetoacetoxy)ethyl methacrylate) (PAcEMA), which can form complexes with transition metals such as iron. These may be used as metal source for the formation iron oxide particles within the brushes to achieve magnetic-responsiveness.

To further enhance the switch in remote-controlled bioactivities of grafted polymer brushes the introduction of block-copolymer (BCP) should be considered. Therefore, controlled radical polymerization techniques (CRP) would need to be applied such as nitroxide-mediated polymerization (NMP), reversible addition fragmentation chain transfer (RAFT) polymerization or metal-free ring-strain promoted atom transfer radical polymerization (ATRP). Applying these methodologies of course would come with the tradeoff of complicating the fabrication process.

Nevertheless, BCP would allow for example to bury certain functionalities such as enzymatic centers in brush systems lowering the initial catalytic activity close to zero, while full activity would be achieved through a response towards *i.e.* UV-light irradiation.

8. References

1. Advincula, R. C.; Brittain, W. J.; Caster, K. C.; Rühe, J., *Polymer brushes*. WILEY-VCH Verlag GmbH & Co- KGaA: Weinheim, 2004.

2. Ruhe, J.; Novotny, V.; Clarke, T.; Street, G. B. *J. Tribol.-Trans. ASME* **1996,** 118, (3), 663-668.

3. Ruoslahti, E. *Annu. Rev. Cell Dev. Biol.* **1996,** 12, 697-715.

4. Prime, K. L.; Whitesides, G. M. *J. Am. Chem. Soc.* **1993,** 115, (23), 10714-10721.

5. R.A.L.;, J.; Richards, R. W., *Polymers at surfaces and interfaces*. Cambridge University Press: Cambridge, 1999.

6. Ulman, A., *An introduction to ultrathin organic films: From Langmuir-Blodgett to self-assembly*. Academic Press: New York, 1991.

7. Jiang, H.; Xu, F. J. *Chem. Soc. Rev.* **2013,** 42, (8), 3394-3426.

8. Klein, J.; Kumacheva, E.; Mahalu, D.; Perahia, D.; Fetters, L. J. *Nature* **1994,** 370, (6491), 634-636.

9. Tsujii, Y.; Ohno, K.; Yamamoto, S.; Goto, A.; Fukuda, T., *Structure and properties of high-density polymer brushes prepared by surface-initiated living radical polymerization*. In *Surface-Initiated Polymerization I*, Jordan, R., Ed. Springer-Verlag: Berlin, 2006.

10. Zajac, R.; Chakrabarti, A. *Phys. Rev. E* **1995,** 52, (6), 6536-6549.

11. Ishida, H.; Chiang, C. H.; Koenig, J. L. *Polymer* **1982,** 23, (2), 251-257.

12. Prucker, O.; Ruhe, J. *Macromolecules* **1998,** 31, (3), 592-601.

13. Prucker, O.; Schimmel, M.; Tovar, G.; Knoll, W.; Ruhe, J. *Adv. Mater.* **1998,** 10, (14), 1073-1077.

14. Kumar, A.; Whitesides, G. M. *Appl. Phys. Lett.* **1993,** 63, (14), 2002-2004.

15. Azzaroni, O.; Brown, A. A.; Huck, W. T. S. *Angew. Chem.-Int. Edit.* **2006,** 45, (11), 1770-1774.

16. Piner, R. D.; Zhu, J.; Xu, F.; Hong, S. H.; Mirkin, C. A. *Science* **1999,** 283, (5402), 661-663.

17. Liu, Y.; Klep, V.; Luzinov, I. *J. Am. Chem. Soc.* **2006,** 128, (25), 8106-8107.

18. Kaholek, M.; Lee, W. K.; LaMattina, B.; Caster, K. C.; Zauscher, S. *Nano Lett.* **2004,** 4, (2), 373-376.

19. Liu, X. G.; Guo, S. W.; Mirkin, C. A. *Angew. Chem.-Int. Edit.* **2003,** 42, (39), 4785-4789.

20.   Ahn, S. J.; Kaholek, M.; Lee, W. K.; LaMattina, B.; LaBean, T. H.; Zauscher, S. *Adv. Mater.* **2004,** 16, (23-24), 2141-2145.

21.   Ballav, N.; Schilp, S.; Zharnikov, M. *Angew. Chem.-Int. Edit.* **2008,** 47, (8), 1421-1424.

22.   Husemann, M.; Morrison, M.; Benoit, D.; Frommer, K. J.; Mate, C. M.; Hinsberg, W. D.; Hedrick, J. L.; Hawker, C. J. *J. Am. Chem. Soc.* **2000,** 122, (8), 1844-1845.

23.   Prucker, O.; Habicht, J.; Park, I. J.; Ruhe, J. *Mater. Sci. Eng. C-Biomimetic Supramol. Syst.* **1999,** 8-9, 291-297.

24.   Brack, H. P.; Padeste, C.; Slaski, M.; Alkan, S.; Solak, H. H. *J. Am. Chem. Soc.* **2004,** 126, (4), 1004-1005.

25.   Neuhaus, S.; Padeste, C.; Solak, H. H.; Spencer, N. D. *Polymer* **2010,** 51, (18), 4037-4043.

26.   Burns, C. T.; Choi, S. Y.; Dietz, M. L.; Firestone, M. A. *Sep. Sci. Technol.* **2008,** 43, (9-10), 2503-2519.

27.   Theato, P.; Klok, H. A., *Functional polymers by post-polymerization modification*. Wiley-VCH Verlag & Co. KGaA: Weinheim, 2013.

28.   Gauthier, M. A.; Gibson, M. I.; Klok, H. A. *Angew. Chem.-Int. Edit.* **2009,** 48, (1), 48-58.

29.   Gok, O.; Durmaz, H.; Ozdes, E. S.; Hizal, G.; Tunca, U.; Sanyal, A. *J. Polym. Sci. Part a-Polym. Chem.* **2010,** 48, (12), 2546-2556.

30.   Helms, B.; Mynar, J. L.; Hawker, C. J.; Frechet, J. M. J. *J. Am. Chem. Soc.* **2004,** 126, (46), 15020-15021.

31.   Campos, L. M.; Killops, K. L.; Sakai, R.; Paulusse, J. M. J.; Damiron, D.; Drockenmuller, E.; Messmore, B. W.; Hawker, C. J. *Macromolecules* **2008,** 41, (19), 7063-7070.

32.   Nebhani, L.; Barner-Kowollik, C. *Adv. Mater.* **2009,** 21, (34), 3442-3468.

33.   Lutz, J. F. *Angew. Chem.-Int. Edit.* **2008,** 47, (12), 2182-2184.

34.   Sumerlin, B. S.; Vogt, A. P. *Macromolecules* **2010,** 43, (1), 1-13.

35.   Durmaz, H.; Sanyal, A.; Hizal, G.; Tunca, U. *Polym. Chem.* **2012,** 3, (4), 825-835.

36.   Kempe, K.; Krieg, A.; Becer, C. R.; Schubert, U. S. *Chem. Soc. Rev.* **2012,** 41, (1), 176-191.

37.   Hoyle, C. E.; Lowe, A. B.; Bowman, C. N. *Chem. Soc. Rev.* **2010,** 39, (4), 1355-1387.

38.   Kolb, H. C.; Finn, M. G.; Sharpless, K. B. *Angew. Chem.-Int. Edit.* **2001,** 40, (11), 2004-2021.

39. Devenish, S. R. A.; Hill, J. B.; Blunt, J. W.; Morris, J. C.; Munro, M. H. G. *Tetrahedron Lett.* **2006,** 47, (17), 2875-2878.

40. Eberhardt, M.; Mruk, R.; Zentel, R.; Theato, P. *Eur. Polym. J.* **2005,** 41, (7), 1569-1575.

41. Gilbert, H. F. *J. Biol. Chem.* **1982,** 257, (20), 2086-2091.

42. Markovic, I.; Stantchev, T. S.; Fields, K. H.; Tiffany, L. J.; Tomic, M.; Weiss, C. D.; Broder, C. C.; Strebel, K.; Clouse, K. A. *Blood* **2004,** 103, (5), 1586-1594.

43. Wedemeyer, W. J.; Welker, E.; Narayan, M.; Scheraga, H. A. *Biochemistry* **2000,** 39, (15), 4207-4216.

44. Wang, L. X.; Kristensen, J.; Ruffner, D. E. *Bioconjugate Chem.* **1998,** 9, (6), 749-757.

45. Ghosh, S.; Basu, S.; Thayumanavan, S. *Macromolecules* **2006,** 39, (17), 5595-5597.

46. Griesbau.K. *Angew. Chem.-Int. Edit.* **1970,** 9, (4), 273-287.

47. Justynska, J.; Hordyjewicz, Z.; Schlaad, H. *Polymer* **2005,** 46, (26), 12057-12064.

48. Navarro-Rodriguez, D.; Rodriguez-Gonzalez, F. J.; Romero-Garcia, J.; Jimenez-Regalado, E. J.; Guillon, D. *Eur. Polym. J.* **1998,** 34, (7), 1039-1045.

49. Edmondson, S.; Huck, W. T. S. *J. Mater. Chem.* **2004,** 14, (4), 730-734.

50. De, S.; Khan, A. *Chem. Commun.* **2012,** 48, (25), 3130-3132.

51. Rostovtsev, V. V.; Green, L. G.; Fokin, V. V.; Sharpless, K. B. *Angew. Chem.-Int. Edit.* **2002,** 41, (14), 2596-2599.

52. Tornoe, C. W.; Christensen, C.; Meldal, M. *J. Org. Chem.* **2002,** 67, (9), 3057-3064.

53. Sumerlin, B. S.; Tsarevsky, N. V.; Louche, G.; Lee, R. Y.; Matyjaszewski, K. *Macromolecules* **2005,** 38, (18), 7540-7545.

54. Li, Y.; Yang, J. W.; Benicewicz, B. C. *J. Polym. Sci. Part a-Polym. Chem.* **2007,** 45, (18), 4300-4308.

55. Gramlich, P. M. E.; Wirges, C. T.; Manetto, A.; Carell, T. *Angew. Chem.-Int. Edit.* **2008,** 47, (44), 8350-8358.

56. Lallana, E.; Riguera, R.; Fernandez-Megia, E. *Angew. Chem.-Int. Edit.* **2011,** 50, (38), 8794-8804.

57. Fournier, D.; Hoogenboom, R.; Schubert, U. S. *Chem. Soc. Rev.* **2007,** 36, (8), 1369-1380.

58. Moses, J. E.; Moorhouse, A. D. *Chem. Soc. Rev.* **2007,** 36, (8), 1249-1262.

59. Tunca, U. *J. Polym. Sci. Part a-Polym. Chem.* **2014,** 52, (22), 3147-3165.

60.   Baskin, J. M.; Prescher, J. A.; Laughlin, S. T.; Agard, N. J.; Chang, P. V.; Miller, I. A.; Lo, A.; Codelli, J. A.; Bertozzi, C. R. *Proc. Natl. Acad. Sci. U. S. A.* **2007,** 104, (43), 16793-16797.

61.   Jewett, J. C.; Bertozzi, C. R. *Chem. Soc. Rev.* **2010,** 39, (4), 1272-1279.

62.   Singh, I.; Zarafshani, Z.; Lutz, J. F.; Heaney, F. *Macromolecules* **2009,** 42, (15), 5411-5413.

63.   Mantovani, G.; Lecolley, F.; Tao, L.; Haddleton, D. M.; Clerx, J.; Cornelissen, J.; Velonia, K. *J. Am. Chem. Soc.* **2005,** 127, (9), 2966-2973.

64.   Sun, F. X.; Luo, X. L.; Kang, L. C.; Peng, X. Y.; Lu, C. X. *Polym. Chem.* **2015,** 6, (8), 1214-1225.

65.   Becer, C. R.; Hoogenboom, R.; Schubert, U. S. *Angew. Chem.-Int. Edit.* **2009,** 48, (27), 4900-4908.

66.   Chan, J. W.; Hoyle, C. E.; Lowe, A. B. *J. Am. Chem. Soc.* **2009,** 131, (16), 5751-5753.

67.   Dondoni, A. *Angew. Chem.-Int. Edit.* **2008,** 47, (47), 8995-8997.

68.   Killops, K. L.; Campos, L. M.; Hawker, C. J. *J. Am. Chem. Soc.* **2008,** 130, (15), 5062-5064.

69.   Lowe, A. B. *Polym. Chem.* **2014,** 5, (17), 4820-4870.

70.   Lowe, A. B. *Polym. Chem.* **2010,** 1, (1), 17-36.

71.   Gupta, N.; Lin, B. F.; Campos, L.; Dimitriou, M. D.; Hikita, S. T.; Treat, N. D.; Tirrell, M. V.; Clegg, D. O.; Kramer, E. J.; Hawker, C. J. *Nat. Chem.* **2010,** 2, (2), 138-145.

72.   Nandivada, H.; Jiang, X. W.; Lahann, J. *Adv. Mater.* **2007,** 19, (17), 2197-2208.

73.   Stolz, R. M.; Northrop, B. H. *J. Org. Chem.* **2013,** 78, (16), 8105-8116.

74.   Chatani, S.; Nair, D. P.; Bowman, C. N. *Polym. Chem.* **2013,** 4, (4), 1048-1055.

75.   Geng, J.; Mantovani, G.; Tao, L.; Nicolas, J.; Chen, G. J.; Wallis, R.; Mitchell, D. A.; Johnson, B. R. G.; Evans, S. D.; Haddleton, D. M. *J. Am. Chem. Soc.* **2007,** 129, (49), 15156-15163.

76.   Pounder, R. J.; Stanford, M. J.; Brooks, P.; Richards, S. P.; Dove, A. P. *Chem. Commun.* **2008**, (41), 5158-5160.

77.   Bailey, G. C.; Swager, T. M. *Macromolecules* **2006,** 39, (8), 2815-2818.

78.   Kwart, H.; King, K. *Chem. Rev.* **1968,** 68, (4), 415-447.

79.   Gacal, B.; Durmaz, H.; Tasdelen, M. A.; Hizal, G.; Tunca, U.; Yagci, Y.; Demirel, A. L. *Macromolecules* **2006,** 39, (16), 5330-5336.

80. Sinnwell, S.; Synatschke, C. V.; Junkers, T.; Stenzel, M. H.; Barner-Kowollik, C. *Macromolecules* **2008,** 41, (21), 7904-7912.

81. Inglis, A. J.; Sinnwell, S.; Davis, T. P.; Barner-Kowollik, C.; Stenzel, M. H. *Macromolecules* **2008,** 41, (12), 4120-4126.

82. Zhu, J.; Kell, A. J.; Workentin, M. S. *Org. Lett.* **2006,** 8, (22), 4993-4996.

83. Sanyal, A. *Macromol. Chem. Physic.* **2010,** 211, (13), 1417-1425.

84. Hizal, G.; Tunca, U.; Sanyal, A. *J. Polym. Sci. Part a-Polym. Chem.* **2011,** 49, (19), 4103-4120.

85. Kavitha, A. A.; Singha, N. K. *ACS Appl. Mater. Interfaces* **2009,** 1, (7), 1427-1436.

86. Chen, X. X.; Dam, M. A.; Ono, K.; Mal, A.; Shen, H. B.; Nutt, S. R.; Sheran, K.; Wudl, F. *Science* **2002,** 295, (5560), 1698-1702.

87. McElhanon, J. R.; Wheeler, D. R. *Org. Lett.* **2001,** 3, (17), 2681-2683.

88. Kose, M. M.; Yesilbag, G.; Sanyal, A. *Org. Lett.* **2008,** 10, (12), 2353-2356.

89. Liu, Y. L.; Chen, Y. W. *Macromol. Chem. Physic.* **2007,** 208, (2), 224-232.

90. Kosif, I.; Park, E. J.; Sanyal, R.; Sanyal, A. *Macromolecules* **2010,** 43, (9), 4140-4148.

91. Xia, F.; Feng, L.; Wang, S. T.; Sun, T. L.; Song, W. L.; Jiang, W. H.; Jiang, L. *Adv. Mater.* **2006,** 18, (4), 432-436.

92. Zhang, Q. L.; Xia, F.; Sun, T. L.; Song, W. L.; Zhao, T. Y.; Liu, M. C.; Jiang, L. *Chem. Commun.* **2008**, (10), 1199-1201.

93. Nakahata, M.; Takashima, Y.; Yamaguchi, H.; Harada, A. *Nat. Commun.* **2011,** 2, 1-6.

94. Kim, P.; Hu, Y. H.; Alvarenga, J.; Kolle, M.; Suo, Z. G.; Aizenberg, J. *Adv. Opt. Mater.* **2013,** 1, (5), 381-388.

95. Gao, G. Z.; Dallmeyer, J. I.; Kadla, J. F. *Biomacromolecules* **2012,** 13, (11), 3602-3610.

96. Kim, H. S.; Crosby, A. J. *Adv. Mater.* **2011,** 23, (36), 4188-4192.

97. Digilov, R. *Langmuir* **2000,** 16, (16), 6719-6723.

98. Ichimura, K.; Oh, S. K.; Nakagawa, M. *Science* **2000,** 288, (5471), 1624-1626.

99. Sinha, M. K.; Purkait, M. K. *J. Membr. Sci.* **2014,** 464, 20-32.

100. Dai, S.; Ravi, P.; Tam, K. C. *Soft Matter* **2009,** 5, (13), 2513-2533.

101. Minkin, V. I. *Chem. Rev.* **2004,** 104, (5), 2751-2776.

102. Chen, C. S.; Mrksich, M.; Huang, S.; Whitesides, G. M.; Ingber, D. E. *Science* **1997,** 276, (5317), 1425-1428.

103. Kwon, O. H.; Kikuchi, A.; Yamato, M.; Okano, T. *Biomaterials* **2003,** 24, (7), 1223-1232.

104. Cunliffe, D.; Alarcon, C. D.; Peters, V.; Smith, J. R.; Alexander, C. *Langmuir* **2003,** 19, (7), 2888-2899.

105. Wang, X. L.; Huang, J.; Chen, X. Z.; Yu, X. H. *Desalination* **2002,** 146, (1-3), 337-343.

106. Kanazawa, H.; Sunamoto, T.; Ayano, E.; Matsushima, Y.; Kikuchi, A.; Okano, T. *Anal. Sci.* **2002,** 18, (1), 45-48.

107. Beebe, D. J.; Moore, J. S.; Yu, Q.; Liu, R. H.; Kraft, M. L.; Jo, B. H.; Devadoss, C. *Proc. Natl. Acad. Sci. U. S. A.* **2000,** 97, (25), 13488-13493.

108. Duncan, R.; Kopecek, J. *Adv. Polym. Sci.* **1984,** 57, 51-101.

109. Qing, S.; Yanlei, S.; Xue, N.; Wenjuan, C.; Jinming, P.; Zhongyi, J. *J. Membr. Sci.* **2010,** 347, (1-2), 62-68.

110. Schacher, F.; Ulbricht, M.; Mueller, A. H. E. *Adv. Func. Mater.* **2009,** 19, (7), 1040-1045.

111. Qiu, X.; Yu, H.; Karunakaran, M.; Pradeep, N.; Nunes, S. P.; Peinemann, K.-V. *ACS Nano* **2013,** 7, (1), 768-776.

112. Chu, L.; Xie, R.; Ju, X. *Chin. J. Chem. Eng.* **2011,** 19, (6), 891-903.

113. Xiang, Y.; Shen, J.; Wang, Y.; Liu, F.; Xue, L. *RSC Advances* **2015,** 5, (30), 23530-23539.

114. Chakrabarty, T.; Shahi, V. K. *RSC Advances* **2014,** 4, (110), 64731-64732.

115. Hasegawa, S.; Ohashi, H.; Maekawa, Y.; Katakai, R.; Yoshida, M. *Polymer* **2009,** 41, (7), 533-540.

116. Stuart, M. A. C.; Huck, W. T. S.; Genzer, J.; Mueller, M.; Ober, C.; Stamm, M.; Sukhorukov, G. B.; Szleifer, I.; Tsukruk, V. V.; Urban, M.; Winnik, F.; Zauscher, S.; Luzinov, I.; Minko, S. *Nat. Mater.* **2010,** 9, (2), 101-113.

117. Jarvinen, K.; Akerman, S.; Svarfvar, B.; Tarvainen, T.; Viinikka, P.; Paronen, P. *Pharm. Res.* **1998,** 15, (5), 802-805.

118. Tripathi, B. P.; Dubey, N. C.; Choudhury, S.; Simon, F.; Stamm, M. *J. Mater. Chem. B* **2013,** 1, (27), 3397-3409.

119. Klajn, R. *Chem. Soc. Rev.* **2014,** 43, (1), 148-184.

120. Kudernac, T.; van der Molen, S. J.; van Wees, B. J.; Feringa, B. L. *Chem. Commun.* **2006,** (34), 3597-3599.

121. Kasatani, K.; Kambe, S.; Irie, M. *J. Photochem. Photobiol. A* **1999,** 122, (1), 11-15.

122. Chen, Y.; Wang, C. M.; Fan, M. G.; Yao, B. L.; Menke, N. *Optical Materials* **2004,** 26, (1), 75-77.

123. Heinz, B.; Malkmus, S.; Laimgruber, S.; Dietrich, S.; Schulz, C.; Ruck-Braun, K.; Braun, M.; Zinth, W.; Gilch, P. *J. Am. Chem. Soc.* **2007,** 129, (27), 8577-8584.

124. Fuss, W.; Kosmidis, C.; Schmid, W. E.; Trushin, S. A. *Angew. Chem.-Int. Edit.* **2004,** 43, (32), 4178-4182.

125. Henzl, J.; Mehlhorn, M.; Gawronski, H.; Rieder, K. H.; Morgenstern, K. *Angew. Chem.-Int. Edit.* **2006,** 45, (4), 603-606.

126. Berkovic, G.; Krongauz, V.; Weiss, V. *Chem. Rev.* **2000,** 100, (5), 1741-1753.

127. Becker, R. S.; Michl, J. *J. Am. Chem. Soc.* **1966,** 88, (24), 5931-5933.

128. Levitus, M.; Glasser, G.; Neher, D.; Aramendia, P. F. *Chem. Physic. Lett.* **1997,** 277, (1-3), 118-124.

129. Fischer, E.; Hirshberg, Y. *J. Chem. Soc.* **1952**, (NOV), 4522-4524.

130. Bertelson, R. C., Photochromic processes involving heterolytic cleavage. In *Photochromism (Techniques of Chemistry)*, Brown, G. H., Ed. Wiley Interscience: New York, 1971.

131. R., G., Photochromism: Molecules and systems. In *Studies in Organic Chemistry*, H.;, D.; H., B.-L., Eds. Elsevier: Amsterdam, 1990.

132. Saragi, T. P. I.; Spehr, T.; Siebert, A.; Fuhrmann-Lieker, T.; Salbeck, J. *Chem. Rev.* **2007,** 107, (4), 1011-1065.

133. Oh, S. K.; Nakagawa, M.; Ichimura, K. *J. Mater. Chem.* **2002,** 12, (8), 2262-2269.

134. Klajn, R.; Stoddart, J. F.; Grzybowski, B. A. *Chem. Soc. Rev.* **2010,** 39, (6), 2203-2237.

135. Samanta, S.; Locklin, J. *Langmuir* **2008,** 24, (17), 9558-9565.

136. Piech, M.; Bell, N. S. *Macromolecules* **2006,** 39, (3), 915-922.

137. Bell, N. S.; Piech, M. *Langmuir* **2006,** 22, (4), 1420-1427.

138. Irie, M. *Chem. Rev.* **2000,** 100, (5), 1683-1683.

139. Breyne, O.; Chan, Y. P.; Henry, D.; Lafosse, X.; Chan, Y.; Henri, D.; Breyen, O.; Xavier, L.; David, H.; Olivier, B. *Photochromic compositions for use in ophthalmic optics*. WO9850807-A.

140. Ikeda, T.; Tsutsumi, O. *Science* **1995,** 268, (5219), 1873-1875.

141. Kawata, S.; Kawata, Y. *Chem. Rev.* **2000,** 100, (5), 1777-1788.

142. Hugel, T.; Holland, N. B.; Cattani, A.; Moroder, L.; Seitz, M.; Gaub, H. E. *Science* **2002,** 296, (5570), 1103-1106.

143.   Barachevsky, V. A.; Alfimov, M. V.; Nazarov, V. B. *Opt. Mem. Neural Netw.* **1998,** 7, (3), 205-212.

144.   Willner, I. *Accounts Chem. Res.* **1997,** 30, (9), 347-356.

145.   Nayak, A.; Liu, H. W.; Belfort, G. *Angew. Chem.-Int. Edit.* **2006,** 45, (25), 4094-4098.

146.   LaVan, D. A.; McGuire, T.; Langer, R. *Nat. Biotechnol.* **2003,** 21, (10), 1184-1191.

147.   Gong, C. B.; Wong, K. L.; Lam, M. H. W. *Chem. Mater.* **2008,** 20, (4), 1353-1358.

148.   Baumann, L.; de Courten, D.; Wolf, M.; Rossi, R. M.; Scherer, L. J. *ACS Appl. Mater. Interfaces* **2013,** 5, (13), 5894-5897.

149.   Baumann, L.; Schoeller, K.; de Courten, D.; Marti, D.; Frenz, M.; Wolf, M.; Rossi, R. M.; Scherer, L. J. *RSC Advances* **2013,** 3, (45), 23317-23326.

150.   Zhao, B.; Moore, J. S.; Beebe, D. J. *Science* **2001,** 291, (5506), 1023-1026.

151.   Sumaru, K.; Ohi, K.; Takagi, T.; Kanamori, T.; Shinbo, T. *Langmuir* **2006,** 22, (9), 4353-4356.

152.   Chung, D. J.; Ito, Y.; Imanishi, Y. *J. Appl. Polym. Sci.* **1994,** 51, (12), 2027-2033.

153.   Blossey, R. *Nat. Mater.* **2003,** 2, (5), 301-306.

154.   Khademhosseini, A.; Langer, R.; Borenstein, J.; Vacanti, J. P. *Proc. Natl. Acad. Sci. U. S. A.* **2006,** 103, (8), 2480-2487.

155.   Sniadecki, N.; Desai, R. A.; Ruiz, S. A.; Chen, C. S. *Ann. Biomed. Eng.* **2006,** 34, (1), 59-74.

156.   Falconnet, D.; Csucs, G.; Grandin, H. M.; Textor, M. *Biomaterials* **2006,** 27, (16), 3044-3063.

157.   Senaratne, W.; Andruzzi, L.; Ober, C. K. *Biomacromolecules* **2005,** 6, (5), 2427-2448.

158.   Besson, E.; Gue, A. M.; Sudor, J.; Korri-Youssoufi, H.; Jaffrezic, N.; Tardy, J. *Langmuir* **2006,** 22, (20), 8346-8352.

159.   Feng, C. L.; Zhong, X. H.; Steinhart, M.; Caminade, A. M.; Majoral, J. P.; Knoll, W. *Adv. Mater.* **2007,** 19, (15), 1933-1936.

160.   Reuther, C.; Hajdo, L.; Tucker, R.; Kasprzak, A. A.; Diez, S. *Nano Lett.* **2006,** 6, (10), 2177-2183.

161.   Cabane, E.; Zhang, X.; Langowska, K.; Palivan, C. G.; Meier, W. *Biointerphases* **2012,** 7, (1-4), 1-27.

162.   Colson, Y. L.; Grinstaff, M. W. *Adv. Mater.* **2012,** 24, (28), 3878-3886.

163.   Kelley, E. G.; Albert, J. N. L.; Sullivan, M. O.; Epps, T. H. *Chem. Soc. Rev.* **2013,** 42, (17), 7057-7071.

164.   Goddard, J. M.; Hotchkiss, J. H. *Prog. Polym. Sci.* **2007,** 32, (7), 698-725.

165.   Rusmini, F.; Zhong, Z. Y.; Feijen, J. *Biomacromolecules* **2007,** 8, (6), 1775-1789.

166.   Wang, Z. G.; Wan, L. S.; Liu, Z. M.; Huang, X. J.; Xu, Z. K. *J. Mol. Catal. B-Enzym.* **2009,** 56, (4), 189-195.

167.   Ward, M. A.; Georgiou, T. K. *Polymers* **2011,** 3, (3), 1215-1242.

168.   Gormally, M. V.; McKibben, R. K.; Johal, M. S.; Selassie, C. R. D. *Langmuir* **2009,** 25, (17), 10014-10019.

169.   Lu, Y.; Wittemann, A.; Ballauff, M. *Macromol. Rapid Commun.* **2009,** 30, (9-10), 806-815.

170.   Haupt, B.; Neumann, T.; Wittemann, A.; Ballauff, M. *Biomacromolecules* **2005,** 6, (2), 948-955.

171.   Samaratunga, A.; Kudina, O.; Nahar, N.; Zakharchenko, A.; Minko, S.; Voronov, A.; Pryor, S. W. *Appl. Biochem. Biotechnol.* **2015,** 175, (6), 2872-2882.

172.   Parthasarathy, R. V.; Martin, C. R. *Nature* **1994,** 369, (6478), 298-301.

173.   Arica, M. Y.; Altintas, B.; Bayramoglu, G. *Bioresour. Technol.* **2009,** 100, (2), 665-669.

174.   Angenendt, P.; Glokler, J.; Murphy, D.; Lehrach, H.; Cahill, D. J. *Anal. Biochem.* **2002,** 309, (2), 253-260.

175.   Castellana, E. T.; Cremer, P. S. *Surf. Sci. Rep.* **2006,** 61, (10), 429-444.

176.   Killops, K. L.; Gupta, N.; Dimitriou, M. D.; Lynd, N. A.; Jung, H.; Tran, H.; Bang, J.; Campos, L. M. *ACS Macro Lett.* **2012,** 1, (6), 758-763.

177.   Netz, R. R.; Andelman, D. *Phys. Rep.* **2003,** 380, (1-2), 1-95.

178.   Costantini, F.; Benetti, E. M.; Reinhoudt, D. N.; Huskens, J.; Vancso, G. J.; Verboom, W. *Lab Chip* **2010,** 10, (24), 3407-3412.

179.   Kuzmyn, A. R.; Pereira, A. D.; Pop-Georgievski, O.; Bruns, M.; Brynda, E.; Rodriguez-Emmenegger, C. *Polym. Chem.* **2014,** 5, (13), 4124-4131.

180.   Zhang, Z. B.; Yuan, S. J.; Zhu, X. L.; Neoh, K. G.; Kang, E. T. *Biosens. Bioelectron.* **2010,** 25, (5), 1102-1108.

181.   Jackeray, R.; Jain, S.; Chattopadhyay, S.; Yadav, M.; Shrivastav, T. G.; Singh, H. *J. Appl. Polym. Sci.* **2010,** 116, (3), 1700-1709.

182.   Yuan, W.; Li, C. Y.; Zhao, C.; Sui, C. G.; Yang, W. T.; Xu, F. J.; Ma, J. *Adv. Func. Mater.* **2012,** 22, (9), 1835-1842.

183.   Xu, F. J.; Wang, Z. H.; Yang, W. T. *Biomaterials* **2010,** 31, (12), 3139-3147.

184.   Srinivasan, N.; Bhagawati, M.; Ananthanarayanan, B.; Kumar, S. *Nat. Commun.* **2014,** 5, 1-8.

185.   Bar, M.; Bar-Ziv, R. H. *Nano Lett.* **2009,** 9, (12), 4462-4466.

186.   Antonio, T.; Cabral, M. F.; Cesarino, I.; Machado, S. A. S.; Pedrosa, V. A. *Electrochem. Commun.* **2013,** 29, 41-44.

187.   Wang, X. M.; Zhou, J.; Tam, T. K.; Katz, E.; Pita, M. *Bioelectrochemistry* **2009,** 77, (1), 69-73.

188.   Bocharova, V.; Tam, T. K.; Halamek, J.; Pita, M.; Katz, E. *Chem. Commun.* **2010,** 46, (12), 2088-2090.

189.   Crulhas, B. P.; Sempionatto, J. R.; Cabral, M. F.; Minko, S.; Pedrosa, V. A. *Electroanalysis* **2014,** 26, (4), 815-822.

190.   Privman, M.; Tam, T. K.; Pita, M.; Katz, E. *J. Am. Chem. Soc.* **2009,** 131, (3), 1314-1321.

191.   Katz, E.; Fernandez, V. M.; Pita, M. *Electroanalysis* **2015,** 27, (9), 2063-2073.

192.   Yu, Q.; Ista, L. K.; Lopez, G. P. *Nanoscale* **2014,** 6, (9), 4750-4757.

193.   Yin, Z.; Zhang, J.; Jiang, L.-P.; Zhu, J.-J. *J. Phys. Chem. C* **2009,** 113, (36), 16104-16109.

194.   Ebara, M.; Yamato, M.; Aoyagi, T.; Kikuchi, A.; Sakai, K.; Okano, T. *Biomacromolecules* **2004,** 5, (2), 505-510.

195.   Xu, F. J.; Zhong, S. P.; Yung, L. Y. L.; Tong, Y. W.; Kang, E. T.; Neoh, K. G. *Biomaterials* **2006,** 27, (8), 1236-1245.

196.   Xu, F. J.; Zhong, S. P.; Yung, L. Y. L.; Kang, E. T.; Neoh, K. G. *Biomacromolecules* **2004,** 5, (6), 2392-2403.

197.   Hatakeyama, H.; Kikuchi, A.; Yamato, M.; Okano, T. *Biomaterials* **2005,** 26, (25), 5167-5176.

198.   Yamada, M. D.; Nakajima, Y.; Maeda, H.; Maruta, S. *J. Biochem.* **2007,** 142, (6), 691-698.

199.   Schierling, B.; Noel, A. J.; Wende, W.; Hien, L. T.; Volkov, E.; Kubareva, E.; Oretskaya, T.; Kokkinidis, M.; Rompp, A.; Spengler, B.; Pingoud, A. *Proc. Natl. Acad. Sci. U. S. A.* **2010,** 107, (4), 1361-1366.

200. Hien, L. T.; Zatsepin, T. S.; Schierling, B.; Volkov, E. M.; Wende, W.; Pingoud, A.; Kubareva, E. A.; Oretskaya, T. S. *Bioconjugate Chem.* **2011,** 22, (7), 1366-1373.

201. Harvey, J. H.; Trauner, D. *ChemBioChem* **2008,** 9, (2), 191-193.

202. Willner, I.; Liondagan, M.; Marxtibbon, S.; Katz, E. *J. Am. Chem. Soc.* **1995,** 117, (24), 6581-6592.

203. Willner, I.; Willner, B. *Bioelectrochem. Bioenerg.* **1997,** 42, (1), 43-57.

204. Garcia, A.; Marquez, M.; Cai, T.; Rosario, R.; Hu, Z. B.; Gust, D.; Hayes, M.; Vail, S. A.; Park, C. D. *Langmuir* **2007,** 23, (1), 224-229.

205. Reuther, C.; Tucker, R.; Ionov, L.; Diez, S. *Nano Lett.* **2014,** 14, (7), 4050-4057.

206. Poloni, C.; Szymanski, W.; Feringa, B. L. *Chem. Commun.* **2014,** 50, (84), 12645-12648.

207. Fissi, A.; Pieroni, O.; Ruggeri, G.; Ciardelli, F. *Macromolecules* **1995,** 28, (1), 302-309.

208. Kessler, D.; Jochum, F. D.; Choi, J.; Char, K.; Theato, P. *ACS Appl. Mater. Interfaces* **2011,** 3, (2), 124-128.

209. Dispinar, T.; Sanyal, R.; Sanyal, A. *J. Polym. Sci. Part a-Polym. Chem.* **2007,** 45, (20), 4545-4551.

210. Farquet, P.; Padeste, C.; Solak, H. H.; Gursel, S. A.; Scherer, G. G.; Wokaun, A. *Macromolecules* **2008,** 41, (17), 6309-6316.

211. Strongman, C. *The Architects' Journal* **03.07.2008**.

212. Schiers, J., *Modern Fluoropolymers*. John Wiley & Sons Ltd.: Chichester, 1997.

213. Gomez, D.; Menendez, A.; Sanchez, P.; Martinez, A.; Andres, L. J.; Menendez, M. F.; Campos, N.; Garcia, A.; Sanchez, B., *Novel concepts for low-cost and high-efficient thin film solar cells*. In *Thin Film Solar Technology Iii*, Eldada, L. A., 2011.

214. Vasko, K.; Noller, K.; Mikula, M.; Amberg-Schwab, S.; Weber, U. *Cent. Eur. J. Phys.* **2009,** 7, (2), 371-378.

215. Cherian, J. T.; Castner, D. G. *Surf. Interface Anal.* **2000,** 29, (11), 729-734.

216. Choi, J.; Schattling, P.; Jochum, F. D.; Pyun, J.; Char, K.; Theato, P. *J. Polym. Sci. Part a-Polym. Chem.* **2012,** 50, (19), 4010-4018.

217. Padeste, C.; Solak, H. H.; Brack, H. P.; Slaski, M.; Gursel, S. A.; Scherer, G. G. *J. Vac. Sci. Technol. B* **2004,** 22, (6), 3191-3195.

218. Wang, L.; Terhalle, B.; Guzenko, V. A.; Farhan, A.; Hojeij, M.; Ekinci, Y. *Appl. Phys. Lett.* **2012,** 101, (9).

219.   Rosario, R.; Gust, D.; Hayes, M.; Jahnke, F.; Springer, J.; Garcia, A. A. *Langmuir* **2002,** 18, (21), 8062-8069.

220.   Tokarev, I.; Minko, S. *Adv. Mater.* **2010,** 22, (31), 3446-3462.

221.   Wandera, D.; Wickramasinghe, S. R.; Husson, S. M. *J. Membr. Sci.* **2010,** 357, (1-2), 6-35.

222.   Nicoletta, F. P.; Cupelli, D.; Formoso, P.; De Filpo, G.; Colella, V.; Gugliuzza, A. *Membranes* **2012,** 2, (1), 134-197.

223.   Lee, H.-i.; Pietrasik, J.; Sheiko, S. S.; Matyjaszewski, K. *Prog. Polym. Sci.* **2010,** 35, (1-2), 24-44.

224.   Cabane, E.; Zhang, X. Y.; Langowska, K.; Palivan, C. G.; Meier, W. *Biointerphases* **2012,** 7, (1-4), 27.

225.   Ulbricht, M. *React. Func. Polym.* **1996,** 31, (2), 165-177.

226.   Zhao, C. S.; Nie, S. Q.; Tang, M.; Sun, S. D. *Prog. Polym. Sci.* **2011,** 36, (11), 1499-1520.

227.   Reber, N.; Kuchel, A.; Spohr, R.; Wolf, A.; Yoshida, M. *J. Membr. Sci.* **2001,** 193, (1), 49-58.

228.   Liu, Z.; Luo, F.; Ju, X. J.; Xie, R.; Luo, T.; Sun, Y. M.; Chu, L. Y. *Adv. Func. Mater.* **2012,** 22, (22), 4742-4750.

229.   Chen, H.; Palmese, G. R.; Elabd, Y. A. *Macromolecules* **2007,** 40, (4), 781-782.

230.   Yang, Q.; Xu, Z. K.; Dai, Z. W.; Wang, J. L.; Ulbricht, M. *Chem. Mater.* **2005,** 17, (11), 3050-3058.

231.   Naixin, W.; Guojun, Z.; Shulan, J.; Zhenping, Q.; Zhongzhou, L. *J. Membr. Sci.* **2010,** 354, (1-2), 14-22.

232.   Yu, W. H.; Kang, E. T.; Neoh, K. G. *Langmuir* **2005,** 21, (1), 450-456.

233.   Ying, L.; Yu, W. H.; Kang, E. T.; Neoh, K. G. *Langmuir* **2004,** 20, (14), 6032-6040.

234.   Hai-Yin, Y.; Wei, L.; Jin, Z.; Jia-Shan, G.; Lei, H.; Zhao-Qi, T.; Xian-Wen, W. *J. Membr. Sci.* **2009,** 343, (1-2), 82-89.

235.   Bo, D.; Xuanxuan, Y.; Leidong, X.; Jingye, L.; Zhengchi, H.; Yao, S.; Guoming, L.; Kanglong, S.; Qing, H. *J. Membr. Sci.* **2009,** 330, (1-2), 363-368.

236.   Barbey, R.; Lavanant, L.; Paripovic, D.; Schuwer, N.; Sugnaux, C.; Tugulu, S.; Klok, H. A. *Chem. Rev.* **2009,** 109, (11), 5437-5527.

237.   Hegemann, D.; Brunner, H.; Oehr, C. *Nucl. Instrum. Methods Phys. Res. Sect. B-Beam Interact. Mater. Atoms* **2003,** 208, 281-286.

238. Shinkai, S.; Kinda, H.; Manabe, O. *J. Am. Chem. Soc.* **1982,** 104, (10), 2933-2934.

239. Bouas-Laurent, H.; Durr, H. *Pure Appl. Chem.* **2001,** 73, (4), 639-665.

240. Dübner, M.; Spencer, N. D.; Padeste, C. *Langmuir* **2014,** 30, (49), 14971-14981.

241. Dübner, M.; Gevrek, T. N.; Sanyal, A.; Spencer, N. D.; Padeste, C. *ACS Appl. Mater. Interfaces* **2015,** 7, (21), 11337-11345.

242. Subramani, C.; Cengiz, N.; Saha, K.; Gevrek, T. N.; Yu, X.; Jeong, Y.; Bajaj, A.; Sanyal, A.; Rotello, V. M. *Adv. Mater.* **2011,** 23, (28), 3165-3169.

243. Onbulak, S.; Tempelaar, S.; Pounder, R. J.; Gok, O.; Sanyal, R.; Dove, A. P.; Sanyal, A. *Macromolecules* **2012,** 45, (3), 1715-1722.

244. Yilmaz, II; Arslan, M.; Sanyal, A. *Macromol. Rapid Commun.* **2012,** 33, (9), 856-862.

245. Miyadera, T.; Kosower, E. M. *J. Med. Chem.* **1972,** 15, (5), 534-537.

246. Ghosh, S. S.; Kao, P. M.; McCue, A. W.; Chappelle, H. L. *Bioconjugate Chem.* **1990,** 1, (1), 71-76.

247. Gindy, M. E.; Ji, S. X.; Hoye, T. R.; Panagiotopoulos, A. Z.; Prud'homme, R. K. *Biomacromolecules* **2008,** 9, (10), 2705-2711.

248. Xiao, S. J.; Textor, M.; Spencer, N. D.; Wieland, M.; Keller, B.; Sigrist, H. *J. Mater. Sci-Mater. Med.* **1997,** 8, (12), 867-872.

249. Schlapak, R.; Pammer, P.; Armitage, D.; Zhu, R.; Hinterdorfer, P.; Vaupel, M.; Fruhwirth, T.; Howorka, S. *Langmuir* **2006,** 22, (1), 277-285.

250. Gevrek, T. N.; Bilgic, T.; Klok, H.-A.; Sanyal, A. *Macromolecules* **2014,** 47, (22), 7842-7851.

251. Mautner, A.; Qin, X. H.; Kapeller, B.; Russmueller, G.; Koch, T.; Stampfl, J.; Liska, R. *Macromol. Rapid Commun.* **2012,** 33, (23), 2046-2052.

252. De, P.; Li, M.; Gondi, S. R.; Sumerlin, B. S. *J. Am. Chem. Soc.* **2008,** 130, (34), 11288-11289.

253. Zhang, J.; Peppas, N. A. *Macromolecules* **2000,** 33, (1), 102-107.

254. Kong, S. D.; Zhang, W. Z.; Lee, J. H.; Brammer, K.; Lal, R.; Karin, M.; Jin, S. H. *Nano Lett.* **2010,** 10, (12), 5088-5092.

255. Amir, R. J.; Zhong, S.; Pochan, D. J.; Hawker, C. J. *J. Am. Chem. Soc.* **2009,** 131, (39), 13949-13951.

256. Schumers, J. M.; Fustin, C. A.; Gohy, J. F. *Macromol. Rapid Commun.* **2010,** 31, (18), 1588-1607.

257. Huang, W. M.; Jia, J. B.; Zhang, Z. L.; Han, X. J.; Tang, J. L.; Wang, J. G.; Dong, S. J.; Wang, E. K. *Biosensors & Bioelectronics* **2003,** 18, (10), 1225-1230.

258. Gooding, J. J.; Erokhin, P.; Losic, D.; Yang, W. R.; Policarpio, V.; Liu, J. Q.; Ho, F. M.; Situmorang, M.; Hibbert, D. B.; Shapter, J. G. *Anal. Sci.* **2001,** 17, (1), 3-9.

9. Acknowledgements

I would like to thank Prof. Nicholas D. Spencer for supervising my PhD project. I always appreciated his scientific input, drive and attitude towards science which continuously promoted our projects and made it very easy for me to conserve my focus and high level of motivation. I envy his ability for time-management which allows him to maintain his work-life balance to act out his passion for traveling, dancing and wine, aside from handling such a big group as the Laboratory of Surface Science and Technology (LSS) and teaching at ETH Zurich. And if that wasn't enough, none of this would ever stop him from proof-reading any of your drafts and manuscripts in between meetings, at the airport or on any vehicle for transportation you can imagine. Even if you are (again) very close to submission deadline, you can be sure that he replies instantaneously and that he will always end with kind words such as "All the best from … (enter a random destination), Nic". I thank him for introducing me into his world of surface and material science, as well as into the art of enjoying life, including Tango and Argentinian wine on our countless group events.

A great piece of gratitude is due to Dr. Celestino Padeste who initiated the project and acted as my direct supervisor at the Laboratory of Micro- and Nanotechnology (LMN) of the Paul-Scherrer-Institute (PSI). I thank him for his contributions, discussions and enthusiasm throughout the entire four years. In an environment full of engineers and physicists, I was very happy to have someone at my side that "speaks my language", as one of the very few chemists at LMN. I admire his broad expertise, ranging from chemistry, over surface science and microfabrication, all the way to biosensing and crystallography. His diverse interests inspired me to also span my projects into directions further than what we have planned in the very beginning. I thank him for the unlimited flexibility – not only in my working hours, turning more than one blind eye on me not being at work at 9.00 am sharp – but also in what to prioritize and how to tackle upcoming challenges. The absolute freedom of choice on what to work and focus on was probably what I enjoyed the most and what let me unfold this project to its full beauty. He proved over and over strong intuition on how to handle his students creating a comfort zone with a familiar atmosphere which offers unequaled opportunities. On top of that, I thank him for his endless patience in general and in particular with reading and re-reading of my always too long manuscripts. Skills such as cutting drafts by half and avoiding so-called "Matthias loops" in my findings are just two examples on how he made me become a better scientist. I don't know if I

will ever be able to pay back what he has done for me, but I will try by starting with finally attending one of his classical concerts.

Thanks are also due to our collaborators Tuğçe Nihal Gevrek and Prof. Amitav Sanyal from Boğaziçi University in Bebek (Istanbul, Turkey), not only for providing the furan-protected maleimide monomer, but also for very fruitful meetings *via* Skype. What started from a random discussion at a poster session of a conference in Italy, turned out to be a very successful and straight-forward collaboration across Europe. Certainly, without their contribution of introducing us into the world of highly-efficient reactions, this dissertation would not have been the same.

I would like to thank Prof. A. Dieter Schlüter for accepting to be co-examiner of my PhD thesis and Prof. Manfred Fiebig, who agreed to lead the PhD defense as representative of the Department of Materials of ETH Zurich. I gratefully acknowledge financial support from the Swiss National Science Foundation without this PhD project never would have even started.

Many thanks go to my colleagues from PSI. In particular, I would like to thank Prof. Jens Gobrecht and Dr. Helmut Schift for accepting me as PhD student at LMN and the cross-institutional INKA group of PSI and FHNW. I thank the heart and soul of LMN, Edith Meisel, for her support in administrative issues, organizing our social events and always putting a smile back on my face when things went wrong and I came into her office for a desperately needed coffee break. I thank Dr. Lorenz Gubler for providing our substrate materials, Konrad Vogelsang for preparing all the flat-pressed polymer foils for countless grafting reactions, Prof. Kurt Ballmer and Dr. Dmitry Veprintsev for assistance with Fluorescence microscopy, Dr. Camelia N. Borca and Dr. Sonia Pin with IR microscopy, Rolf Schelldorfer with Atomic Force Microscopy, Stefan Stutz with UV/vis Microscopy and Michaela Vockenhuber with EUV-IL exposures, respectively.

But all the projects of my thesis could not have been as extensive without the help of our apprentices Désirée Burkart and Yves Erdin, as well as our Bachelor and Master students Sabrina Baumann, Sandro Bellini, Katarzyna Gajos and Maria-Eleni Naoum. They created a very nice atmosphere in the lab and conducted uncountable experiments discussed in this thesis. It was my pleasure to supervise their work and help them develop their future careers. I also would like to thank our in-house collaborators Dr. Robert Kirchner, Dr. Victor J. Cadarso and visiting PhD student Sahan A. Ranamukhaarachchi from University of British Columbia in Vancouver (Canada), as well as Dr. Guido Panzarasa from Università del Piemonte Orientale in Alessandria (Italy) for very interesting and fruitful projects aside my PhD thesis which led to additional published manuscripts.

10.   Curriculum Vitae

Name	Matthias Dübner
Date of Birth	May 19th, 1987
Nationality	German
Present Address	Nordstrasse 397, 8037 Zürich

Education

06/2012-06/2016	Doctoral Student in Materials Science at the Laboratory for Micro- and Nanotechnology, Paul-Scherrer Institute, Villigen and at the Laboratory for Surface Science and Technology, Department of Material, ETH Zurich
09/2010-04/2012	Master of Science in Chemistry, ETH Zurich. Thesis on Synthesis of Phenanthro[9,10-*b*]benzofuranes for OLED Application.
09/2007-07/2010	Bachelor of Science in Chemistry, University of Heidelberg. Thesis on Analysis of a Perylenediimide-bis-(DPA-Zn(II)) Complex as a Fluorescence Sensor for Nucleoside Phosphates.

Employment

05/2013-04/2014	Visitor Guide at the PSI Forum, Villigen.
10/2011-03/2012	Intern for Master Thesis Project at the OLED Division, BASF AG, Basel.
07/2009-09/2009	Intern for a Research Project at the INE, Karlsruhe Institute of Technology.
08/2006-08/2007	Kindergarten Teacher for Voluntary Social Year Abroad at the Rudolf Steiner School, Kings Langley, London.
05/2006-08/2006	Intern at Bondioli & Pavesi GmbH, Groß-Gerau.

Publications

2016	Reversible Light-Switching of Enzymatic Activity on Orthogonally Functionalized Polymer Brushes. M. Dübner, V.J. Cadarso, T.N. Gevrek, A. Sanyal, N.D. Spencer, C. Padeste, *Nat. Mater.* **2016**, in preparation.

From pH- to Light-Response: Post-Polymerization Modification of Polymer Brushes Grafted onto Polymeric Membranes.

M. Dübner, M.-E. Naoum, N.D. Spencer, C. Padeste, *ACS Appl. Mater. Interfaces* **2016**, in preparation.

Integrated hollow microneedle optofluidic biosensor for therapeutic drug monitoring in sub-nanoliter volumes.

S.A. Ranamukhaarachchi, C. Padeste, M. Dübner, U.O. Häfeli, B. Stoeber, V.J. Cadarso, *Scientific Reports* **2016**, accepted. DOI: 10.1038/srep29075.

ON/OFF Switching of Silicon Wafer Electrochemistry by pH-Responsive Polymer Brushes.

G. Panzarasa, M. Dübner, V. Pifferi, G. Soliveri, C. Padeste, *J. Mater. Chem. C* **2016**, *4*, 6287−6294.

2015   Fabrication of Thiol-Ene "Clickable" Copolymer-Brush Nanostructures on Polymeric Substrates *via* Extreme Ultraviolet Interference Lithography.

M. Dübner, T.N. Gevrek, A. Sanyal, N.D. Spencer, C. Padeste, *ACS Appl. Mater. Interfaces* **2015**, *7*, 11337−11345.

2014   Light-Responsive Polymer Surfaces *via* Post-Polymerization Modification of Grafted Polymer-Brush Structures.

M. Dübner, N.D. Spencer, C. Padeste, *Langmuir* **2014**, *30*, 14971−14981.

2013   Phenanthro[9,10-*b*]furan polymers and small molecules for electronic applications.

M. Welker, T. Schäfer, N. Chebotareva, M. Dübner, M.G.R. Turbiez, Patent WO/2013/149897.

Presentations

2016   Light-Controlled Enzymatic Activity on Orthogonally Functionalized
                 Polymer Brushes Grafted from Polymeric Substrates (Talk).
                 M. Dübner *et al.*, *POC*, Hersonissos (Crete), Greece, June, 13th-16th.

2015   Multifunctional Copolymer-Brush Nanostructures for Smart Surfaces *via*
                 EUV-Interference Lithography (Talk).
                 M. Dübner *et al.*, *INASCON*, Basel, Switzerland, August, 11th-14th.

                 Nanopatterned Thiol-Ene "Clickable" Copolymer-Brushes on Polymeric
                 Substrates *via* EUV-Interference Lithography (Poster).
                 M. Dübner *et al.*, *SCS PolyColl*, Fribourg, Switzerland, July, 3rd.

                 Smart Surfaces *via* Multifunctional Copolymer-Brush Nanostructures on
                 Polymeric Substrates (Talk).
                 M. Dübner *et al.*, *European Polymer Congress*, Dresden, Germany, June,
                 21st-26th.

                 Nano-Patterned   Thiol-Reactive   Copolymer-Brushes   Grafted   from
                 Polymeric Surfaces (Poster).
                 M. Dübner *et al.*, *Frontiers in Polymer Science*, Riva del Garda, Italy,
                 May, 20th-22nd.

                 Thiol-ene 'Clickable' Copolymer-Brush Nanostructures on Polymeric
                 Substrates *via* Extreme Ultraviolet Interference Lithography (Poster).
                 M. Dübner *et al.*, *Swiss Soft Days*, Villigen PSI, Switzerland, May, 4th.

2014   Light-Responsive Polymer Surfaces *via* Post-Polymerization Modification
                 of Grafted Brush Structures (Poster).
                 M. Dübner *et al.*, *EUPOC*, Gargnano, Italy, May, 25th-29th.

Nanostructured Light-Responsive Polymer Brushes (Poster).

M. Dübner *et al.*, *Swiss NanoConvention*, Brugg, Switzerland, May, 21st.

2013   Nanostructured Light-Responsive Polymer Brushes (Talk).

M. Dübner *et al.*, *SLS Symposium*, Villigen, Switzerland, September, 03rd.

Nano-Patterned Light-Responsive Polymer Brushes Grafted from Polymer Surfaces (Poster).

M. Dübner *et al.*, *Frontiers in Polymer Science*, Sitges (Barcelona), Spain, May, 21st-23rd.